Electronic Supplementary Material (ESI) for Journal of Materials Chemistry A.

Designing for conjugate addition: an amine functionalised quinone anolyte for redox flow batteries – Supplementary Information

Rajesh B. Jethwa,[†] Evan Wenbo Zhao,[†] Rachel N. Kerber,[†‡] Erlendur Jónsson,[†] Dominic S. Wright[†*] and Clare P. Grey[†*]

[†]Department of Chemistry, University of Cambridge, Lensfield Road, Cambridge CB2 1EW, United Kingdom

[‡] Johnson Matthey Technology Centre, Core-Science Physical and Chemical Modelling Group, Blounts Ct Rd, Sonning Common, Reading RG4 9NH

Contents

1. Methodology

1.1 Synthesis

Multiple batches of product were used in this paper. The synthesis was carried out in broadly the same way. The preparations are detailed below. Apart from Batch 1, benzoquinone was sublimed under vacuum before use. All other reagents were used as purchased without further purification. Benzoquinone and 4-aminobenzoic acid were sourced from Acros Organics. 2,5-dimethyl-1,4-benzoquinone was sourced from Aldrich and absolute ethanol was sourced from VWR Chemicals.

1.1.1 CABQ Synthetic protocol

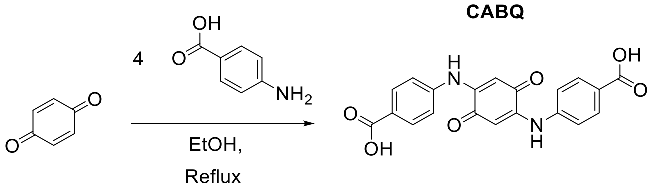

Scheme 1: Reaction scheme illustrating the synthesis of CABQ.

General protocol:

1,4-benzoquinone (1 eq) was added to 4-aminobenzoic acid (4 eq) under inert atmosphere. Ethanol (20 ml) was then added. The suspension was stirred for 70 mins after which further ethanol (20 ml) was added. The red-brown suspension was then heated under reflux (100 °C, ~100 hrs) causing the suspension to darken. The system was then exposed to air and refluxed further (100 hrs). The suspension was cooled to ambient conditions and then filtered under vacuum, washing with cold ethanol followed by cold ether then pentane. The resulting brown powder was then dried under elevated temperature (100 °C) and under vacuum for 20 mins.

Justification:

Amine functionalisation of the quinone framework was initially attempted using the protocol suggested by Nain-Perez *et al.*[1] However, due to the difficulty found when attempting to isolate the target molecule, the protocol suggested for aminobenzoic acid functionalisation by Macgregor *et al.*[2] was instead adopted. However, due to this protocol producing a significant proportion of impurities, the protocol was modified to use an increased excess of the amine and a greater reaction time (see SI for further details). The crude yield for all batches (see SI) was approximately 37%. Of the 37% solid crude yield that was isolated, approximately 80% comprised of CABQ with the remainder being one minor by-product (measured by comparison of major aromatic doublets to minor aromatic doublets in the ^{1}H NMR spectra). The minor by-product is thought to be CABHQ.[3] Separation of the major product from the minor, was achieved by dissolution in basic aqueous media followed by neutralisation and re-precipitation with aqueous acidic media and washing with ethyl acetate, water and diethyl ether (Figure S 3). However, the crude product was used for all electrochemical analyses reported in this work as the electrochemical performance between the crude and purified products did not differ significantly, consistent with the minor product simply representing the reduced form of CABQ (Figure S 21, Figure S 22, Figure S 28, Figure

S 29 and Figure S 30). The low yields can be explained by the need for re-oxidation of the molecule after the first substitution, which is carried out by either the quinone substrate itself or by atmospheric oxygen.[4]

Batch 1

1,4-benzoquinone (1.0626 g, 9.83 mmol) was added to 4-aminobenzoic acid (5.3741 g, 39.19 mmol). A dark brown powder (1.6598 g) was obtained. ^{1}H NMR confirmed that the product had been made along-side a by-product (presumed to be the hydroquinone analogue) and some solvent impurities.

A (Yield = 37%, Purity = 82%) was used for all further characterisation techniques i.e. NMR, IR, CV and elemental analysis.
Elemental Analysis: Found: C, 62.6; H, 3.9; N, 7.4; Calculated: C, 63.5; H, 3.7; N, 7.4.

^{1}H-NMR (400.13 MHz, d$_6$-DMSO) δ 9.49 (2H, s, NH), 7.97 (4H, d, J = 8.71 Hz, H$_{Ar}$ – meta to NH), 7.52 (4H, d, J = 8.71 Hz, H$_{Ar}$ – ortho to NH), 6.07 (2H, s, H$_{quinone}$), 12.74 (2H, br s, CO$_2$H).
IR: 3267 cm^{-1}, 1671 cm^{-1}, 1647 cm^{-1}, 1582 cm^{-1}, 1525 cm^{-1}, 1505 cm^{-1}.

Sublimation point: ~275 °C; Melting point of residue: >340 °C (Literature melting point: >250 °C).[2]

Solubility: 66 mM in both H_2O and D_2O.

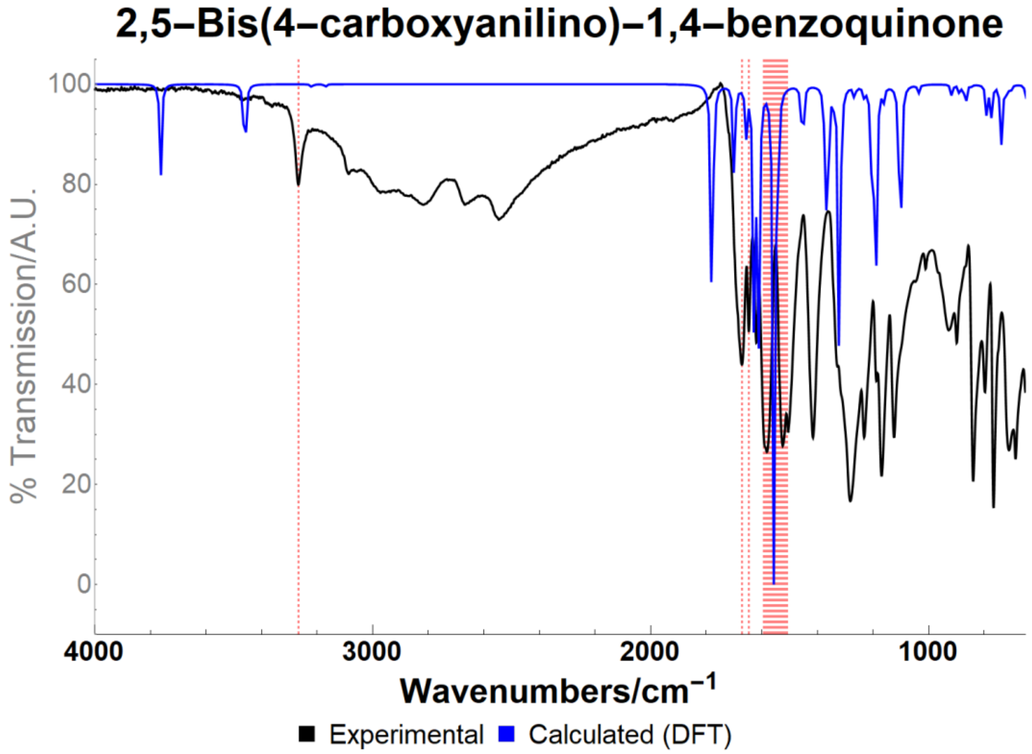

Figure S 1: IR spectrum (black) of CABQ with red gridlines highlighted at 3267 cm^{-1} (N-H), 1671 cm^{-1} (C=O - acid), 1647 cm^{-1} (C=O - quinone) and 1600-1800 cm^{-1} (C_6H_5). The calculated DFT spectrum (B3LYP/def2QZVP, blue) is also shown alongside the experimental data for comparison.

1H NMR

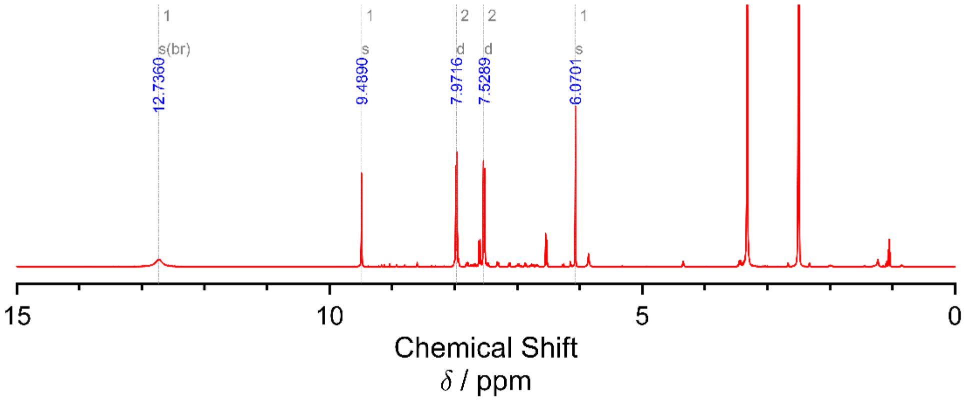

Figure S 2: ^{1}H NMR spectrum of CABQ in d$_6$-DMSO. (400.13 MHz) δ 9.49 (2H, s, NH), 7.97 (4H, d, J = 8.71 Hz, H$_{Ar}$ – meta to NH), 7.53 (4H, d, J = 8.71 Hz, H$_{Ar}$ – ortho to NH), 6.07 (2H, s, H$_{quinone}$), 12.74 (2H, br s, CO$_2$H). Literature values: δ 9.44 (2H, br s, NH), 7.96 (4H, d, J = 8.7 Hz), 7.52 (4H, d, J = 8.7 Hz), 6.06 (2H, s).[2] The peaks at 2.50 and 3.32 ppm are due to DMSO itself and water impurities in the deuterated solvent.[5]

Purification

Purification of the crude sample was achieved by dissolution in basic aqueous media followed by neutralisation and re-precipitation with aqueous acidic media. Ethyl acetate was then used to wash the product yielding only one set of aromatic doublets.

^{1}H NMR

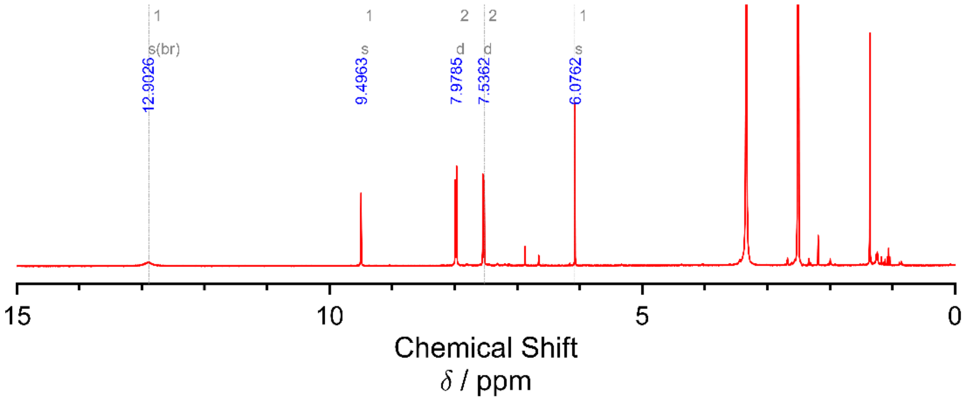

Figure S 3: ^{1}H NMR spectrum of purified CABQ in d$_6$-DMSO. (399.60 MHz) δ 12.90 (2H, br s, CO$_2$H), 9.50 (2H, s, NH), 7.98 (4H, d, J = 8.67 Hz, H$_{Ar}$ – meta to NH), 7.54 (4H, d, J = 8.79 Hz, H$_{Ar}$ – ortho to NH), 6.08 (2H, s, H$_{quinone}$). Literature values: δ 9.44 (2H, br s, NH), 7.96 (4H, d, J = 8.7 Hz), 7.52 (4H, d, J = 8.7 Hz), 6.06 (2H, s).[2] The peaks at 2.51 and 3.34 ppm are due to DMSO itself and water impurities in the deuterated solvent.[5]

Batch 2

1,4-benzoquinone (1.1855 g, 10.97 mmol) was added to 4-aminobenzoic acid (5.3542 g, 38.95 mmol). A dark brown powder (A, 1.5246 g, 37% crude yield) was obtained. The crude sample was used for in-situ NMR analysis without further purification.

^{1}H NMR

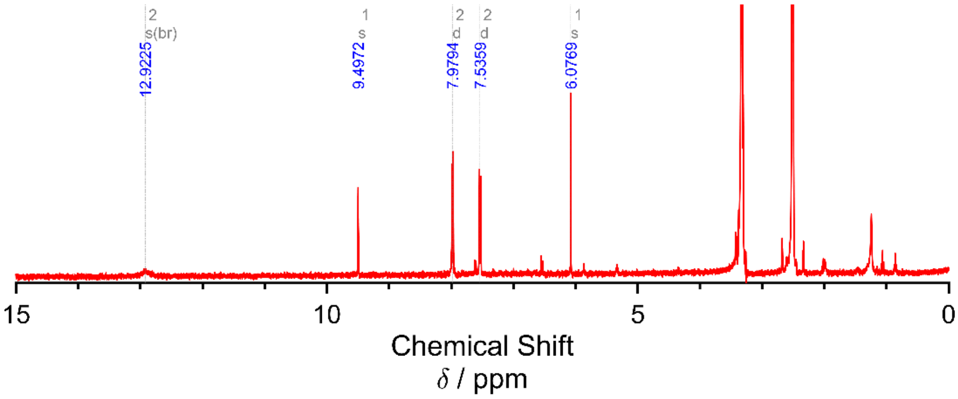

Figure S 4: ^{1}H NMR spectrum of CABQ (Batch 2) in d_6-DMSO. (399.60 MHz) δ 12.92 (2H, br s, CO_2H), 9.50 (2H, s, NH), 7.98 (4H, d, J = 8.70 Hz, H_{Ar} – meta to NH), 7.54 (4H, d, J = 8.73 Hz, H_{Ar} – ortho to NH), 6.08 (2H, s, $H_{quinone}$). Literature values: δ 9.44 (2H, br s, NH), 7.96 (4H, d, J = 8.7 Hz), 7.52 (4H, d, J = 8.7 Hz), 6.06 (2H, s).[2] The peaks at 2.51 and 3.33 ppm are due to DMSO itself and water impurities in the deuterated solvent.[5]

Batch 3

1,4-benzoquinone (2.3034 g, 21.31 mmol) was added to 4-aminobenzoic acid (10.0585 g, 73.35 mmol). A dark brown powder was obtained (A, 2.7614 g, 34% crude yield). The crude sample was used without further purification for the in-situ EPR analysis, Randles-Sevcik analysis and for full-cell battery testing with baked carbon paper.

^{1}H NMR

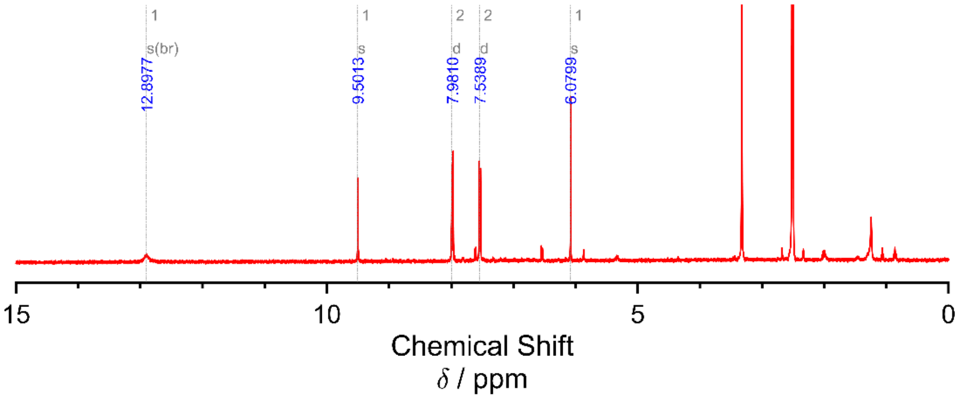

Figure S 5: ^{1}HNMR spectrum of CABQ (Batch 3) in d_6-DMSO. (399.60 MHz) δ 12.90 (2H, br s, CO_2H), 9.50 (2H, s, NH), 7.98 (4H, d, J = 8.65 Hz, H_{Ar} – meta to NH), 7.54 (4H, d, J = 8.73 Hz, H_{Ar} – ortho to NH), 6.08 (2H, s, $H_{quinone}$). Literature values: δ 9.44 (2H, br s, NH), 7.96 (4H, d, J = 8.7 Hz), 7.52 (4H, d, J = 8.7 Hz), 6.06 (2H, s).[2] The peaks at 2.51 and 3.33 ppm are due to DMSO itself and water impurities in the deuterated solvent.[5]

Batch 4

1,4-benzoquinone (1.5901 g, 14.71 mmol) was added to 4-aminobenzoic acid (8.1085 g, 59.13 mmol). A dark brown powder was obtained (1.9858 g). A sample (1.0854 g) of the crude sample was used for further purification. A dark brown powder was obtained after purification (0.4122 g, 38% yield from crude by mass). The purified sample was used for comparison to the crude sample in both electrochemical (10 mM CV) and NMR behaviour.

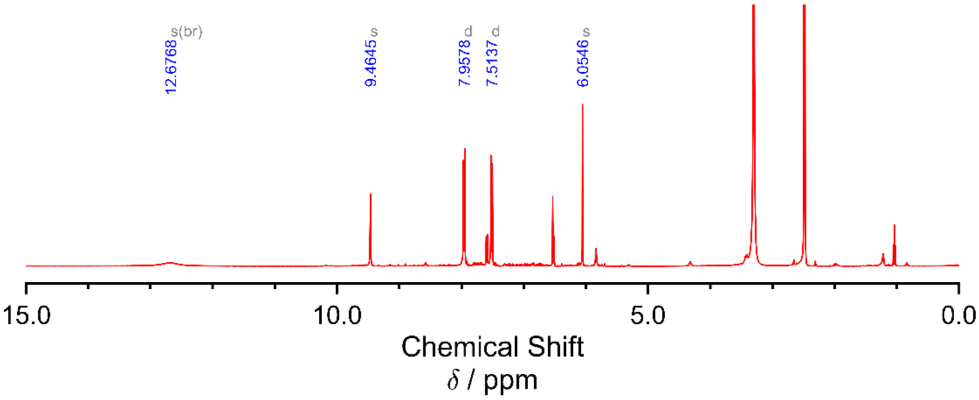

Figure S 6: ^{1}HNMR spectrum of crude CABQ (Batch 4) in d_6-DMSO. (400.13 MHz) δ 12.68 (2H, br s, CO_2H), 9.46 (2H, s, NH), 7.96 (4H, d, J = 8.58 Hz, H_{Ar} – meta to NH), 7.51 (4H, d, J = 8.63 Hz, H_{Ar} – ortho to NH), 6.05 (2H, s, $H_{quinone}$). Literature values: δ 9.44 (2H, br s, NH), 7.96 (4H, d, J = 8.7 Hz), 7.52 (4H, d, J = 8.7 Hz), 6.06 (2H, s).[2] The peaks at 2.51 and 3.33 ppm are due to DMSO itself and water impurities in the deuterated solvent.[5]

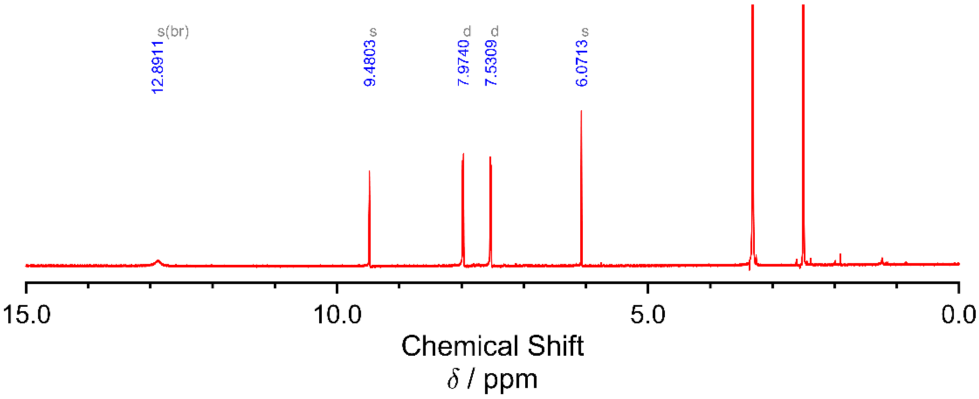

Figure S 7: ^{1}HNMR spectrum of pure CABQ (Batch 4) in d_6-DMSO. (600.13 MHz) δ 12.89 (2H, br s, CO_2H), 9.48 (2H, s, NH), 7.97 (4H, d, J = 8.59 Hz, H_{Ar} – meta to NH), 7.53 (4H, d, J = 8.61 Hz, H_{Ar} – ortho to NH), 6.07 (2H, s, $H_{quinone}$). Literature values: δ 9.44 (2H, br s, NH), 7.96 (4H, d, J = 8.7 Hz), 7.52 (4H, d, J = 8.7 Hz), 6.06 (2H, s).[2] The peaks at 2.51 and 3.33 ppm are due to DMSO itself and water impurities in the deuterated solvent.[5]

Batch 5

1,4-benzoquinone (2.3044 g, 21.32 mmol) was added to 4-aminobenzoic acid (10.0585 g, 86.38 mmol). A dark brown powder was obtained (2.8887 g). The crude sample was used without further purification for the symmetric cell experiment.

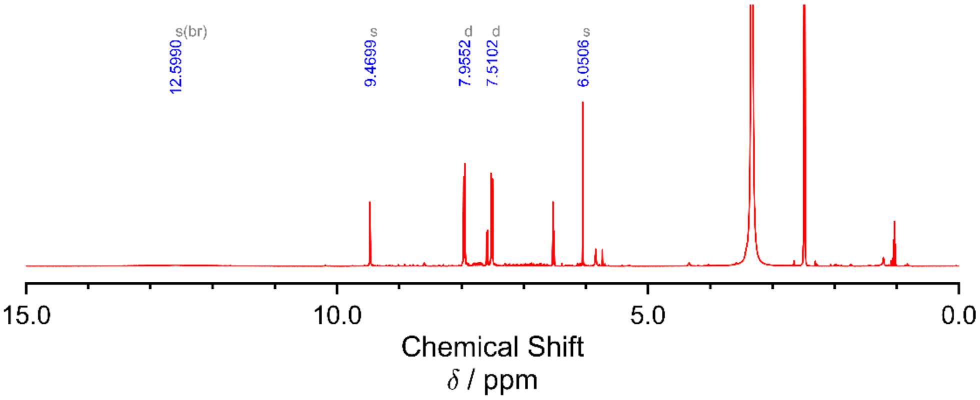

Figure S 8: ^{1}HNMR spectrum of CABQ (Batch 5) in d_6-DMSO. (400.13 MHz) δ 12.60 (2H, br s, CO_2H), 9.47 (2H, s, NH), 7.96 (4H, d, J = 8.67 Hz, H_{Ar} – meta to NH), 7.51 (4H, d, J = 8.74 Hz, H_{Ar} – ortho to NH), 6.05 (2H, s, $H_{quinone}$). Literature values: δ 9.44 (2H, br s, NH), 7.96 (4H, d, J = 8.7 Hz), 7.52 (4H, d, J = 8.7 Hz), 6.06 (2H, s).[2] The peaks at 2.51 and 3.33 ppm are due to DMSO itself and water impurities in the deuterated solvent.[5]

1.1.2 DMCABQ Synthetic protocol

2,5-dimethyl-1,4-benzoquinone (0.9909 g, 7.13 mmol) was dissolved in ethanol (20 ml) with stirring to form a yellow solution under inert atmosphere. 4-aminobenzoic acid (2.1464 g, 15.65 mmol) was then added followed by additional ethanol (10 ml) to form a red-orange solution. The mixture was stirred for 1 hr before being taken to reflux (7 days) during which the solution darkened to dark red colour and began to form a suspension. The suspension was allowed to cool to room temperature overnight and was further cooled to ~5 °C for 3 days. The suspension was then filtered under vacuum and washed onto the filter with cold ethanol. A brown powder (0.1301 g, 5% yield) was obtained.

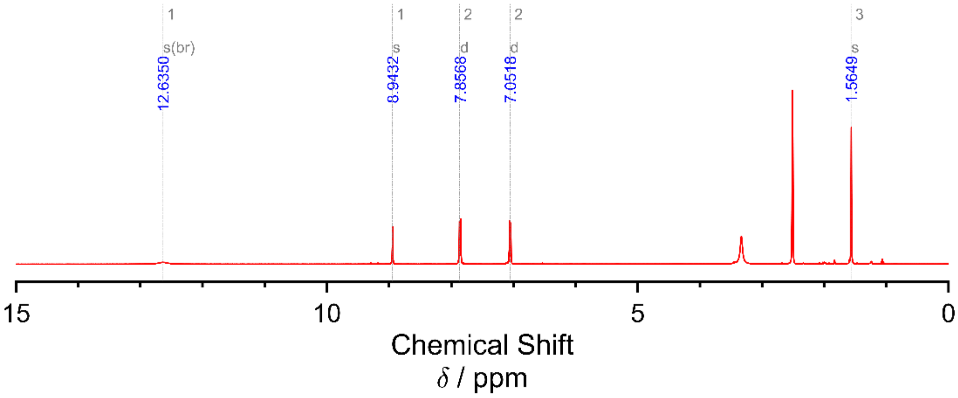

Figure S 9: ^{1}HNMR spectrum of DMCABQ in d_6-DMSO. (399.6 MHz) δ 12.64 (2H, br s, CO_2H), 8.94 (2H, s, NH), 7.86 (4H, d, J = 8.60 Hz, H_{Ar} – meta to NH), 7.05 (4H, d, J = 8.64 Hz, H_{Ar} – ortho to NH), 1.56 (6H, s, $H_{quinone}$). The peaks at 2.51 and 3.33 ppm are due to DMSO itself and water impurities in the deuterated solvent.[5]

1.2 Cycling voltammetry

1.2.1 General process

Electrochemical measurements were performed either on a Biologic potentiostat (SP-150) or on an Ivium CompactStat (B10045) using an in-house small-volume cyclic voltammetry cell. Polished 3 mm diameter glassy carbon (Biologic A-012744) was used as the working electrode while coiled platinum wire was used as the counter-electrode. For the reference, a mercury/mercury oxide (1 M KOH) electrode which has a potential of 0.14 V against the standard hydrogen electrode (SHE) was used. The potassium hydroxide solution (1 M KOH), to be used as supporting electrolyte, was made under inert atmosphere by addition of either de-gassed Millipore water or de-gassed D_2O to a known quantity of potassium hydroxide. Known amounts of the analytes to be studied were then dissolved in the supporting electrolyte solution under inert atmosphere to make a 1 mM solution for electrochemical study. A sample of the solution was then extracted and added to the flushed small-volume electrochemical cell under inert atmosphere. The electrodes were then checked to ensure that no bubbles had formed during the addition before cycling was initiated. The voltage was scanned cathodically (towards negative potentials) first in all cases. The cell was kept under an active pressure of dried nitrogen to ensure an inert atmosphere throughout the experiments.

1.2.2 Preparation of CV sample – batch 1

CABQ (13.3 mg) was dissolved in 1 M KOH aqueous solution (35.15 ml) to form a dark brown-red solution. A sample was transferred, under inert atmosphere, to the in-house cell for testing.

Preparation of CV sample – purified sample from batch 1

Added CABQ (113.9 mg) to 1 M KOH aqueous solution (1.2 ml) followed by further dilution by water (30 ml). The solution was then refluxed (100 °C, 43 hrs). Hydrochloric acid (1 M, 6 ml) was then added dropwise causing a precipitate to form. The precipitate was left to settle before filtration first under vacuum (A, 27.79 mg) followed by filtration under gravity (B, 48.47 mg). The solid (B) was recovered from the filter paper using dissolution in acetone followed by concentration under vacuum.

Added CABQ (108.4 mg) to 1 M KOH aqueous solution (1.2 ml) followed by further dilution by water (8.8 ml). The solution was then stirred while air was bubbled through (93 hrs) during which the dark red solution became a brown suspension. Filtration was attempted through a glass frit but not solid was collected. Ethyl acetate extraction was then attempted on the filtrate, but the organic phase was not discoloured. Hydrochloric acid (1 M, 1.2 ml) was then added, and the mixture was again agitated causing the organic phase to become red while the aqueous phase remained brown. A precipitate was observed, the mixture was filtered to obtain a brown powder (A, 13.28 mg). The organic phase was separated from the aqueous and both fractions were concentrated to dryness under vacuum. From the organic phase a dark red powder was obtained (B, 12.45 mg) while from the aqueous phase a brown powder was obtained (C, 61.55 mg). ^{1}H NMR showed that C contained the purified product.

C (12.5 mg) was dissolved in 1 M KOH aqueous solution (32.25 ml) to form a red-orange solution. A sample was transferred, under inert atmosphere, to the in-house cell for testing.

Preparation of CV sample for dissolution in potassium chloride solution – neutralisation via stoichiometric addition of KOH solution.

CABQ (15.1 mg) was dissolved in 1 M KOH potassium hydroxide solution (0.8 ml). 0.1 M KCl aqueous solution was then added to generate a solution of the right concentration.

1.2.3 Preparation of CV sample – batch 3

Preparation of CV sample at near neutral pH – deprotonation using triethylamine

CABQ (9.2 mg) was added to aqueous salt solution (1 M KCl, de-ionised H_2O). Triethylamine (1 ml, dry) was then added to cause the quinone to dissolve into the aqueous solution. A sample was then transferred, under inert atmosphere, to the in-house cell for testing.

1.2.4 DMCABQ

DMCABQ (3.81 mg) was dissolved in 1 M KOH aqueous solution to form a dark yellow-brown solution. A sample was transferred, under inert atmosphere, to the in-house cell for testing.

1.3 Galvanostatic cycling

1.3.1 Flow cell assembly

The same setup was used as in our previous work,[6] the setup is described again here for convenience:

> “The hardware of the flow battery was purchased from Scribner Associates. Ultra-high purity and sealed graphite flow plates with serpentine flow patterns were used for both electrodes. Each electrode comprised of carbon felt (6 mm,

SGL, 5 cm^2 active area). Nafion® 212 was used as the ion transport membrane. Pre-treatment was carried out by first heating the membrane (80 C, 20 mins) in de-ionized water and then soaking it in hydrogen peroxide solution (5%, 35 mins). The treated membranes were stored in 0.1 M KOH solution at room temperature. PTFE frames with a thickness of 3 mm were used to position the electrodes with Viton gaskets of 0.7 mm in thickness on each side. The current collectors consisted of gold-plated copper sheets. Anodized aluminium end plates with ports for electrolyte input/output were also used. It was found that the aluminium coatings were easily corroded by basic solutions and therefore direct contact should be avoided. The inlet and outlet tubing were therefore carefully inserted through the Viton O-ring seals. A stock solution of 1 M KOH dissolved in D_2O was prepared and used as the solvent. Custom-made Pyrex glassware with specific connections for gas inlet and outlet, and liquid inlet and outlet were used as electrolyte reservoirs. Prior to the experiments, all solutions were degassed with N_2 gas rigorously (bubbling, 30-60 mins). The torque applied on the cell bolts was found to affect the battery performance significantly. It was therefore optimized at 2 N.m on each bolt.”

1.3.2 Potentiostat

A Biologic SP-150 potentiostat was used for all lab-scale full-cell testing.

1.3.3 In-situ NMR and EPR

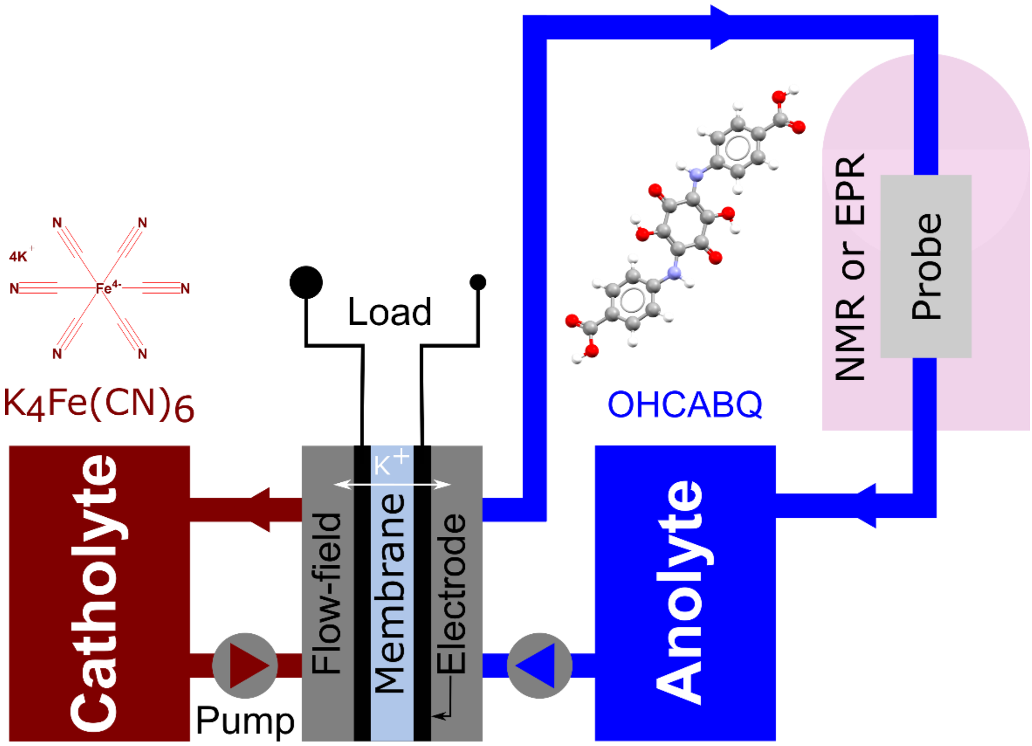

Scheme 2: Schematic of the in-situ NMR/EPR setup used for characterisation purposes.

For more experimental details, please see references 6 and 7 for further details. In general, in-situ characterisation was carried out by flowing the electrolyte solution through the cavity of either the NMR or EPR spectrometers while the battery was operated. This allowed for continuous analysis of the solution during both charge and discharge.

1.3.4 Aged electrolyte solution

Batch 2

The electrolyte solution used for the in-situ EPR measurement was left under ambient conditions in a sealed container for 18 days. After this time, the solution was then re-used for galvanostatic cycling.

1.3.5 Baked carbon paper

Preparation of the carbon electrodes

Carbon paper (5 cm^2) was baked under aerobic conditions at 400 °C for 24 hours. The sample was heated to 400 °C within an hour and then allowed to cool naturally to ambient temperature after treatment. A stack of three such samples were used as the electrodes within the flow cell.

1.4 Density Functional Theory

1.4.1 General procedure

DFT calculations with the software package Gaussian 16[8] were performed. Due to its wide and established usage for organic molecules, the hybrid functional B3LYP[9–13] was employed in combination with def2QZVP[14,15] and EPR-III[16] basis sets.
The energetics, vibrational frequencies and NMR were calculated for all species of interest. The absence of imaginary frequencies confirms that the obtained geometry corresponds to a ground state structure. The Gibbs free energy calculations allowed the conversion to redox potential and the NMR calculations allowed the direct comparison to experimental observables.
For the following structures of interest, the solvation environment was either an unsolvated gaseous environment or an aqueous solvation environment. Aqueous solvation was applied implicitly as continuous medium with certain dielectric constant (e.g., water) to the model i.e. a polarizable continuum model (PCM) was used.[17] This neglects to incorporate important interactions such as hydrogen bonding but was chosen to minimize the computational cost while retaining some spatial resolution of the solvent and provides reasonable results at the same time.

2. Additional Results

2.1 Ex-situ ^{1}H NMR

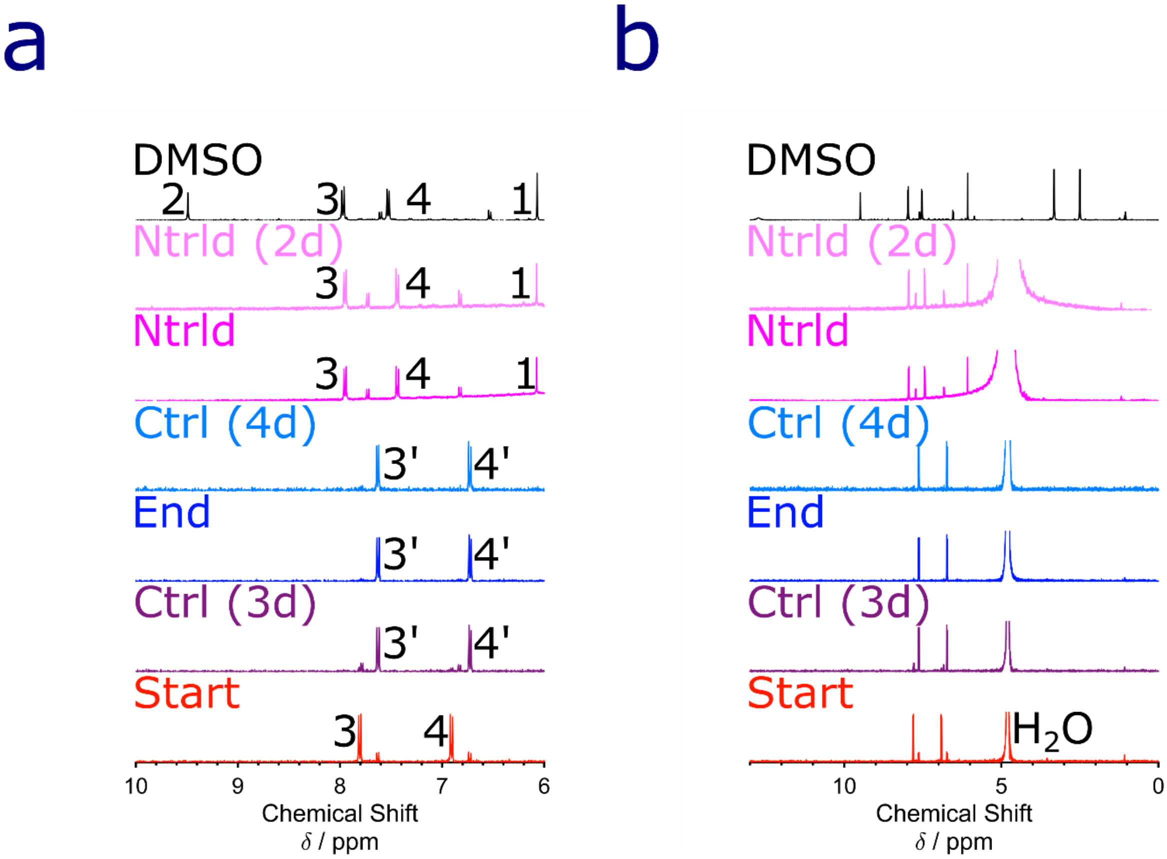

Figure S 10: **(a)** Zoomed in ^{1}H NMR (400.13 MHz) spectra of CABQ under different conditions, from **bottom-to-top:** NMR taken in 1 M KOH/D_2O at the start of CV cycling, NMR taken of the CV control sample in 1 M KOH/D_2O after 3 days, NMR taken in 1 M KOH/D_2O at the end of CV cycling, NMR taken of the CV control sample in 1 M KOH/D_2O after 4 days when the CV cycling finished, NMR taken of CABQ which was first neutralised (Ntrld) with a stoichiometric amount of 1 M KOH before being diluted with D_2O, NMR taken of CABQ neutralised with stoichiometric KOH after 2 days, NMR of the as-synthesised CABQ dissolved in DMSO. **(b)** full-range ^{1}H NMR (400.13 MHz) spectra of CABQ under the previously described conditions. From **bottom-to-top**, the order is the same as in (a).

2.2 Diffusion Ordered NMR (DOSY) Spectra

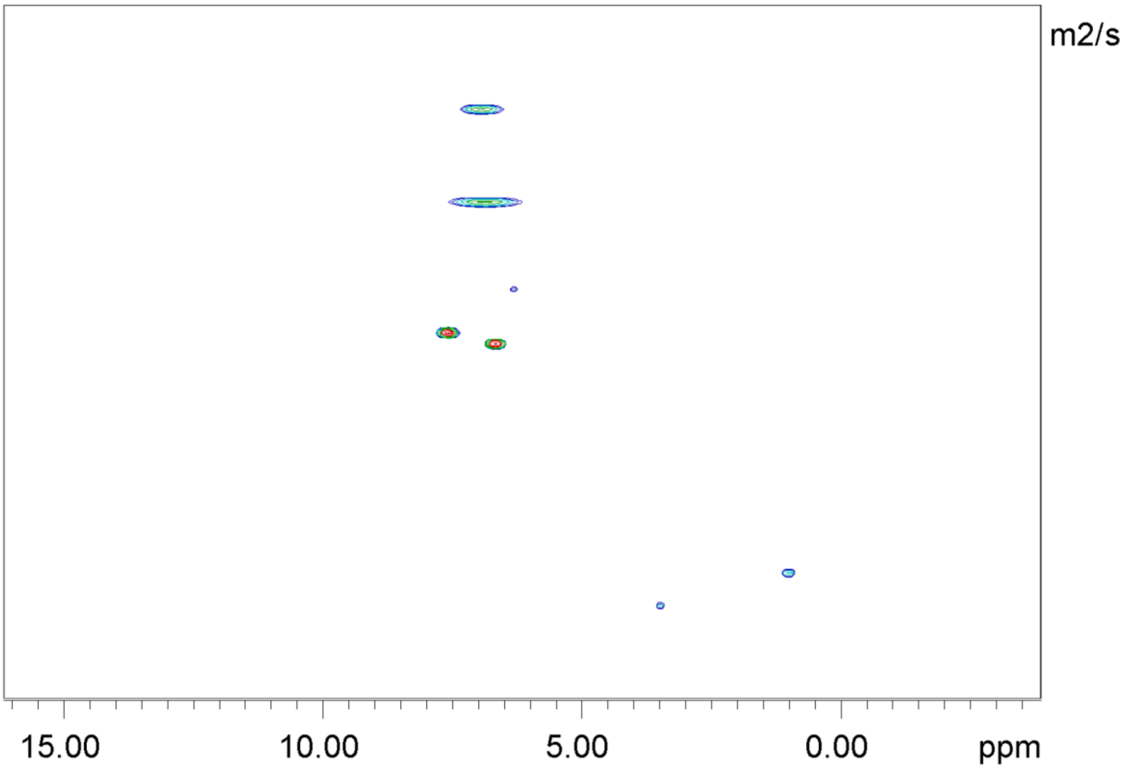

Fitted function:	f (x) = Io * exp (-D * x^2 * gamma^2 * littleDelta^2 (bigDelta-littleDelta/3)* 10^4
used gamma:	26752 rad/(s*Gauss)
used little delta:	0.0016000 s
used big delta:	0.099900 s
used gradient strength:	variable
Random error estimation of data:	RMS per spectrum (or trace/plane)
Systematic error estimation of data:	worst case per peak scenario
Fit parameter Error estimation method:	from Monte Carlo simulations
Confidence level:	95%
Used peaks:	automatically picked peaks
Used integrals:	area integral
Used Gradient strength:	all values (including replicates) used

Peak name	F2 [ppm]	Io	error	D [m2/s]	error
44	7.581	1.11e+09	7.171e+04	5.55e-10	6.542e-14
45	6.663	1.17e+09	7.077e+04	5.70e-10	6.137e-14
46	6.932	9.58e+07	8.483e+04	3.62e-10	6.934e-13
47	6.858	9.75e+07	8.592e+04	4.35e-10	7.599e-13
48	6.302	2.44e+07	7.341e+04	5.14e-10	2.930e-12
49	3.494	3.43e+07	1.194e+05	9.37e-10	5.358e-12
50	1.028	5.25e+07	1.094e+05	8.80e-10	3.099e-12

Figure S 11: DOSY ^{1}H NMR focusing on the integrals of the respective peaks.

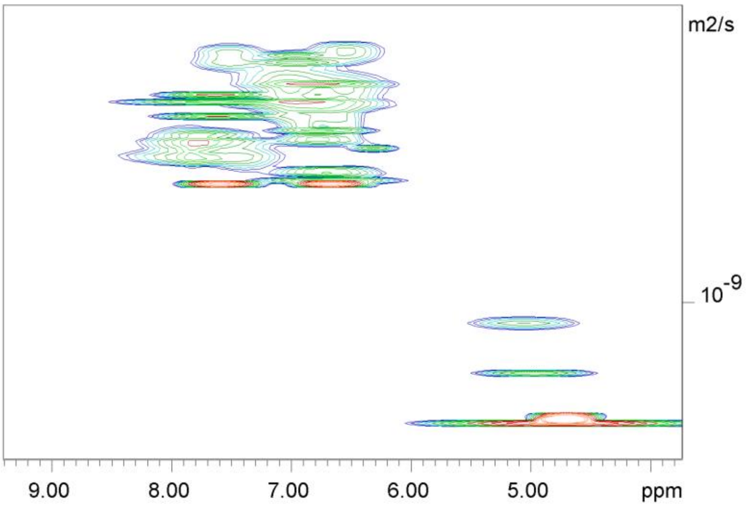

Fitted function:	f (x) = Io * exp (-D * x^2 * gamma^2 * littleDelta^2 (bigDelta-littleDelta/3)* 10^4
used gamma:	26752 rad/(s*Gauss)
used little delta:	0.0016000 s
used big delta:	0.099900 s
used gradient strength:	variable
Random error estimation of data:	RMS per spectrum (or trace/plane)
Systematic error estimation of data:	worst case per peak scenario
Fit parameter Error estimation method:	from Monte Carlo simulations
Confidence level:	95%
Used peaks:	automatically picked peaks
Used integrals:	peak intensities
Used Gradient strength:	all values (including replicates) used

Peak name	F2 [ppm]	Io	error	D [m2/s]	error
1	7.789	6.54e+05	8028	5.04e-10	1.144e-11
2	7.771	7.66e+05	7712	5.10e-10	1.022e-11
3	7.756	6.58e+05	7276	4.82e-10	1.030e-11
4	7.735	6.95e+05	7838	4.75e-10	1.023e-11
5	7.718	7.63e+05	7304	4.74e-10	9.151e-12
6	7.675	1.11e+06	7696	4.71e-10	6.164e-12
7	7.652	2.21e+06	7470	3.91e-10	2.820e-12
8	7.630	3.61e+06	7459	3.76e-10	1.629e-12
9	7.609	3.00e+06	7322	4.18e-10	2.104e-12
10	7.594	3.16e+07	8134	5.73e-10	2.698e-13
11	7.572	3.15e+07	8145	5.76e-10	2.601e-13
12	7.530	7.13e+05	7376	3.24e-10	8.397e-12
13	7.509	6.79e+05	7643	3.08e-10	8.505e-12
14	6.980	4.77e+05	7673	3.52e-10	1.306e-11
15	6.974	5.17e+05	7367	3.69e-10	1.220e-11
16	6.953	1.50e+06	7011	3.16e-10	3.740e-12
17	6.932	1.50e+06	7043	3.27e-10	3.688e-12
18	6.905	6.73e+05	7812	4.19e-10	1.033e-11
19	6.896	5.45e+05	7559	4.41e-10	1.229e-11
20	6.878	1.34e+06	7365	3.90e-10	4.648e-12
21	6.857	1.39e+06	7618	3.96e-10	4.706e-12
22	6.817	1.22e+06	7555	3.91e-10	5.020e-12
23	6.796	1.30e+06	7582	4.04e-10	4.822e-12
24	6.778	1.10e+06	7845	4.72e-10	6.620e-12
25	6.762	2.56e+06	7343	3.62e-10	2.383e-12
26	6.739	1.85e+06	7887	4.45e-10	3.667e-12
27	6.717	1.72e+06	8021	5.43e-10	4.389e-12
28	6.701	2.19e+06	8660	5.63e-10	3.881e-12
29	6.678	3.58e+07	8077	5.79e-10	2.446e-13
30	6.657	3.28e+07	8006	5.79e-10	2.584e-13

Figure S 12: DOSY ^{1}H NMR focussing on the chemical shift of the peaks.

Integrals: 5.55E-10 m^2s^{-1}
Peaks: 3.24E-10 m^2s^{-1}
From this, if taken with the CV data from 2.11 (Figure S 26), the number of electrons for the redox reaction can be back-calculated from the Randles-Sevcik equation. The derived values for the number of electrons being effectively transferred are as follows:
Integrals:

Peaks: 0.9024
Troughs: 1.3223
Peaks:
Peaks: 1.0797
Troughs: 1.5822

2.3 Solubility Tests and Colour Changes

Figure S 13: Picture of a rudimentary solubility test carried out on CABQ in which a micro-spatula full of samples was added to 2 ml of solvent, swirled, and then left to stand. The solvents from left to right are as follows: nitro-ethane, acetonitrile, dichloromethane, acetone, tetrahydrofuran, water, ethanol, ethyl acetate.

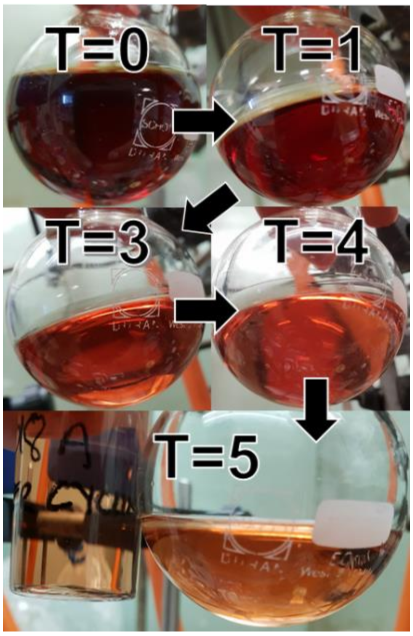

Figure S 14: Images of the solution of CABQ in 1 M KOH/D_2O over the course of 5 days (T = X refers to the time, X, in days in total which has passed). The solution gets gradually lighter as time progresses implying a chemical change. The bottom picture also includes a comparison of the non-cycled sample (right, round-bottomed flask) to the cycled sample (left, vial).

2.4 In-situ – Charge resting

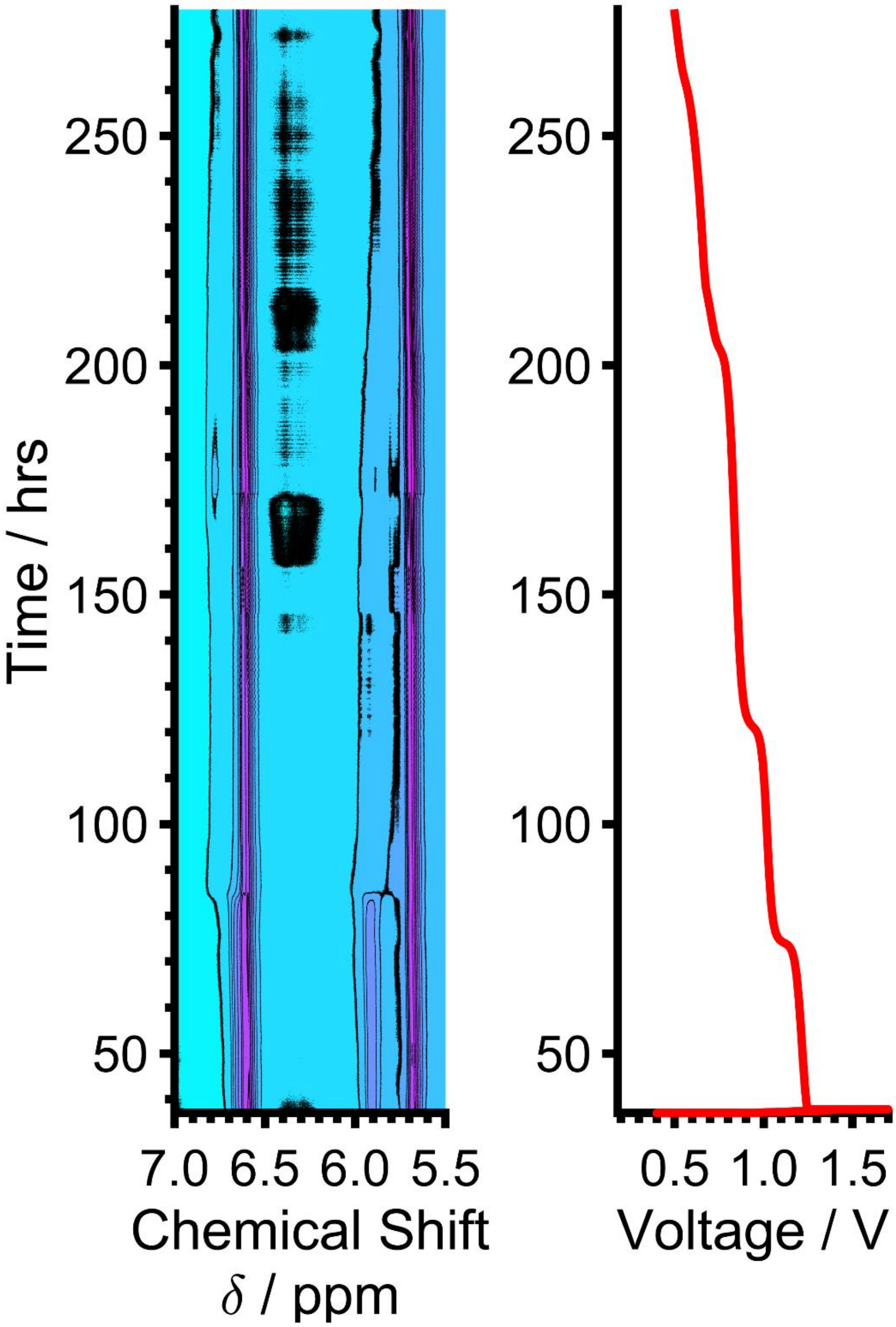

Figure S 15: (**Left**) In-situ ^{1}H NMR (300.13 MHz) of CABQ (Batch 2) taken after cycling and re-charging of the solution. (**Right**) The corresponding galvanostatic cycling data.

2.5 CV of Batch 1 sample

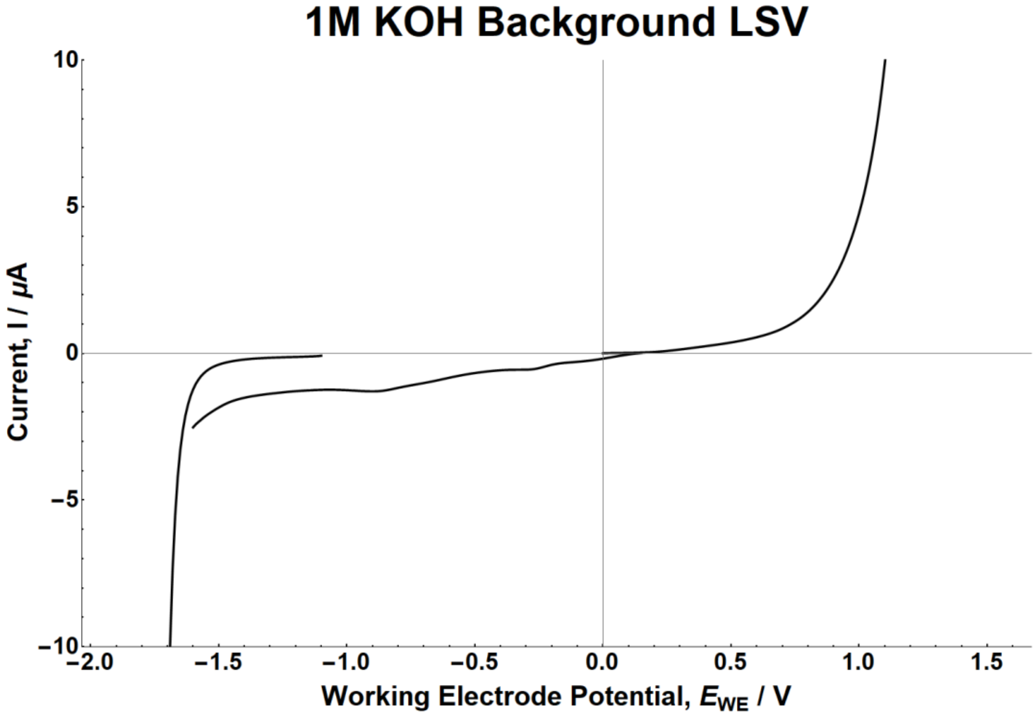

Figure S 16: Background voltammogram (linear scan) of the supporting electrolyte solution used during the CV experiment. No significant redox active impurities appear to be present within the electrochemical window.

2.6 CV peak current vs cycle number fitted variables

The reaction presented in Scheme 2 takes the form of a pseudo $A \overset{k_a}{\rightarrow} B \overset{k_b}{\rightarrow} C$ type reaction due to the large excess of hydroxide ions present in the system if one assumes that any electron transfers are faster than any chemical reactions, where A = CABHQ/CABQ, B = I1/I2 and C = OHCABHQ/OHCABQ. It would therefore be expected that the concentrations of the various species conform to the equations:[18]

$$[A] = [A]_0 \exp(-k_a t) \tag{1}$$

$$[B] = \frac{k_a [A]_0}{k_b - k_a} (\exp(-k_a t) - \exp(-k_b t)) \tag{2}$$

$$[C] = [A]_0 \left(1 + \frac{k_a \exp(-k_b t) - k_b \exp(-k_a t)}{k_b - k_a}\right) \tag{3}$$

Based on these equations and the qualitative peak currents extracted from the CV data (Figure 1), we were able to model the current vs. cycle number graphs shown in Figure 2b (see Table S1, S2 and S3). This allowed for an estimate of the rate constants for the reactions. From averaging across both the oxidative and reductive fitting A_o was determined to be (7 ± 3) x 10^{11} molecules, k_a was estimated to be 7.0 ± 1.6 x10^{-6} s^{-1} and k_b was estimated to be 3.1 ± 0.3 x10^{-5} s^{-1}. The rates are of a similar magnitude, but it appears that k_b i.e., the constant corresponding to the reaction of I1/I2 to OHCABHQ/OHCABQ, is slightly larger than k_a. However, it must be noted that extracting peak currents from cyclic voltammograms is imprecise due to the uncertainty in correcting for the charging current. This is increased on the reverse wave and so CV experiments do not tend to be the ideal method for quantitative analysis based on peak heights e.g. concentrations or rate constants.[19] Therefore, these values are presented as a ball-park estimate only.

The oxidative and reductive waves for α were fit to the form $a\exp(bx)$. β was fit to the form $(a\exp(bx) + \mathrm{c}\exp(dx))$ and γ was fit to the form $a(1 + \frac{b\exp(-cx) - c\exp(-bx)}{c-b})$. The error in the fitting of γ was found to be more difficult than the fitting of α and β and therefore there is a greater inherent error in the coefficients found therein.

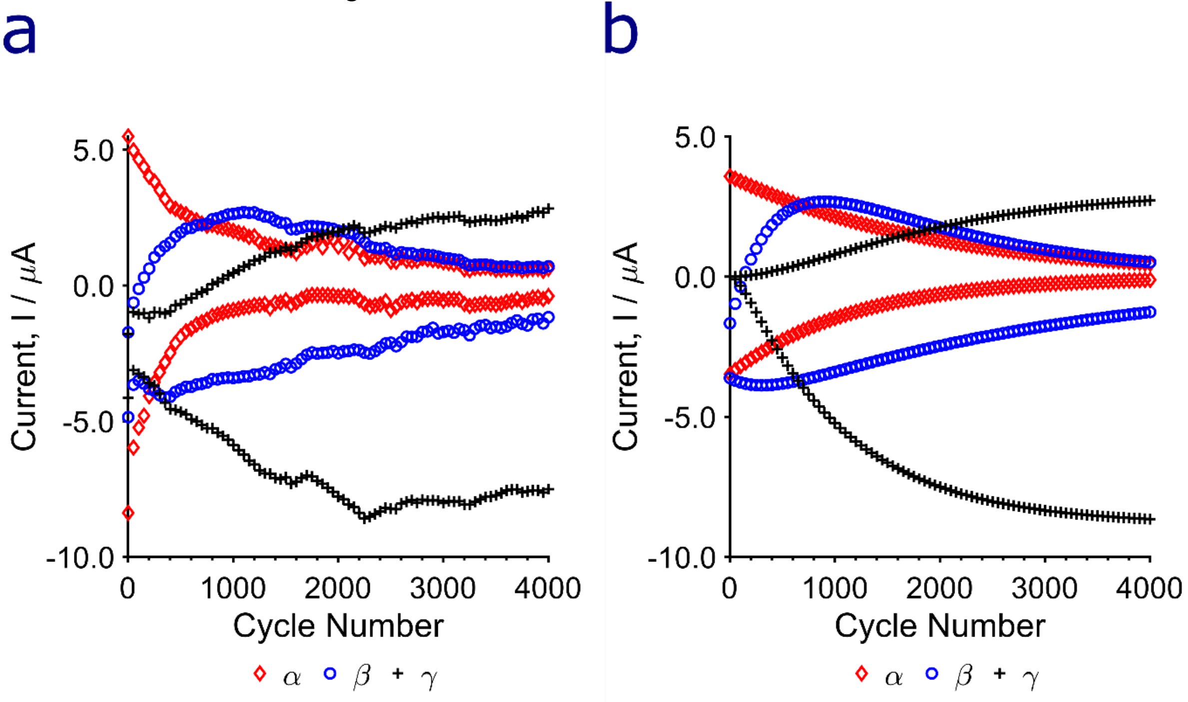

Figure S 17: **(a)** The peak current as a function of cycle number for processes **α**, **β**, and **γ**, shown by the red, blue, and black markers, respectively. **(b)** Plots of the exponential fits applied to the peak current versus cycle number data.

Table S 1: Values of the constants calculated by the fitting functions derived from peak current vs cycle number (shown in Figure S 17.b) to the raw peak currents extracted from the long-term cyclic voltammetry experiment shown in Figure 1.

Variables / 10^{-6}		*a*	*b*	*c*	*d*
Oxidation	α	3.582	-5.093×10^{2}		
	β	6.467	-6.317×10^{2}	-8.146	-2.348×10^{3}
	γ	2.993	9.909×10^{2}	1.003×10^{3}	
Reduction	α	3.482	-8.546×10^{2}		
	β	4.838	-3.360×10^{2}	-1.225	-2.993×10^{3}
	γ	8.826	1.000×10^{4}	1.000×10^{3}	

$A_0 = 4.7 \pm 1.4\ \mu A$; $A_{0,o} = 3.3 \pm 0.3\ \mu A$, $A_{0,r} = 6 \pm 3\ \mu A$

$k_a = (2.2 \pm 1.6) \times 10^{-3}\ \mathrm{cycle}^{-1}$; $k_{a,o} = (7.1 \pm 1.4) \times 10^{-4}\ \mathrm{cycle}^{-1}$, $k_{a,r} = (4 \pm 3) \times 10^{-3}\ \mathrm{cycle}^{-1}$

k_b = (1.8 ± 0.5) x 10^{-3} cycle^{-1}; $k_{b,o}$ = (1.7 ± 0.7) x 10^{-4} cycle^{-1}; $k_{b,r}$ = (2 ± 1) x 10^{-3} cycle^{-1}

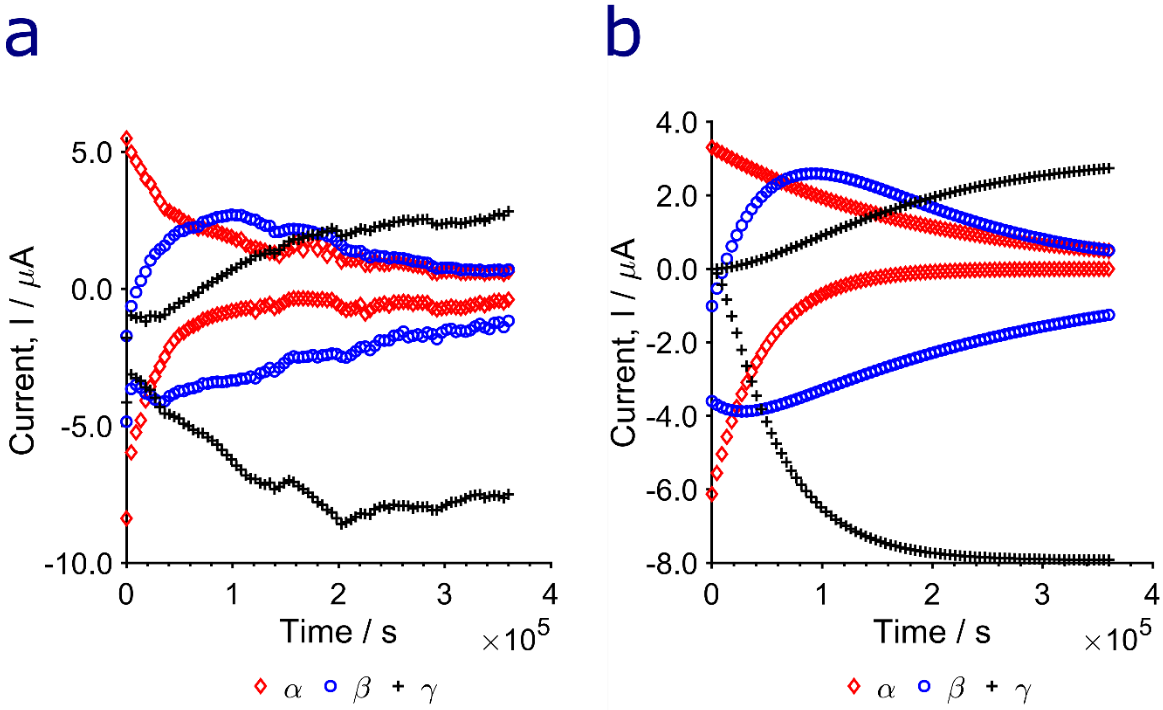

Figure S 18: **(a)** The peak current as a function of time for processes **α**, **β**, and **γ**, shown by the red, blue, and black markers, respectively. **(b)** Plots of the exponential fits applied to the peak current versus time.

Table S 2: Values of the constants calculated by the fitting functions derived from peak current vs time (shown in Figure S 18.b) to the raw peak currents extracted from the long-term cyclic voltammetry experiment shown in Figure 1.

Variables / 10^{-6}		*a*	*b*	*c*	*d*
Oxidation	α	3.305	-5.309		
	β	1.219 x 10^1	-8.659	-1.321 x 10^1	-1.646 x 10^1
	γ	3.034	1.084 x 10^1	1.095 x 10^1	
Reduction	α	6.218	-2.173 x 10^1		
	β	4.868	-3.773	-1.271	-3.313 x 10^1
	γ	7.927	9.600 x 10^1	1.948 x 10^1	

A_0 = 5.1 ± 1.2 μA; $A_{0,o}$ = 3.17 ± 0.14 μA, $A_{0,r}$ = 7.0 ± 0.9 μA
k_a = (2.4 ± 1.5) x 10^{-5} s^{-1}; $k_{a,o}$ = (8.3 ± 1.6) x 10^{-6} s^{-1}, $k_{a,r}$ = (4 ± 3) x 10^{-5} s^{-1}
k_b = (2.0 ± 0.5) x 10^{-5} s^{-1}; $k_{b,o}$ = (1.4 ± 0.3) x 10^{-5} s^{-1}; $k_{b,r}$ = (2.6 ± 0.7) x 10^{-5} s^{-1}

Using the current value estimated for A_0, the number of molecules being sampled can be estimated as follows:

$$No.of\ molecules = \frac{A_0 * t_p}{n * q_e}$$

Where *A_0 = the starting current, t_p = time interval between data points, n = no. electrons transferred per molecule, q_e = elementary charge of an electron.* Following this, an estimate for the number of molecules of (8 ± 3) x 10^{11} was found.

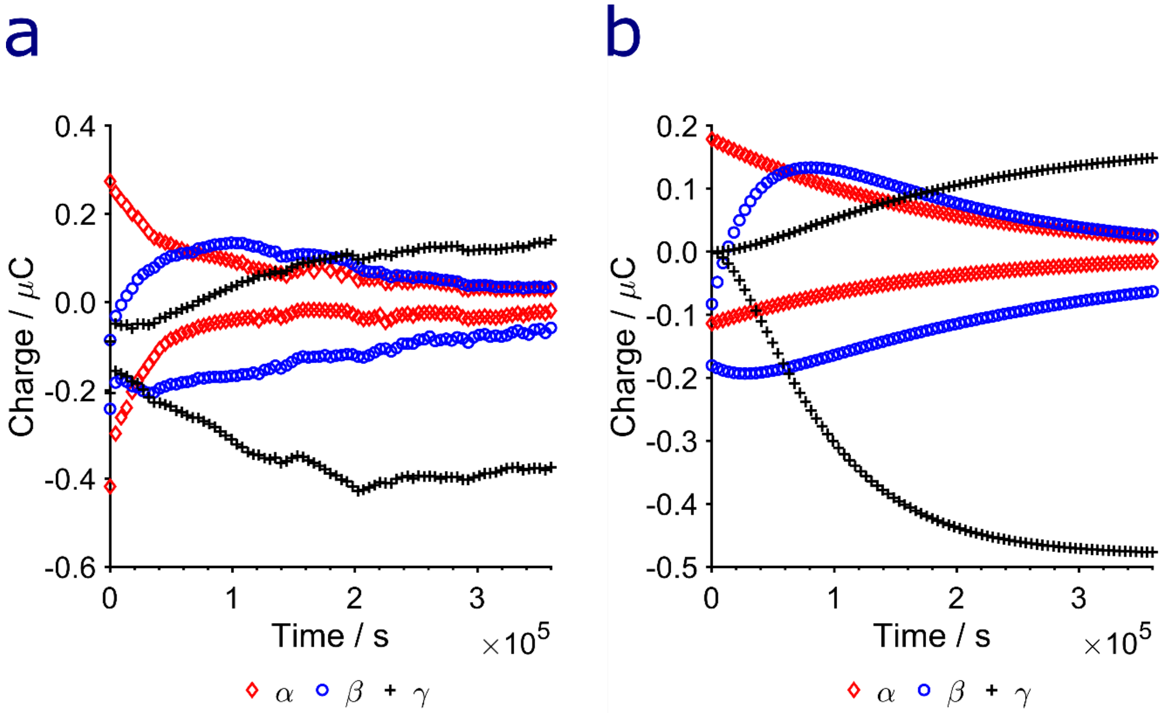

Figure S 19: **(a)** The estimated charge as a function of time for processes **α**, **β**, and **γ**, shown by the red, blue, and black markers, respectively. **(b)** Plots of the exponential fits applied to the estimated charge versus time.

Table S 3: Values of the constants calculated by the fitting functions derived from peak current vs time (shown in Figure S 18.b) to the raw peak currents extracted from the long-term cyclic voltammetry experiment shown in Figure 1.

Variables / 10^{-7}		*a*	*b*	*c*	*d*
Oxidation	α	1.787	-5.661×10^{1}		
	β	3.226	-7.02×10^{1}	-4.061	-2.608×10^{2}
	γ	1.787	5.661×10^{1}	2.608×10^{2}	
Reduction	α	1.139	-5.573×10^{1}		
	β	2.414	-3.735×10^{1}	-6.107×10^{-1}	-3.325×10^{2}
	γ	4.812	1.449×10^{2}	3.679×10^{2}	

$A_0 = 0.24 \pm 0.08$ μC; $A_{0,o} = 0.2 \pm 0.2^*$ μC, $A_{0,r} = 0.3 \pm 0.2$ μC
$k_a = (7.0 \pm 1.6) \times 10^{-6}\ s^{-1}$; $k_{a,o} = (6.1 \pm 0.5) \times 10^{-6}\ s^{-1}$, $k_{a,r} = (8 \pm 4) \times 10^{-6}\ s^{-1}$
$k_b = (3.1 \pm 0.3) \times 10^{-5}\ s^{-1}$; $k_{b,o} = (2.6 \pm 0.3^*) \times 10^{-5}\ s^{-1}$; $k_{b,r} = (3.50 \pm 0.18) \times 10^{-5}\ s^{-1}$
*Standard deviation and therefore standard error between the values was 0. Realistically, error is likely to be greater than this, so the greatest calculated standard error was applied.

Using the charge estimated for A_0, the number of molecules being sampled can be estimated as follows:

$$No.of\ molecules = \frac{A_0}{n * q_e}$$

Where *A_0 = the starting peak current, t_p = time interval between data points, n = no. electrons transferred per molecule, q_e = elementary charge of an electron.* Following this, an estimate for the number of molecules of $(7 \pm 3) \times 10^{11}$ was found.

2.7 CV of potassium salt in potassium chloride solution

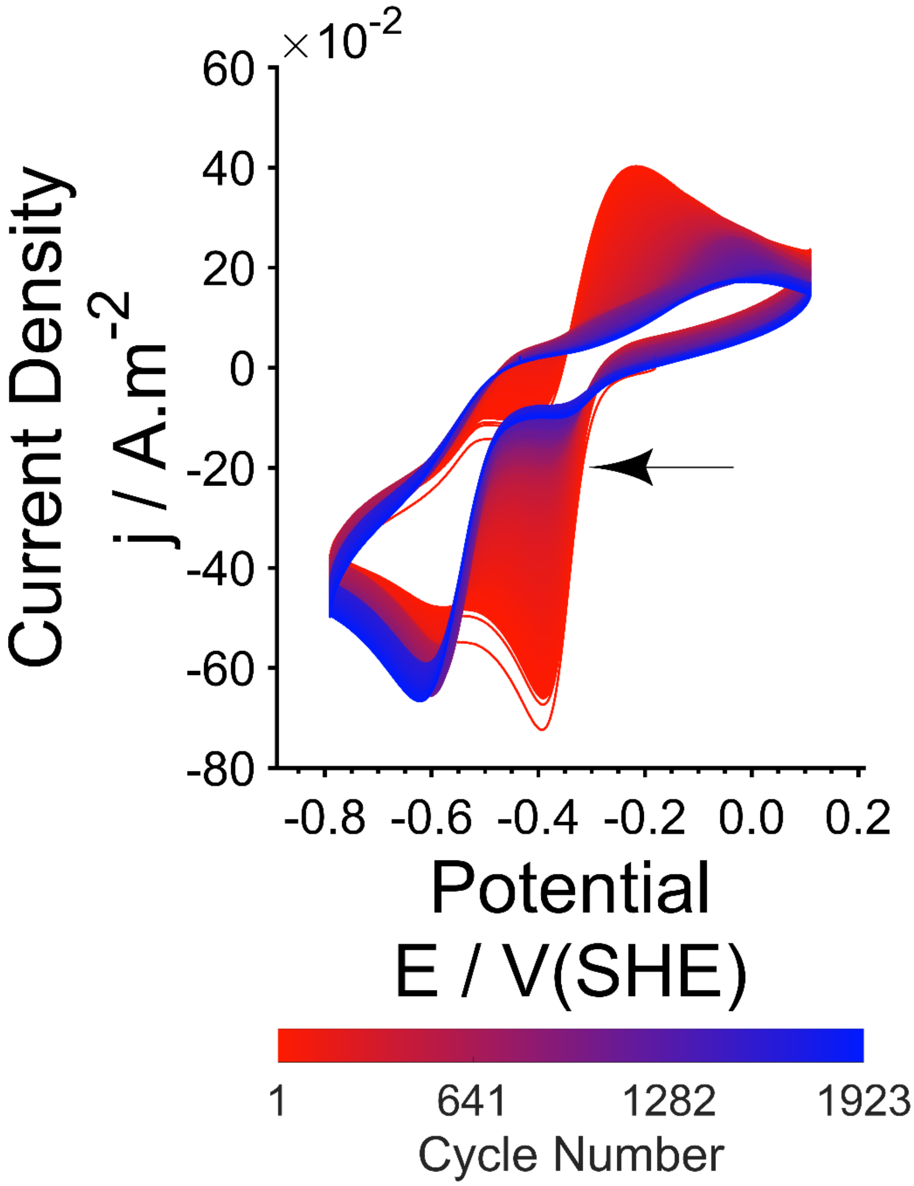

Figure S 20: Cyclic voltammograms corresponding to a long-term CV experiment carried out on 1 mM of the potassium-salt of CABQ. The voltage was scanned at 20 mVs^{-1}, scanning to negative potentials first. The supporting electrolyte was KCl at a concentration of 100 mM in water. The experiment was carried out at ambient temperature.

2.8 CV of Batch 1 purified sample

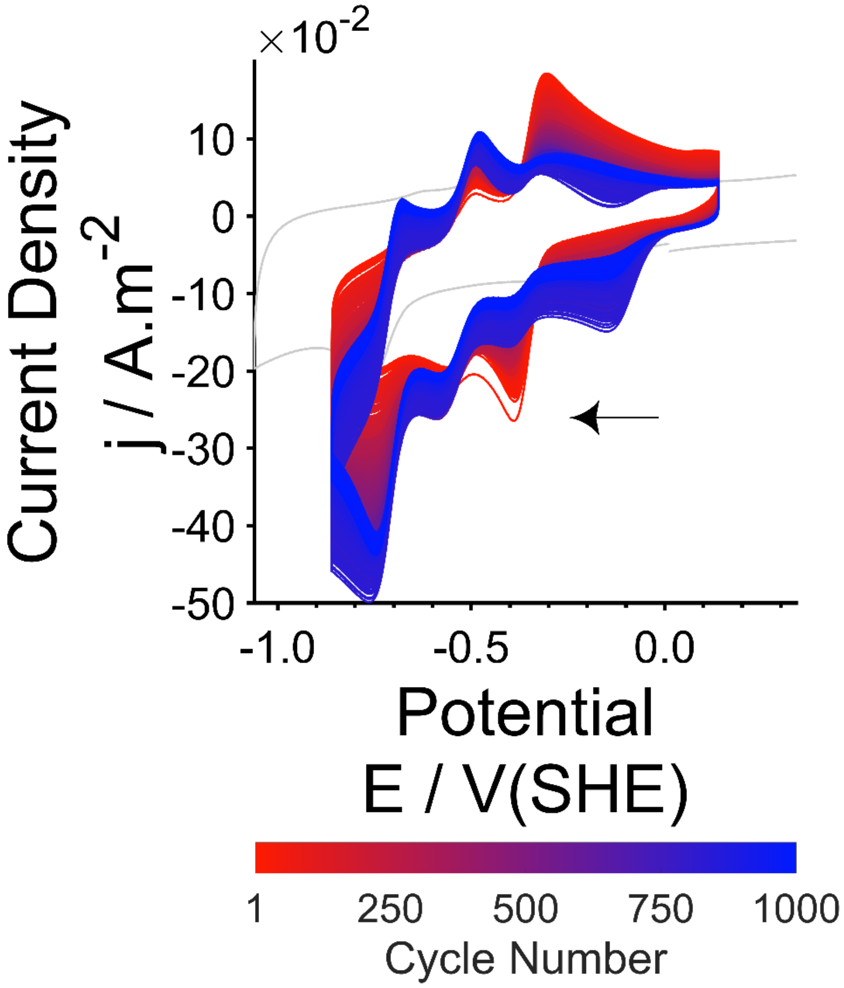

Figure S 21: Cyclic voltammograms of purified 1 mM CABQ dissolved in 1 M KOH/H_2O. The experiment was run at ambient temperature using a 3mm diameter glassy carbon working electrode, a mercury-mercury oxide (1 M KOH) reference electrode and coiled platinum wire as the counter electrode. The scan rate was 20 mVs^{-1}, scanning towards negative potentials first. The background CV is shown behind in gray.

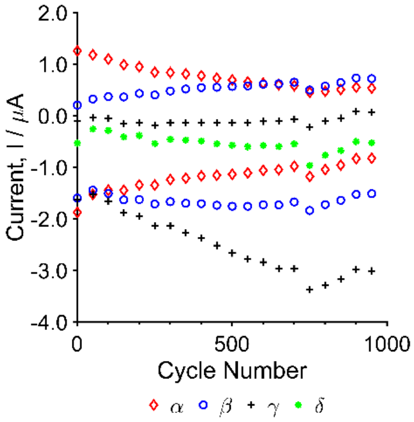

Figure S 22: The change in peak current with cycle number for processes a, b, c, and d which correspond to the red, blue, black and green markers respectively.

2.9 CV of Batch 3 – NEt_3

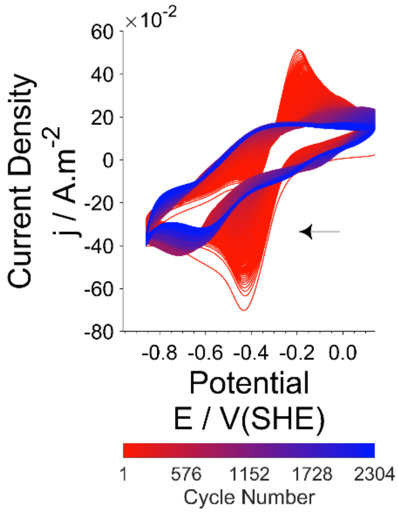

Figure S 23: Cyclic voltammograms of 1 mM CABQ deprotonated initially with NEt_3 before being dissolved in 1 M KCl/H_2O solution. The scan rate was 20 mVs^{-1}, scanning to negative potentials first. The experiment was carried out at ambient temperature against a Ag/AgCl (3 M KCl) reference electrode.

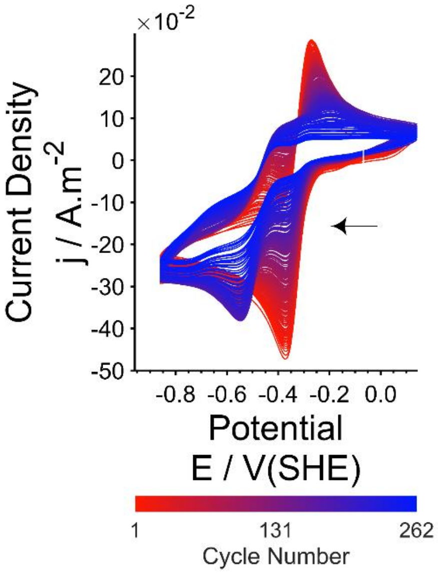

Figure S 24: Cyclic voltammograms of CABQ deprotonated initially with NEt_3 before being dissolved in 1 M KCl solution. The scan rate was 5 mVs^{-1}, scanning to negative potentials first. The experiment was carried out at ambient temperature against a Ag/AgCl (3 M KCl) reference electrode.

2.10 CV of Batch 3 (Aged)

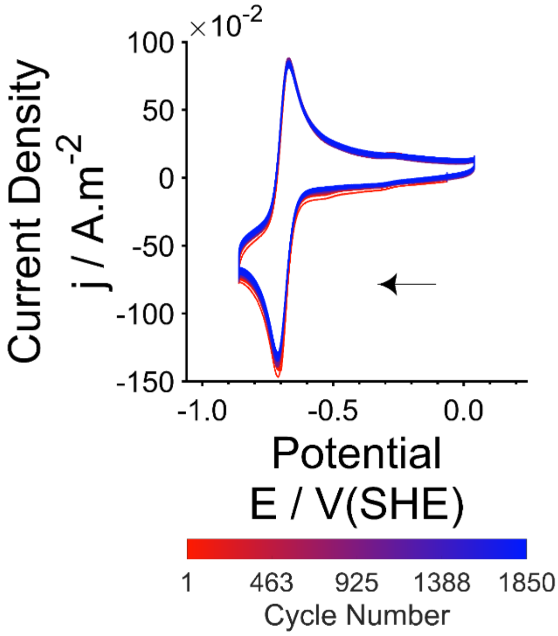

Figure S 25: Cyclic voltammograms of 1 mM CABQ (Batch 3) dissolved and aged in 1 M KOH/H_2O. The experiment was run at 298 K using a 3mm diameter glassy carbon working electrode, a mercury-mercury oxide (1 M KOH) reference electrode and coiled platinum wire as the counter electrode. The scan rate was 20 mVs^{-1}, scanning towards negative potentials first.

2.11 Randles-Sevcik Analysis (Aged)

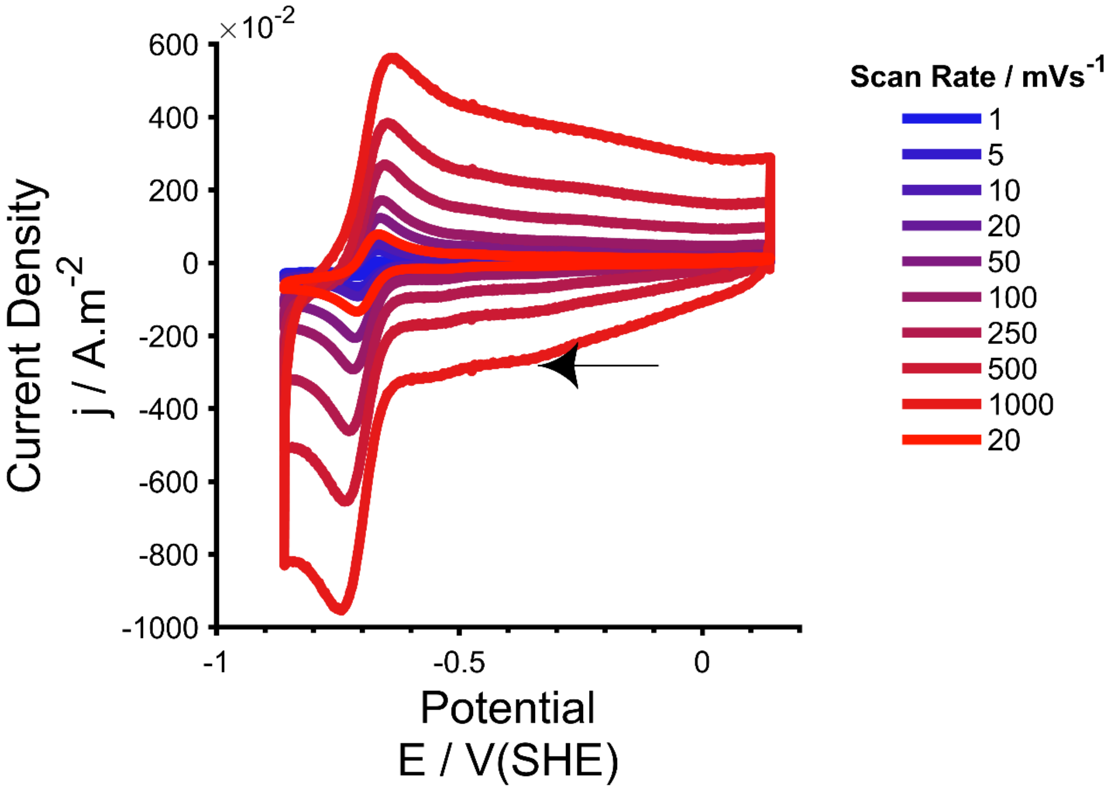

Figure S 26: Cyclic voltammograms of an aged 1 mM sample of CABQ (Batch 3) taken at different scan rates (1 to 100 mVs^{-1}) in 1 M KOH/H_2O solution at 298 K.

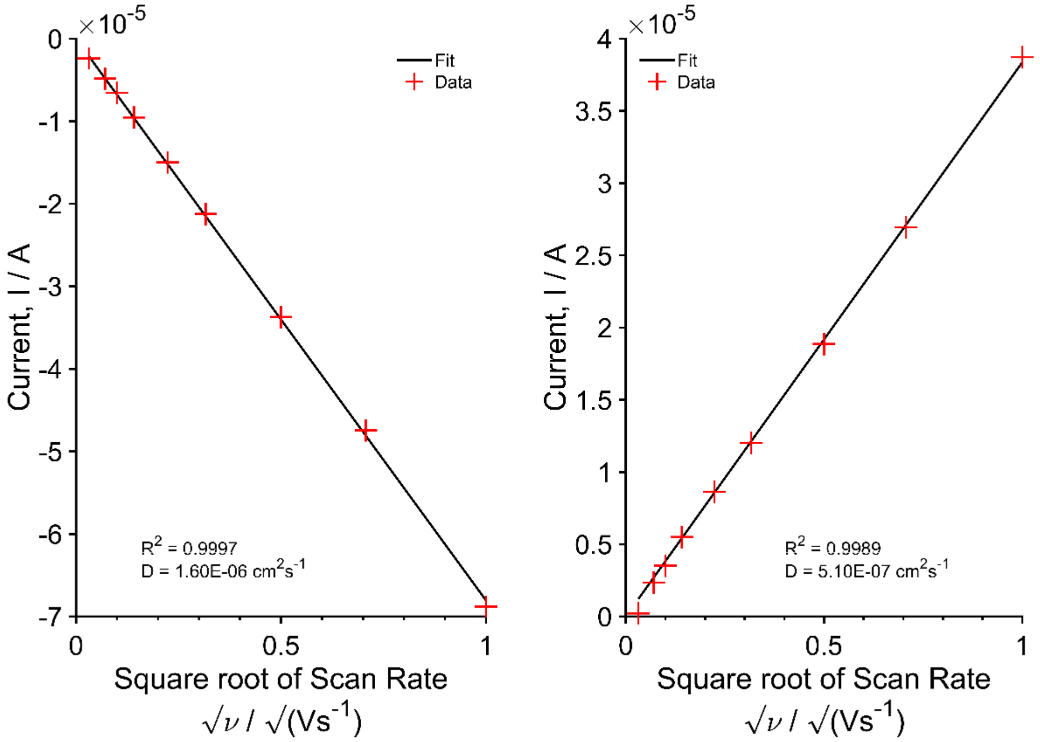

Figure S 27: Plots and linear regressions of peak current versus the square root of scan rate for (left) the cathodic and (right) anodic processes for an aged 1 mM sample of CABQ (Batch 3) taken at different scan rates (1 to 100 mVs^{-1}) in 1 M KOH/H_2O solution at 298 K.

2.12 Crude vs Pure

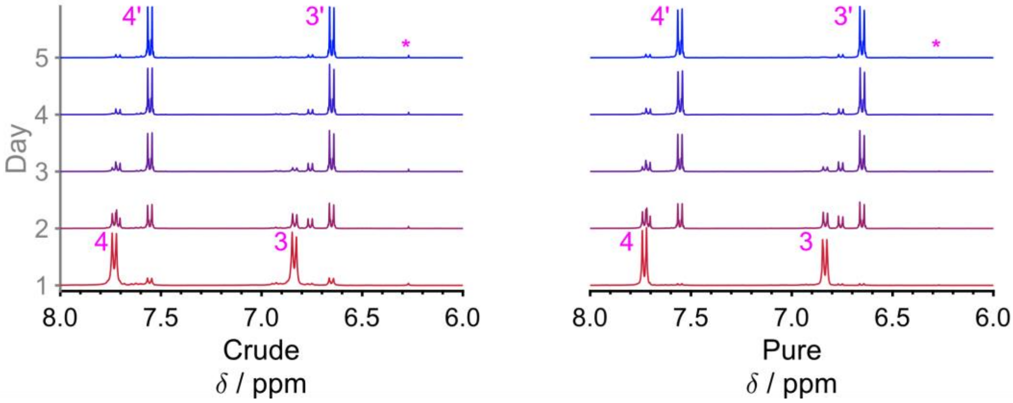

Figure S 28: Ex-situ ^{1}H NMR (400.13 MHz) of a 10 mM CABQ (Crude on the left, Pure on the right) solution in 1 M KOH/D_2O. The sample was kept in a sealed J Young's NMR Tube and NMR was recorded daily for the purpose of tracking the conjugate addition reaction.

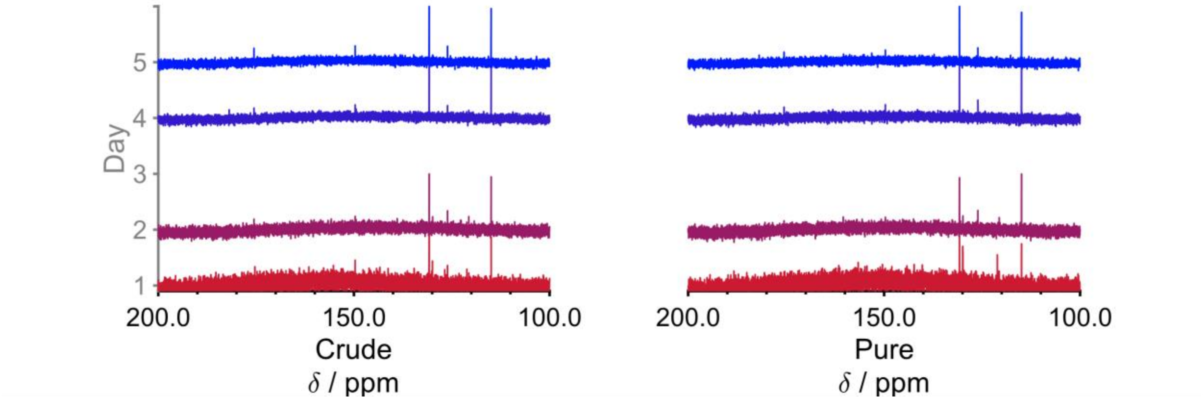

Figure S 29: Ex-situ ^{13}C NMR (100.61 MHz) of a 10 mM CABQ (Crude on the left, Pure on the right) solution in 1 M KOH/D_2O. The sample was kept in a sealed J Young's NMR Tube and NMR was recorded daily for the purpose of tracking the conjugate addition reaction.

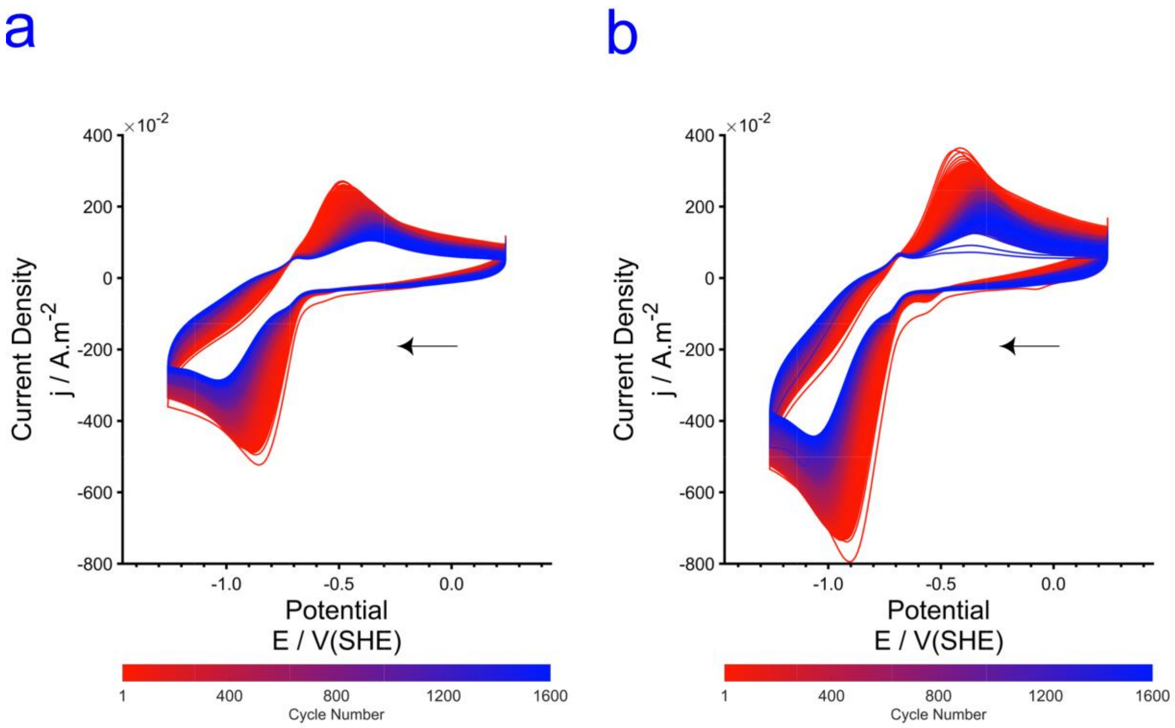

Figure S 30: Cyclic voltammograms of 10 mM CABQ dissolved in 1 M KOH/D_2O (**(a)** crude, **(b)** pure). The experiment was run at 298 K using a 3mm diameter glassy carbon working electrode, a mercury-mercury oxide (1 M KOH) reference electrode and coiled platinum wire as the counter electrode. The scan rate was 20 mVs^{-1}, scanning towards negative potentials first (as indicated by the arrow).

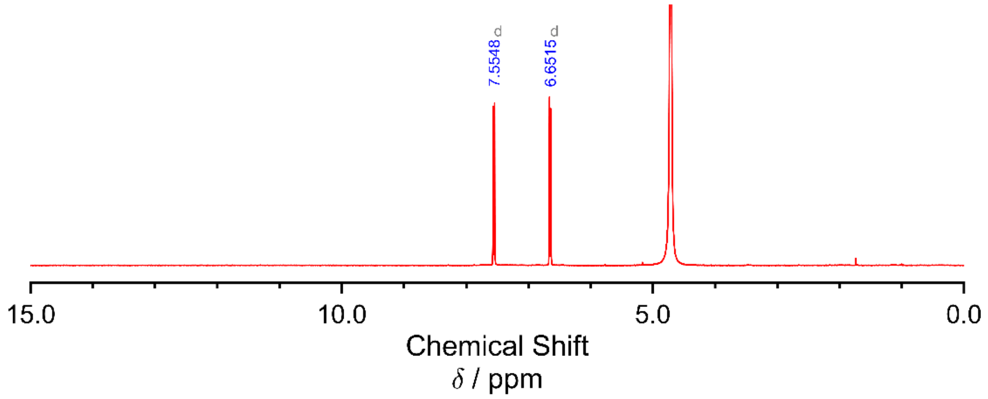

Figure S 31: Ex-situ ^{1}H NMR (400.13 MHz) of a 10 mM pure CABQ solution in 1 M KOH/D_2O taken after CV characterisation.

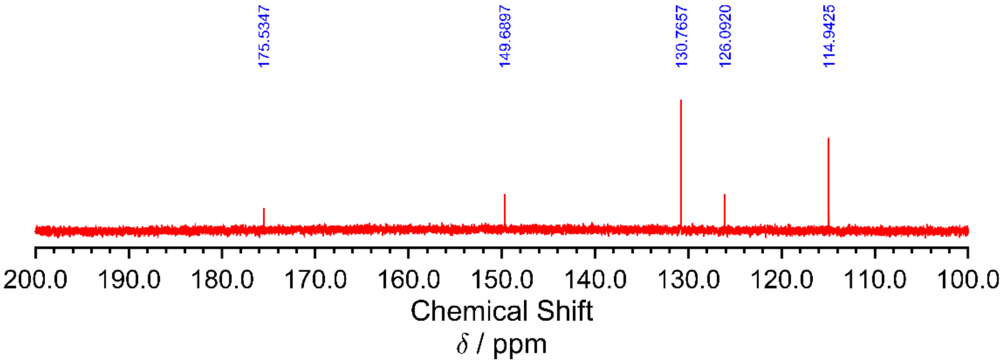

Figure S 32: Ex-situ ^{13}C NMR (100.61 MHz) of a 10 mM pure CABQ solution in 1 M KOH/D_2O taken after CV characterisation.

2.13 GC (In situ NMR) – Carbon felt – NAFION 212

CABQ (0.950 g, mass required for 100 mM) was dissolved in 1 M KOH/D_2O (25.11 ml) to make up the anolyte suspension. Due to the saturation point for CABQ being around 0.066 M, the excess material would settle on standing overnight but under agitation, a suspension would be formed. Potassium ferrocyanide (3.289 g) was dissolved in 2 M KOH/D_2O (26 ml) followed by a further dilution with D_2O (26 ml). This was combined with a previous 150 mM solution (3.252 g dissolved in 51.33 ml 1 M KOH/D_2O) to form the catholyte solution. 25 ml of anolyte suspension was used against 50 ml of catholyte solution. The flow battery was pumped at 15 ml.min^{-1} (60 rpm).

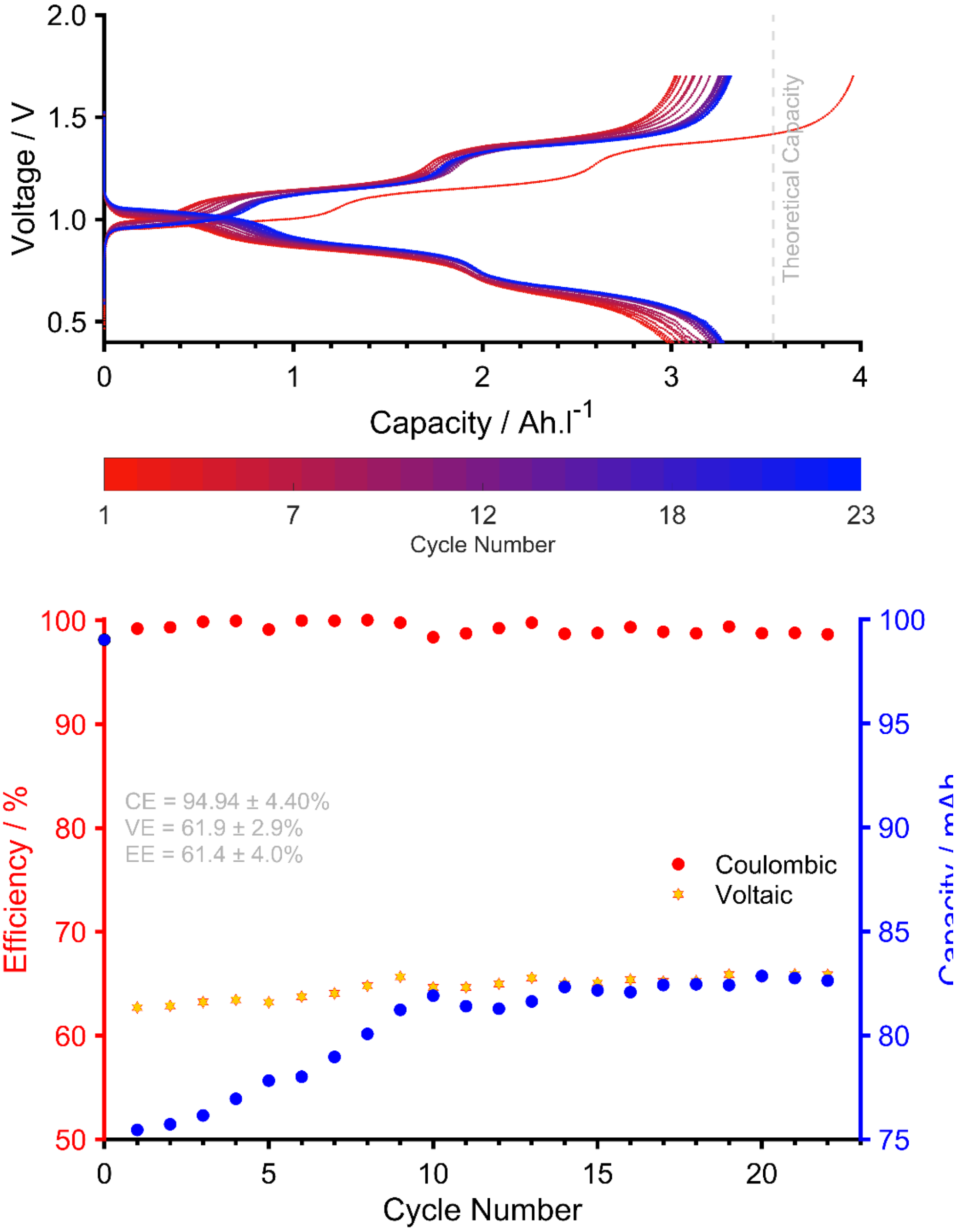

Figure S 33: Galvanostatic cycling data corresponding to the In-situ NMR experiment where 25 ml of 0.066 M CABQ dissolved in 1 M KOH/D_2O solution was cycled against 50 ml of 0.15 M $K_4Fe(CN)_6$ dissolved in 1 M KOH/D_2O solution. The flow battery was charged and discharged at 100 mA with a flow rate of 15 ml.min^{-1}.

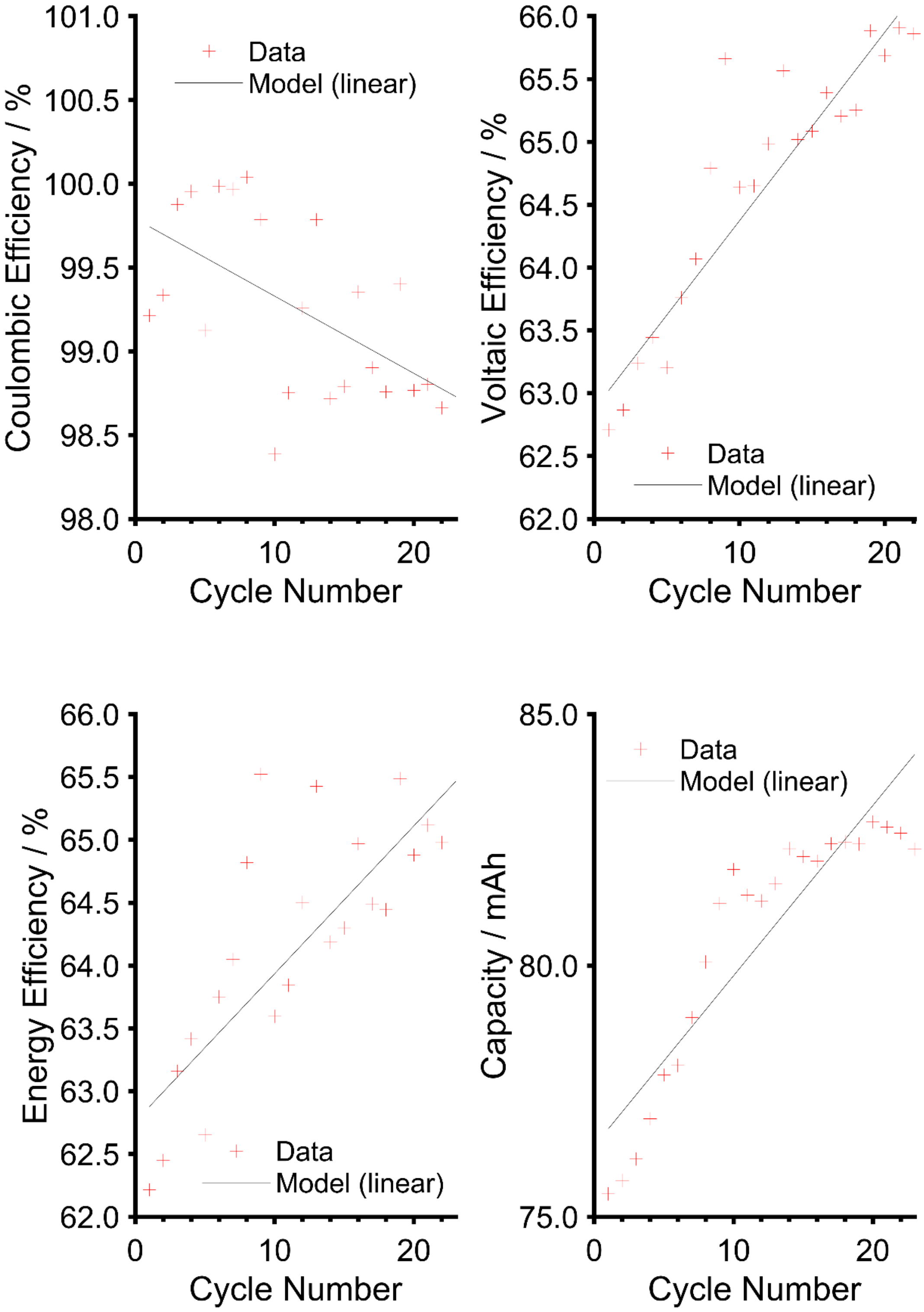

Figure S 34: Linear regression applied to the efficiencies and capacities of the in-situ NMR GC data.

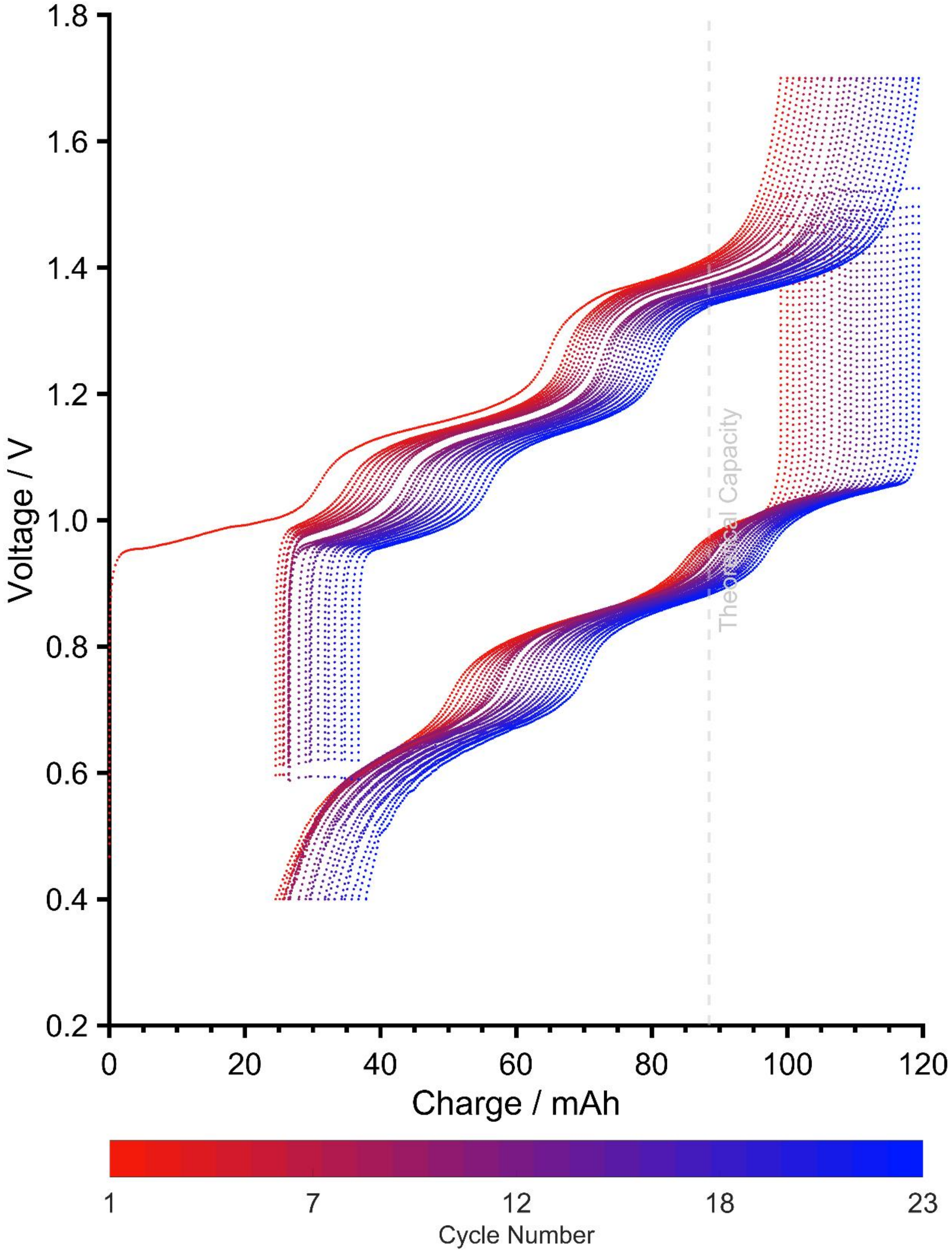

Figure S 35: Capacity-slip representation of the in-situ NMR GC data.

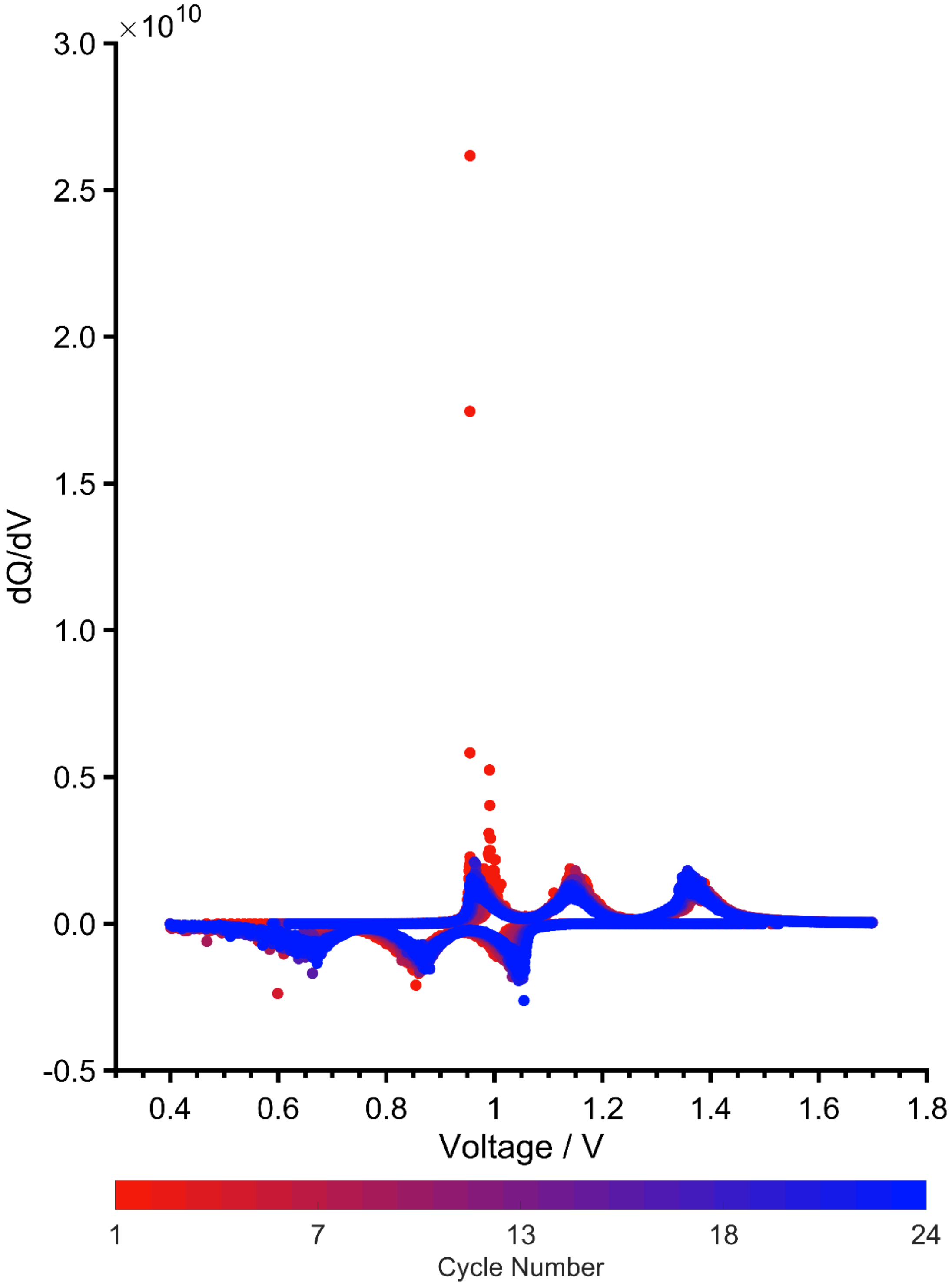

Figure S 36: dQ/dV of the in situ NMR GC data.

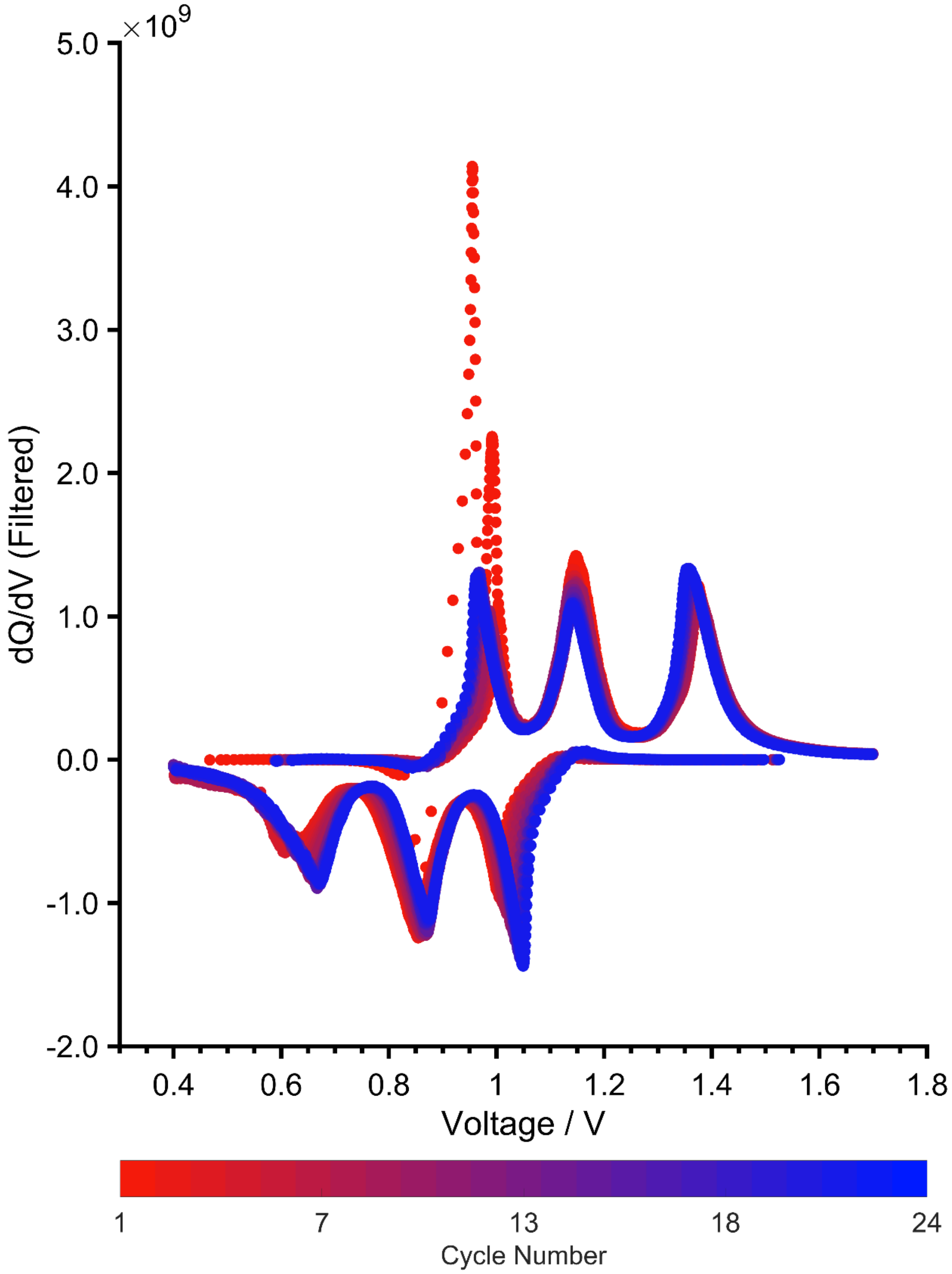

Figure S 37: Filtered dQ/dV data derived from the aged solution GC experiment.

2.14 GC - Aged - Carbon felt - NAFION 212

The solutions from the in-situ NMR experiment were stored in plastic containers for 4 months under air before being cycled in a lab-scale, full cell test.

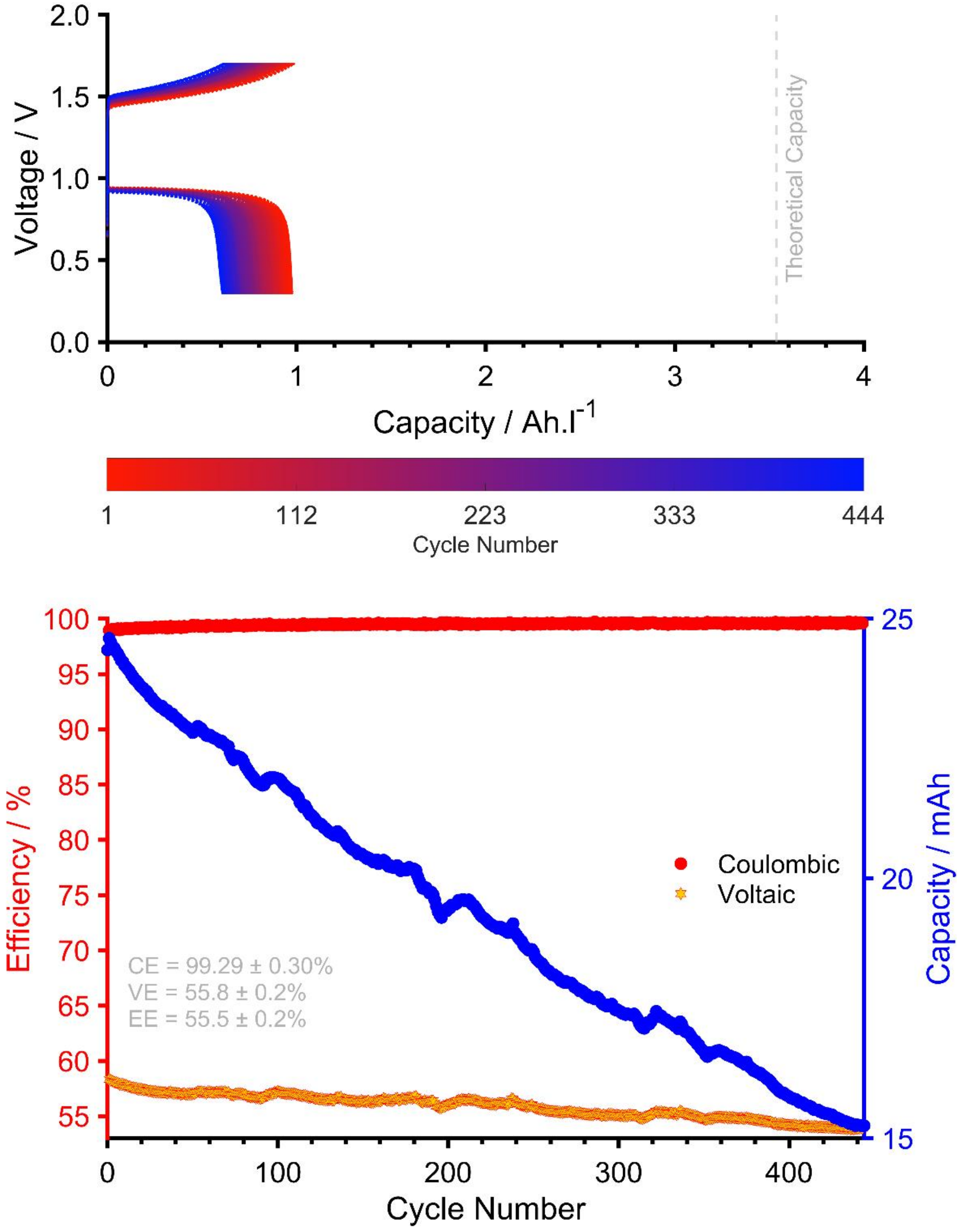

Figure S 38: Galvanostatic cycling data corresponding to an aged CABQ solution where 25 ml of 0.066 M CABQ dissolved in 1 M KOH/D_2O solution was cycled against 50 ml of 0.15 M $K_4Fe(CN)_6$ with 0.0375 M $K_3Fe(CN)_6$ dissolved in 1 M KOH/D_2O solution. The flow battery was charged and discharged at 200 mA with a flow rate of 75 ml.min^{-1}.

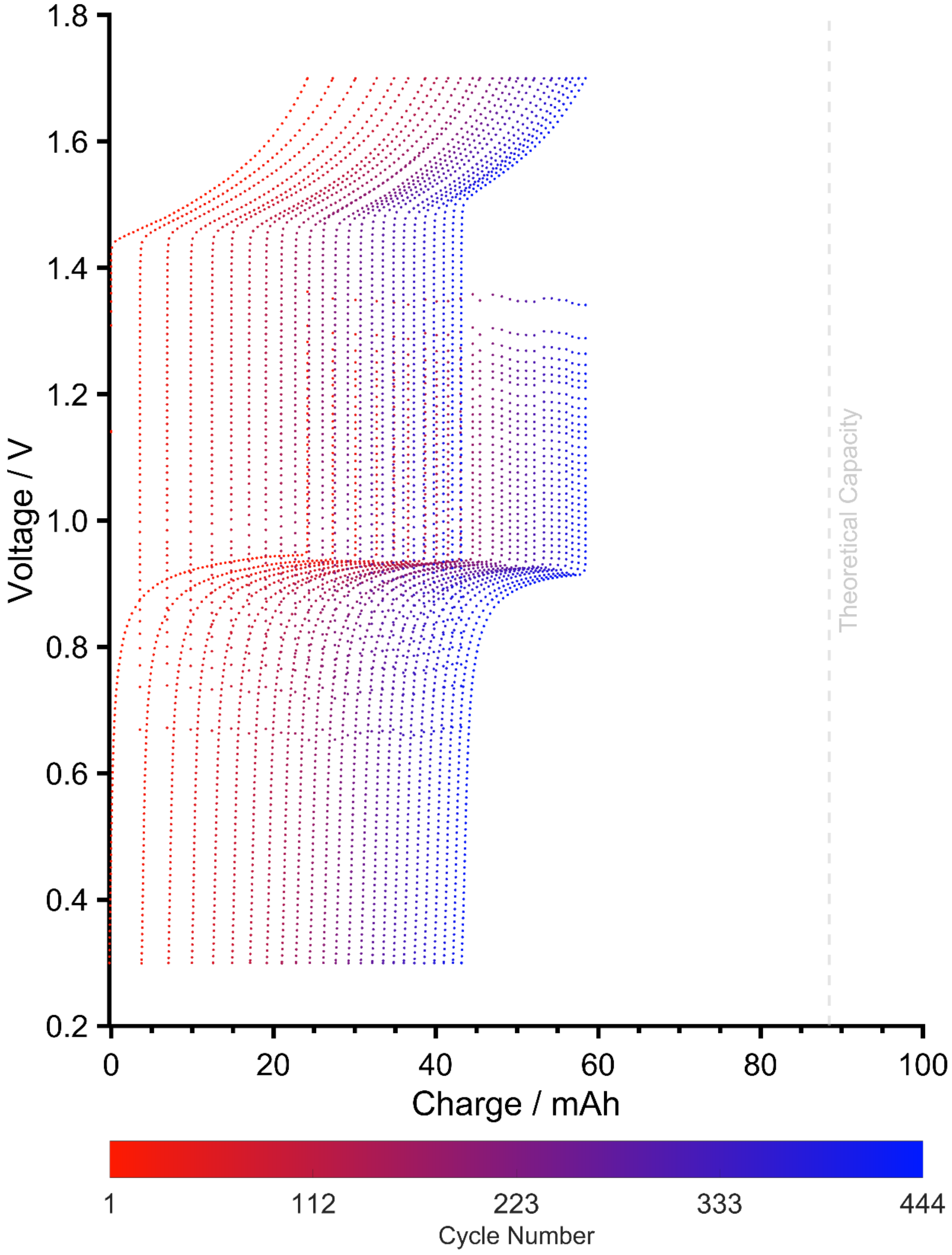

Figure S 39: Capacity-slip representation of the aged solution.

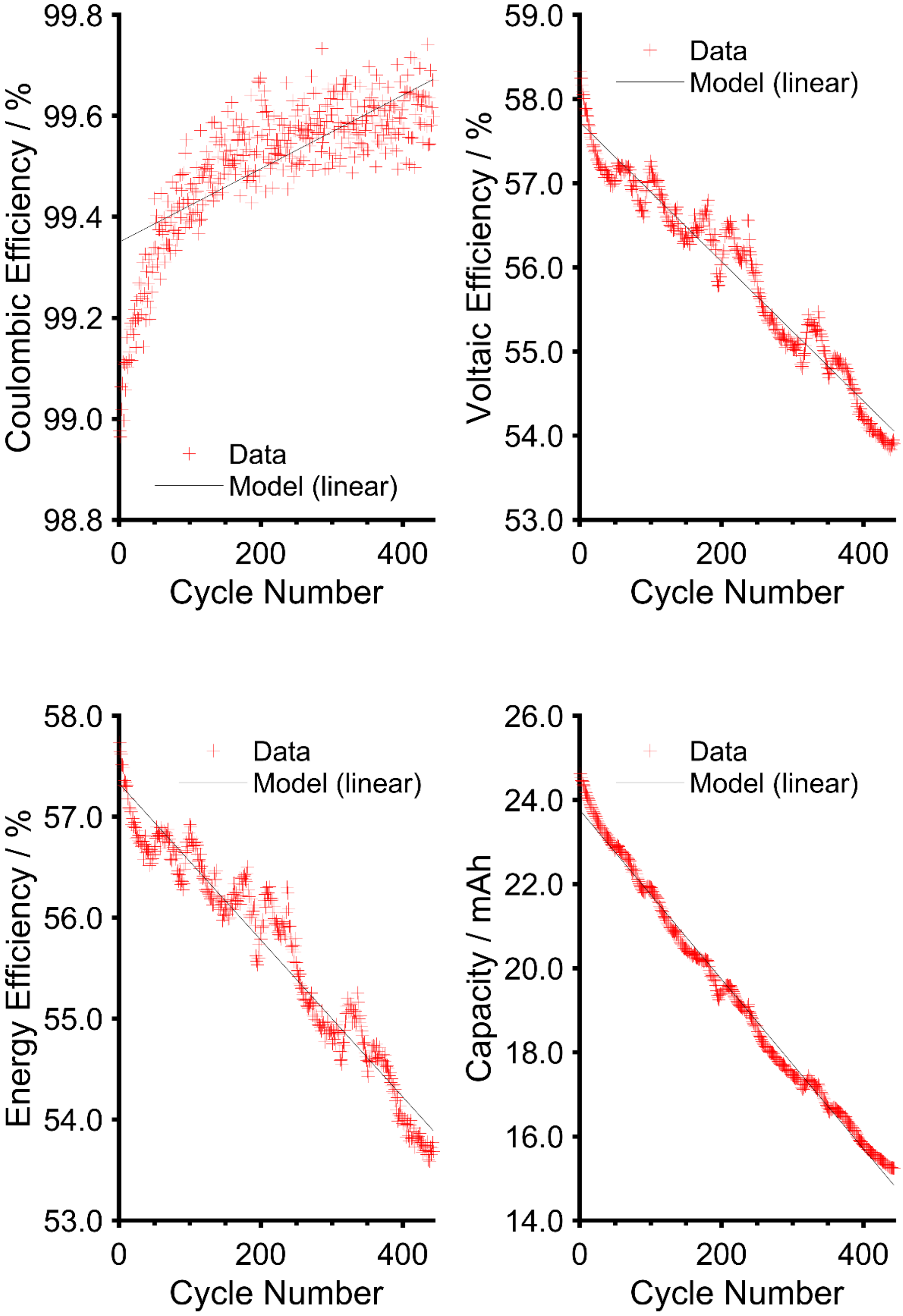

Figure S 40: Linear regression and polynomial models applied to the efficiency and capacity data for the aged solution GC experiment.

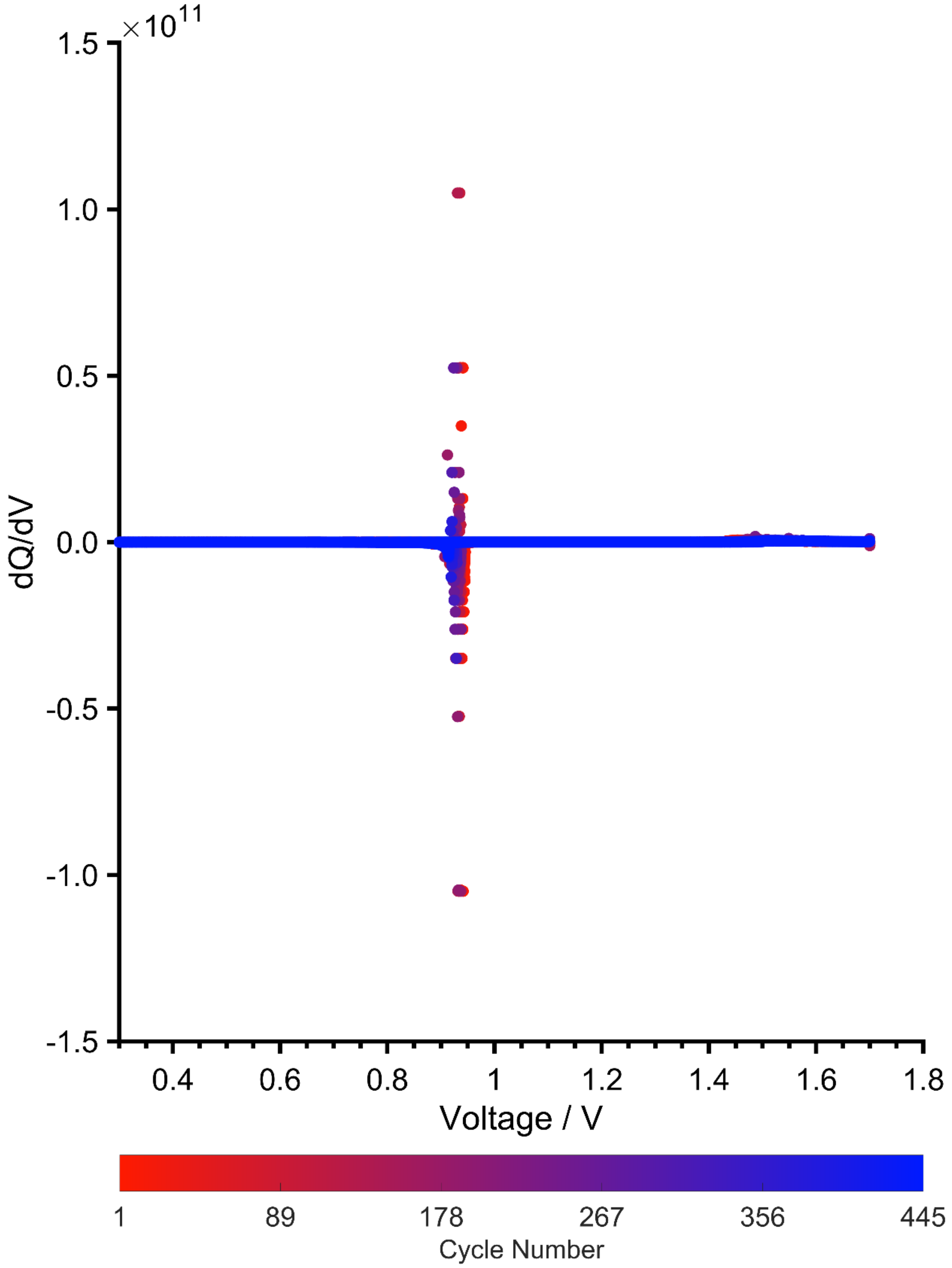

Figure S 41: dQ/dV data derived from the aged solution GC data.

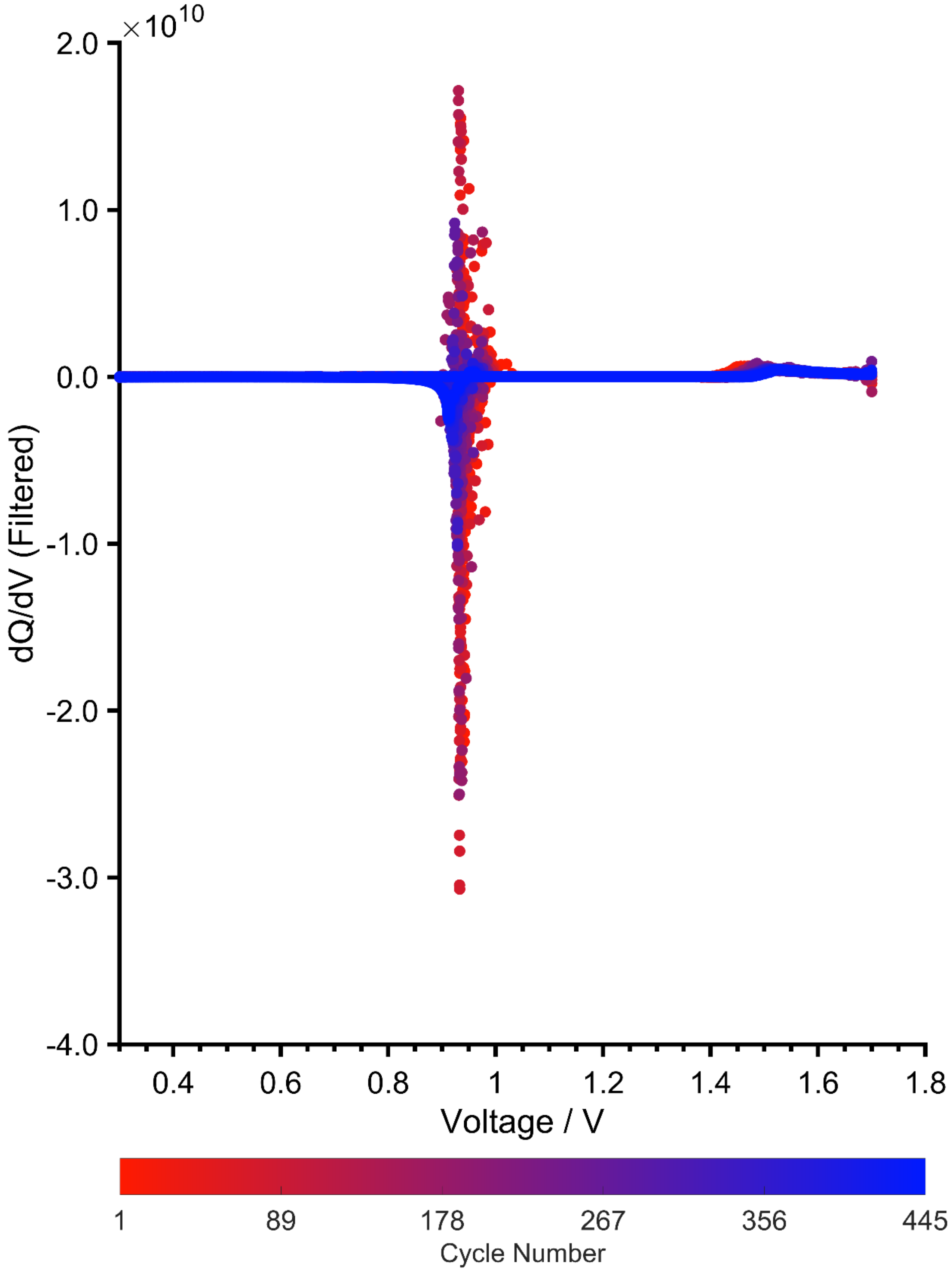

Figure S 42: Filtered dQ/dV data derived from the aged solution GC experiment.

2.14.1 Variable Current

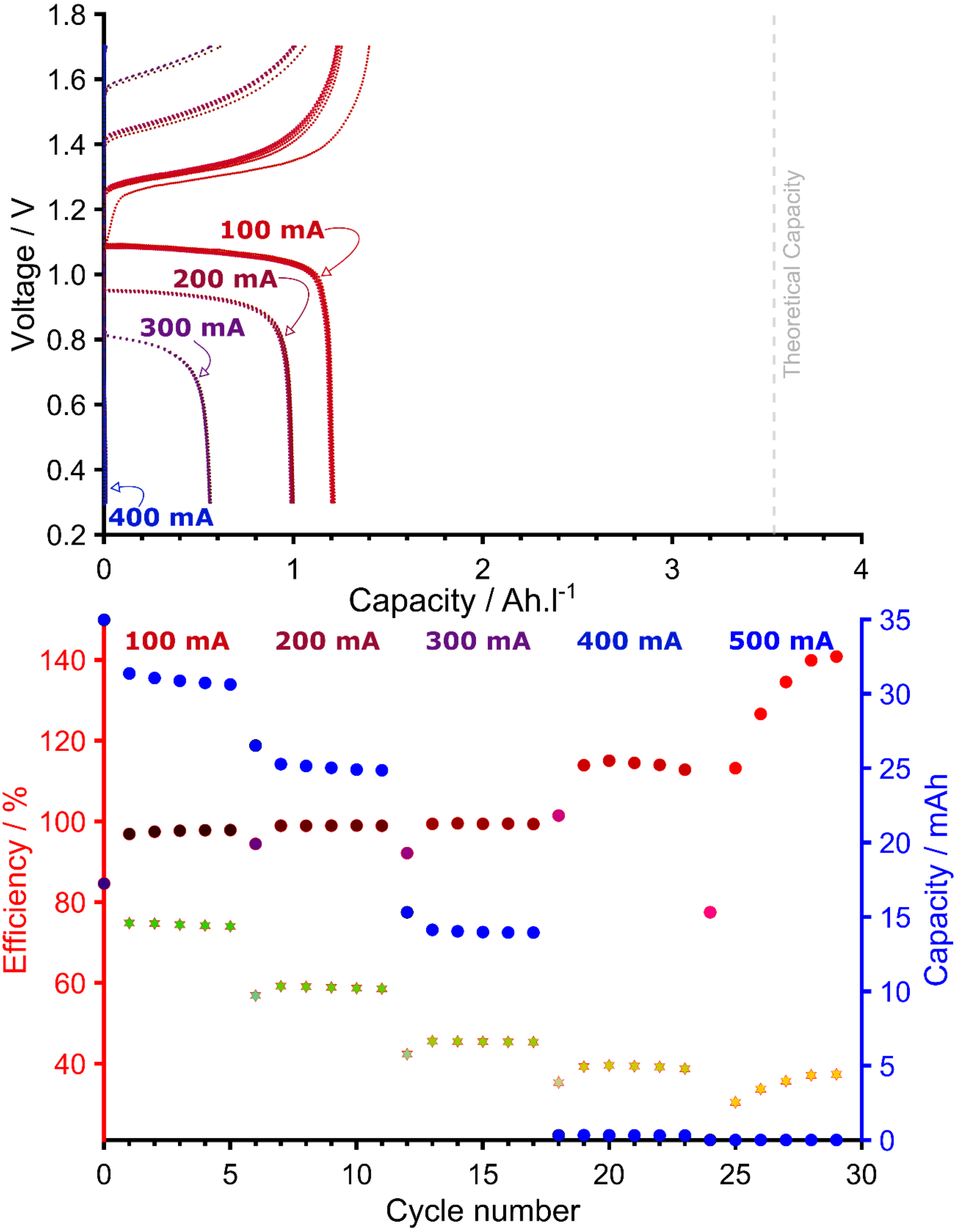

Figure S 43: Variable current data GC corresponding to a scan rates from 100-500 mA in 100 mA steps. The system was the same as in the aged electrolyte experiment.

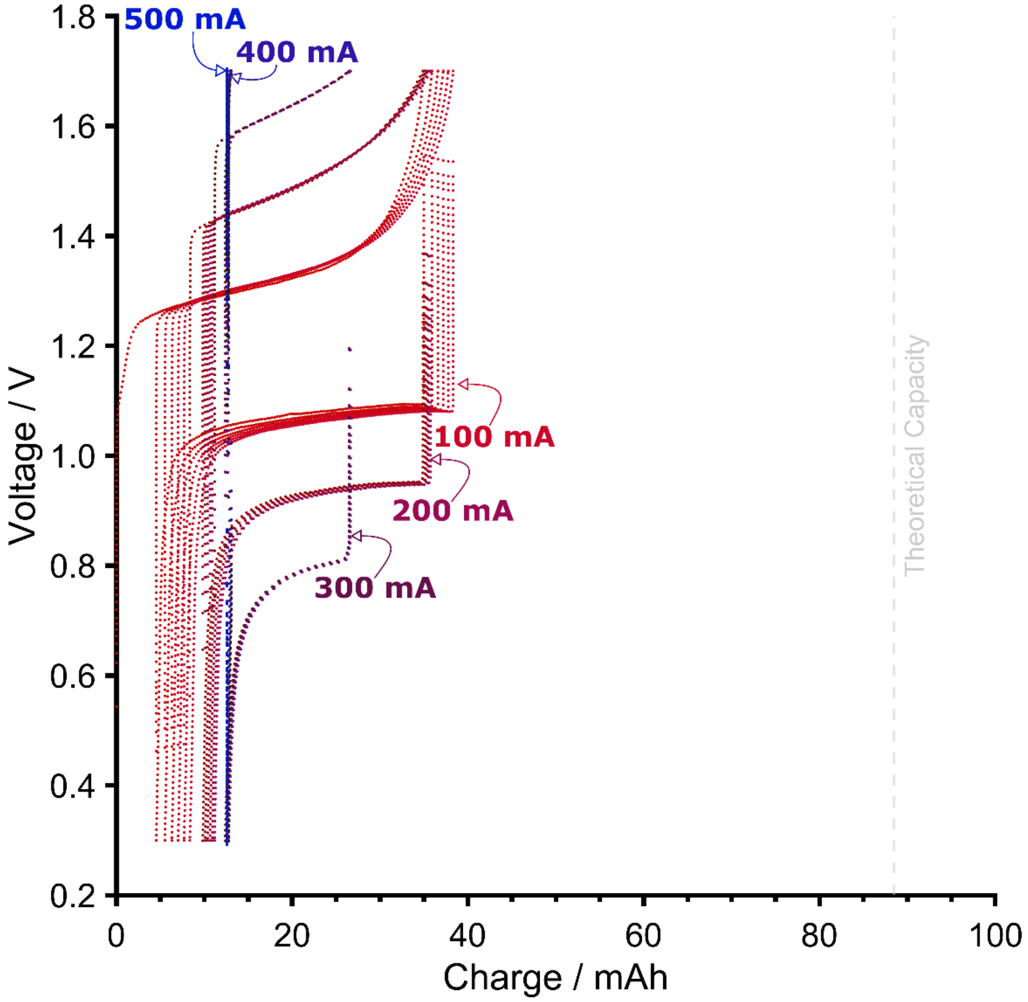

Figure S 44: Capacity-slip representation of the variable current, aged electrolyte experiment.

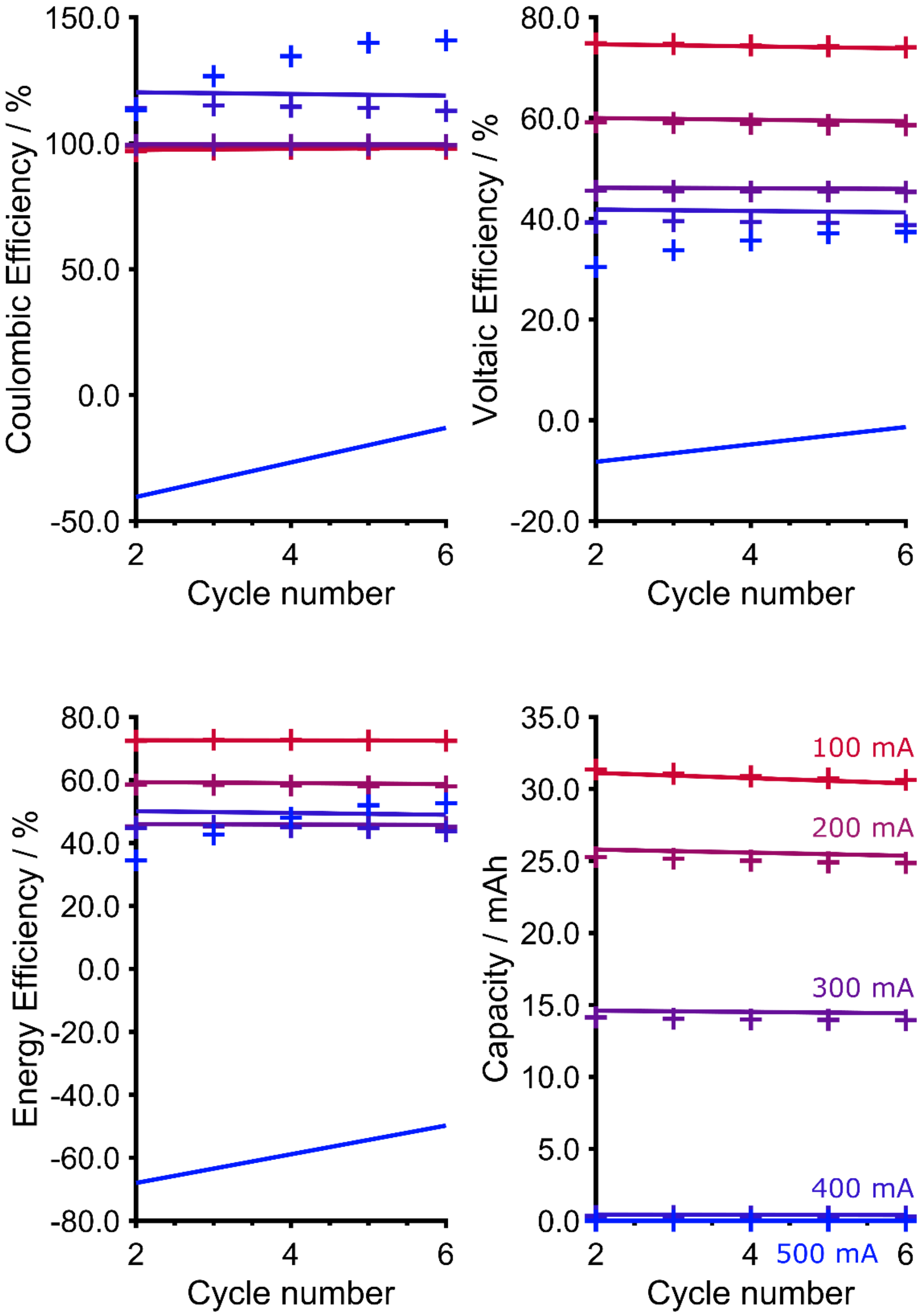

Figure S 45: Line and polynomial fits applied to the variable current, aged electrolyte experiment.

2.15 GC (In situ EPR) – Carbon felt – NAFION 212

CABQ (0.0076 g, mass required for 0.001 M) was dissolved in 1 M KOH/D_2O (20 ml) to make up the anolyte solution. Potassium ferrocyanide (2.534 g, mass required for 200 mM) was dissolved in 1 M KOH/D_2O (30 ml) to form the catholyte solution. 20 ml of anolyte solution was used against 30 ml of catholyte solution. The flow battery was pumped at 13.6 ml.min^{-1} (60 rpm). Using these solutions, in-situ EPR was carried out.

2.16 GC – Baked Carbon Paper – NAFION 212

CABQ (0.748 g) was dissolved in 1 M KOH/D_2O (30 ml) to make a 0.066 M anolyte solution. Ferrocyanide (3.802 g) and ferricyanide (0.950 g) were dissolved in 1 M KOH/D_2O (60 ml) to make a catholyte solution. 15 ml of the anolyte solution was cycled against 30 ml of the catholyte solution at a flow rate of 188 ml.min^{-1} (200 rpm).

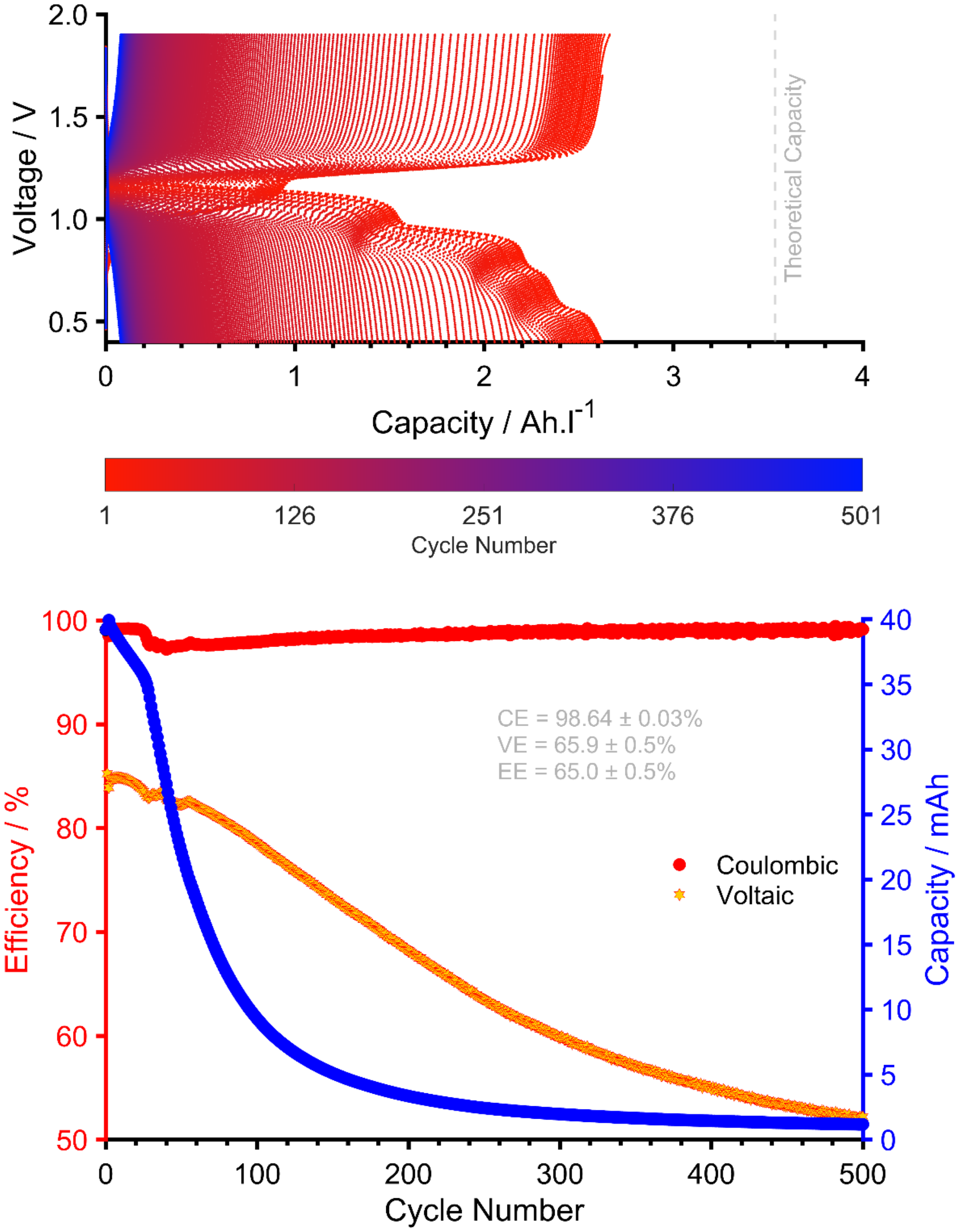

Figure S 46: **[Top]** Galvanostatic cycling data of 0.066 M 2,5-pCApBQ (15 ml) in 1 M KOH/D_2O cycled at 188 ml.min^{-1} at ambient temperature against a 0.15 M: 0.0375 M solution of potassium ferrocyanide: potassium ferricyanide (30 ml), **[Bottom] left:** Coulombic and Voltaic Efficiency versus cycle number, **right:** capacity versus cycle number.

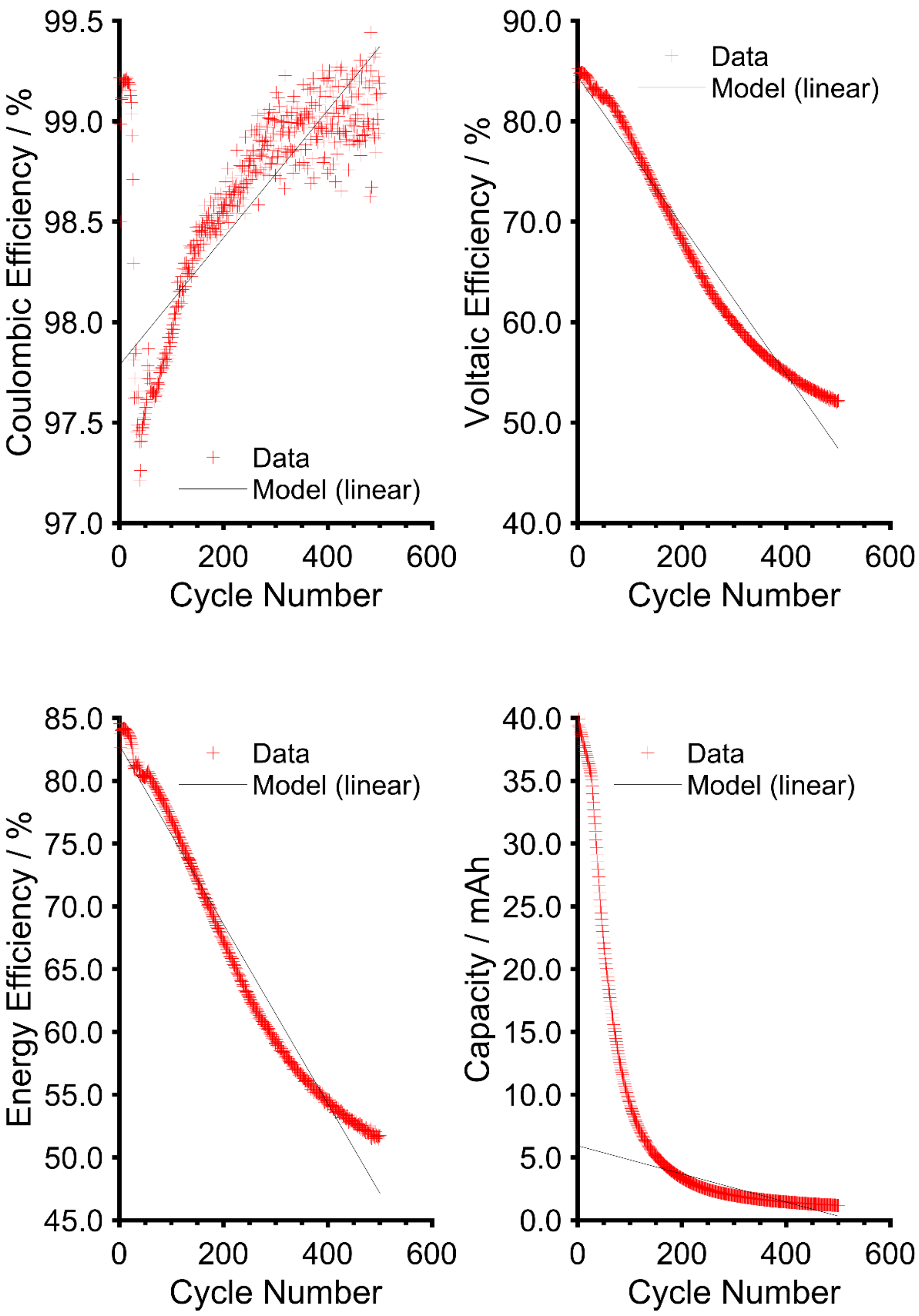

Figure S 47: Graphs showing the fit of the data using a linear regression model for each of Coulombic, Voltaic and Energy efficiencies as well as capacity vs. cycle number.

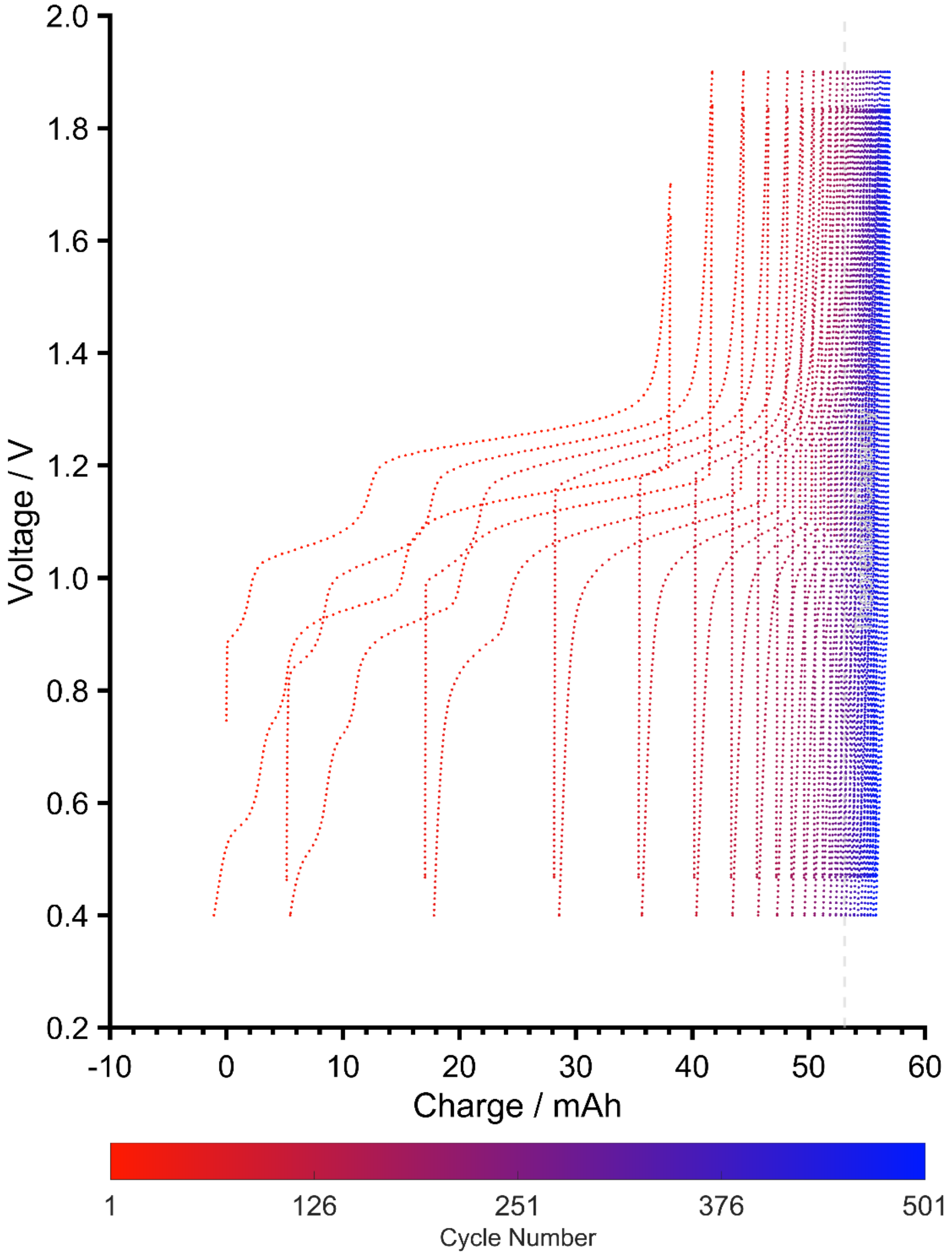

Figure S 48: Charge (Q-Q_0) versus voltage data shown for every 20th cycle to demonstrate the hysteresis involved in the cycling process as well as the loss of plateaus as cycling continues. The data corresponds to 0.066 M 2,5-pCApBQ (15 ml) in 1 M KOH/D_2O cycled at 188 ml.min^{-1} at ambient temperature against a 0.15 M: 0.0375 M solution of potassium ferrocyanide: potassium ferricyanide (30 ml).

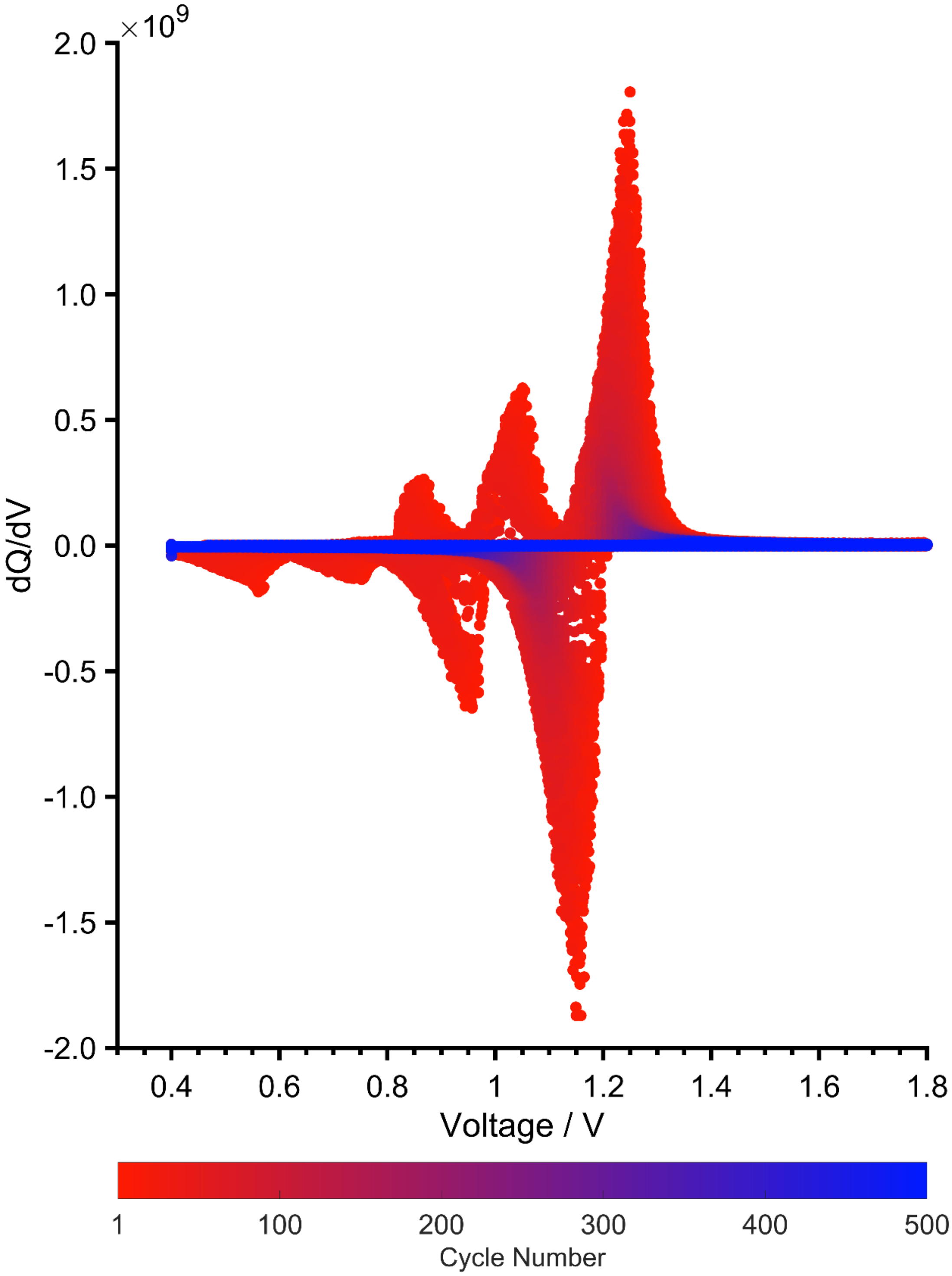

Figure S 49: dQ/dV data derived from the first baked carbon paper GC experiment.

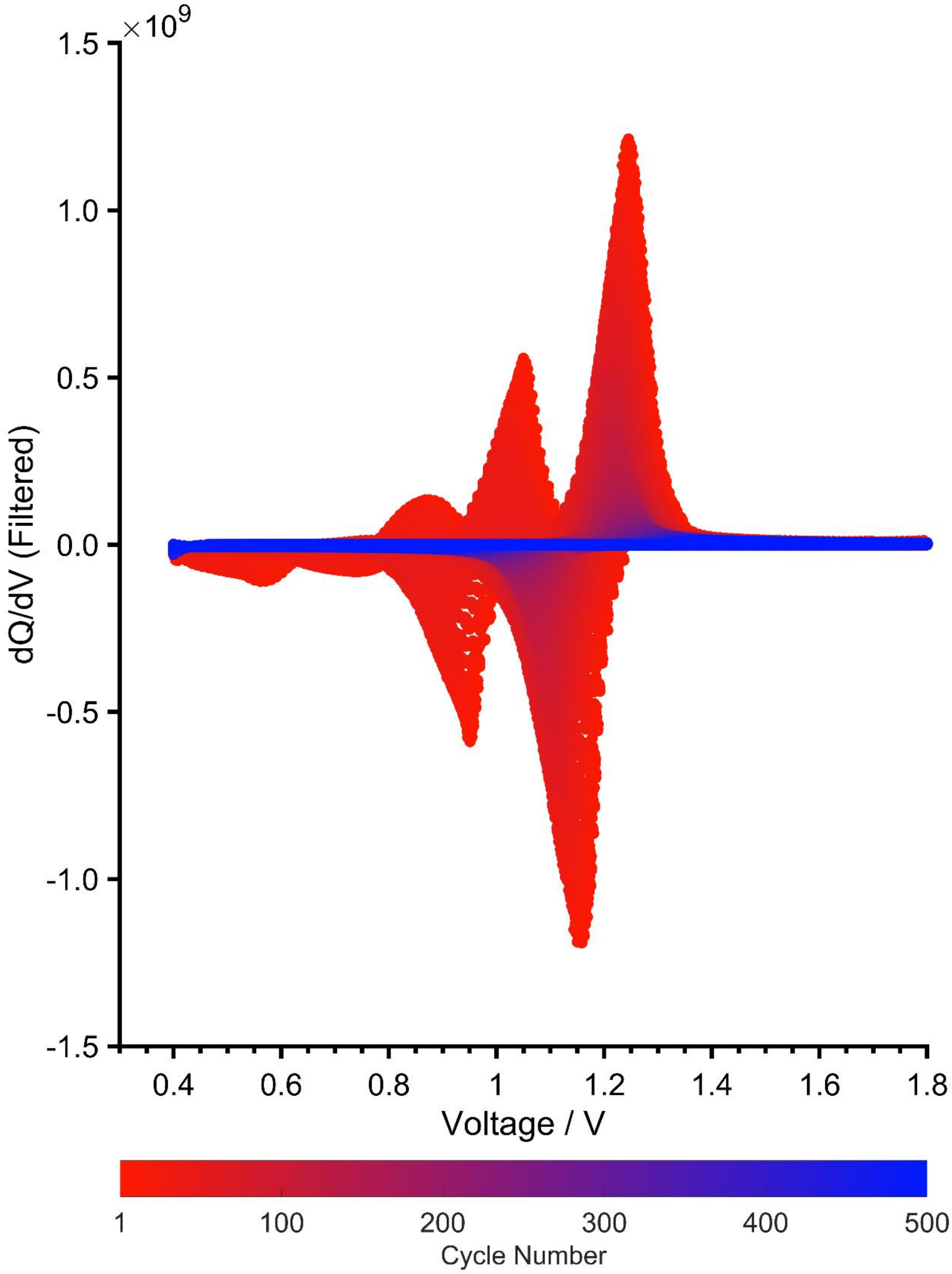

Figure S 50: Filtered dQ/dV data derived from the first baked carbon paper GC experiment.

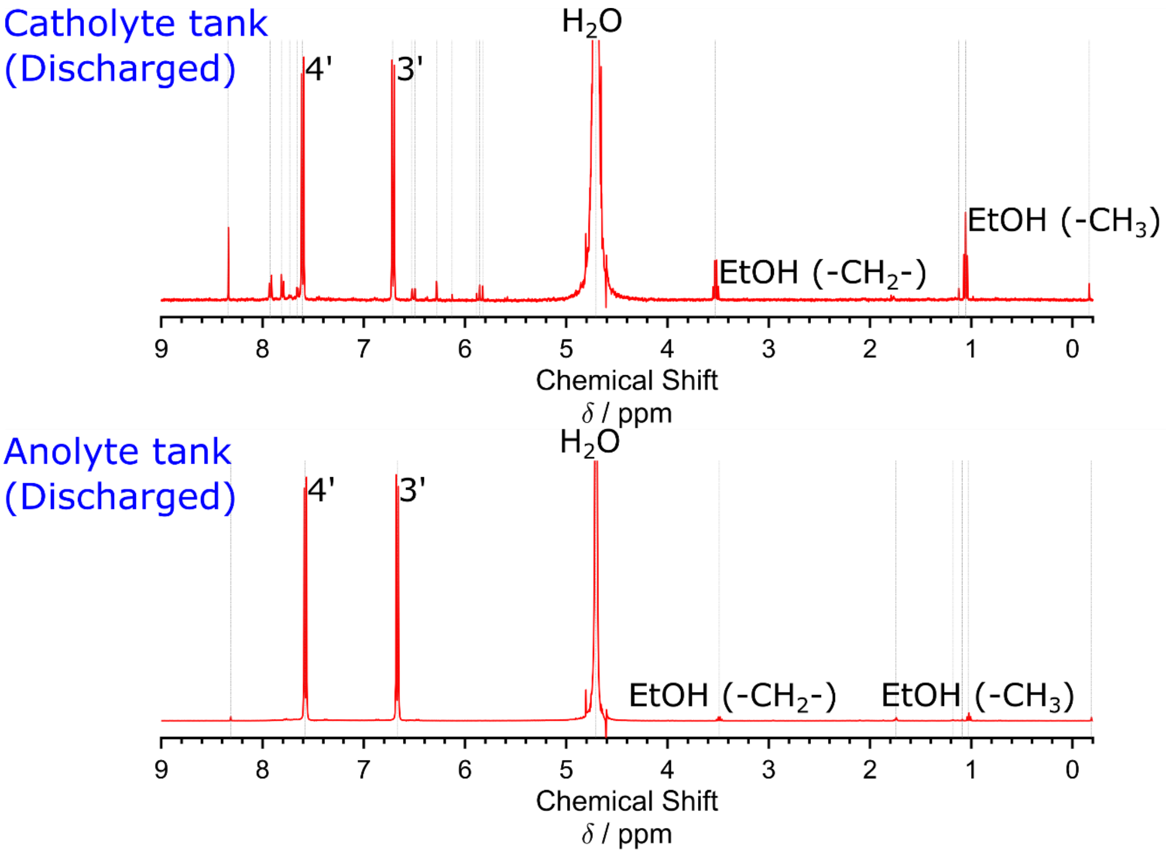

Figure S 51: Ex-situ ^{1}H NMR (400.13 MHz) taken of the discharged anolyte and catholyte tanks.

2.17 GC – Baked Carbon Paper – NAFION 212 x2

The figures shown in this section correspond to the electrochemical data shown in Figure 10 of the main matter. CABQ (0.621 g) was dissolved in 1 M KOH/D_2O (25 ml) to make a 0.066 M anolyte solution. Ferrocyanide (3.166 g) and ferricyanide (0.617 g) were dissolved in 1 M KOH/D_2O (50 ml) to make a catholyte solution. 15 ml of the anolyte solution was cycled against 30 ml of the catholyte solution at a flow rate of 75 ml.min^{-1} (80 rpm).

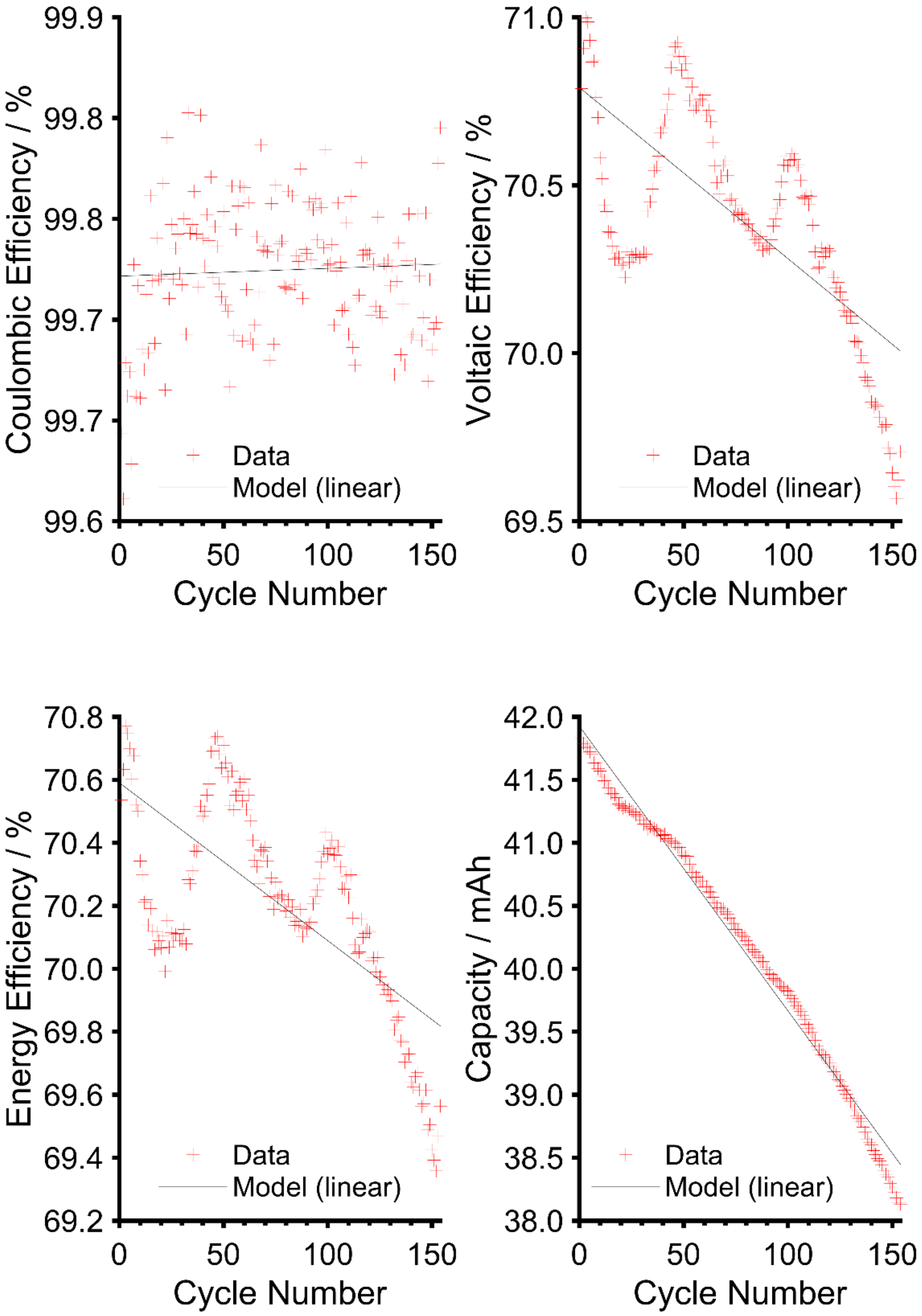

Figure S 52: Linear regression of the efficiencies and capacity derived from the second baked carbon paper GC experiment.

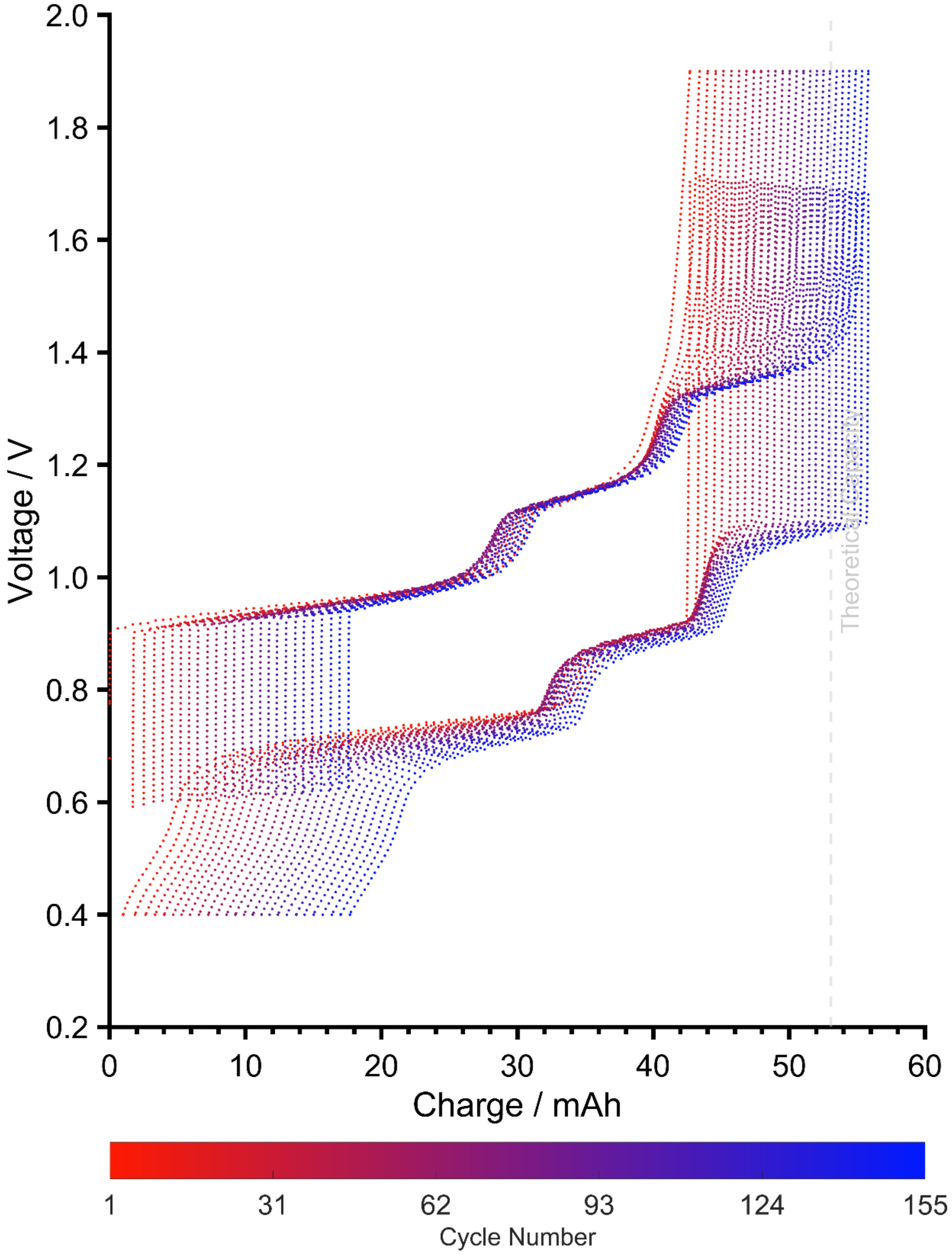

Figure S 53: Capacity slip representation of the second baked carbon paper GC experiment.

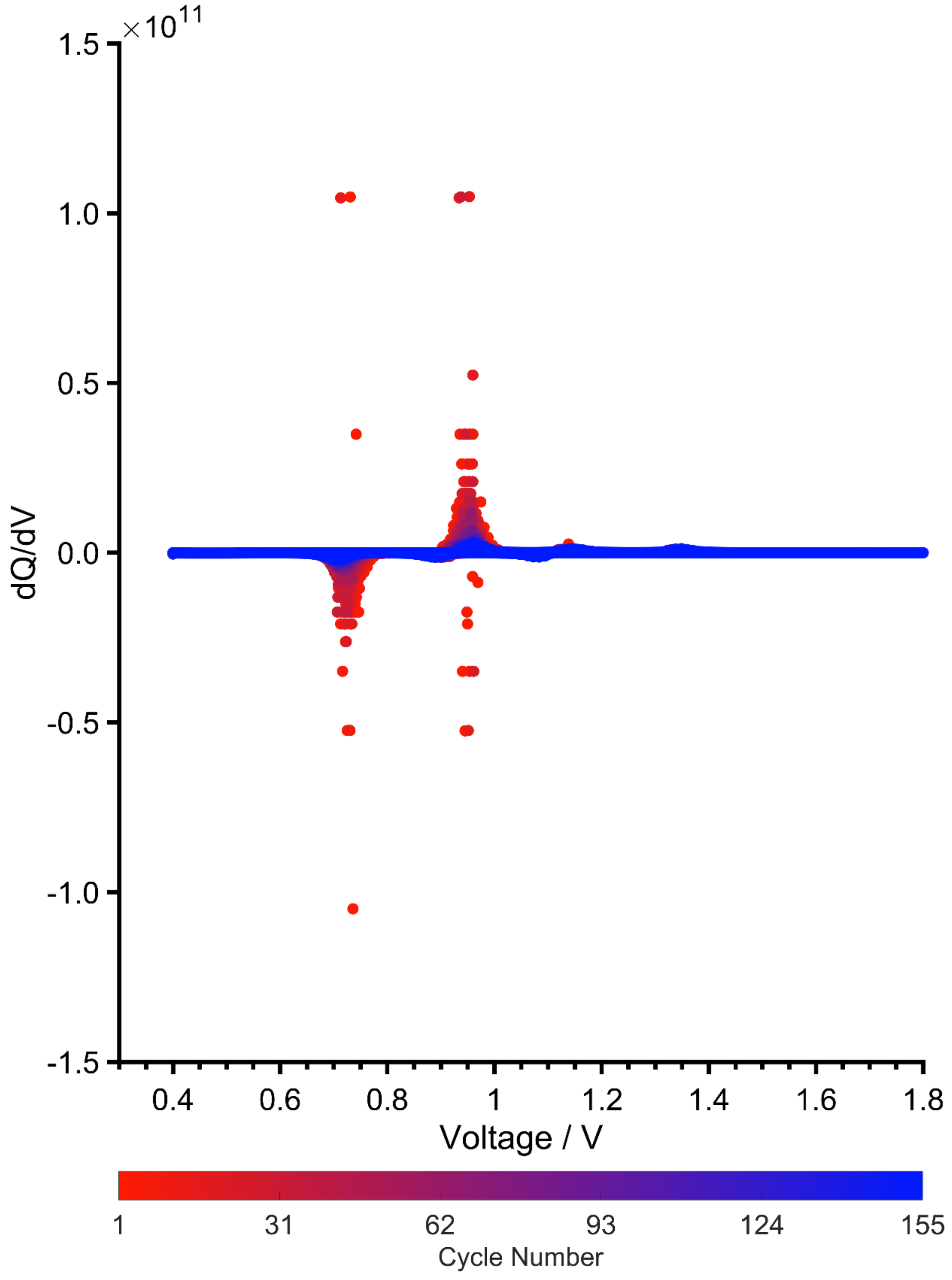

Figure S 54: dQ/dV data derived from the second baked carbon paper experiment.

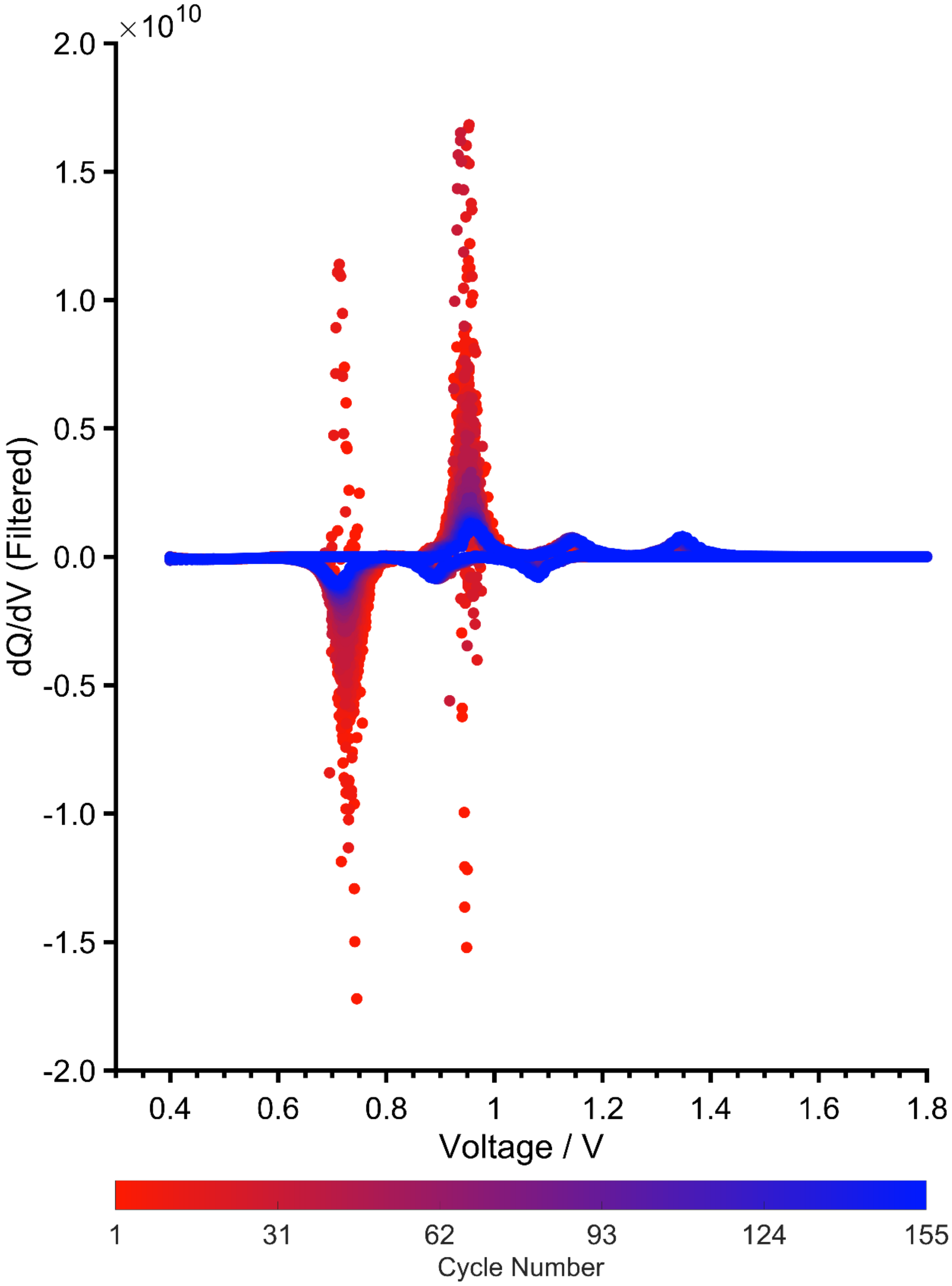

Figure S 55: Filtered dQ/dV data derived from the second baked carbon paper GC experiment.

To compare the difference in resistance between the single-membrane experiment (2.16) and the double-membrane experiment (2.17) the IR drop was calculated using both the charge and the discharge curves for all cycles. The results and their standard deviations are summarised below.

Table S 4: Table detailing the resistance calculated from the IR drop observed between switching from charging to discharging in the galvanostatic charging experiments.

	Single layer / Ω	*Double layer / Ω*
Charge	0.1648 ± 0.0002	0.513 ± 0.002
Discharge	0.1696 ± 0.0002	0.528 ± 0.002
Overall	0.1672 ± 0.0002	0.520 ± 0.002

From the above table, the area-specific resistances are 0.84 Ω.cm^2 and 2.60 Ω.cm^2 for the single-layer and double-layer experiments, respectively, with an increase in resistance of 353 Ω between the two experiments.

Table S 5: Table detailing the peak positions of the dQ/dV plots that derived from the single-layer (2.16) and double-layer (2.17) experiments, respectively.

Plateau	*Single-layer Discharge peak voltage/Charge peak voltage (V)*	*Peak-to-peak separation (V)*	*Double-layer Discharge peak voltage/Charge peak voltage (V)*	*Peak-to-peak separation (V)*
A	0.7515/0.9072	0.1557	0.7159/0.9524	0.2365
B	0.9508/1.0500	0.0992	0.8932/1.1429	0.2497
C	1.1569/1.2553	0.0884	1.0823/1.3372	0.2549
/	Average	0.114	Average	0.247

To validate the above IR drop data, the resistance was also estimated from the dQ/dV plots. From the above table, one can estimate the increase in resistance by first halving the peak-to-peak separation to estimate the overpotential: NAFIONx1 = 57 mV, NAFIONx2 = 120 mV (2 s.f.). Taking the difference of these two values gives: 66 mV (2 s.f.) and then by dividing by the charging current (200 mA), following Ohm's law, we can estimate the resistance change as 0.33 Ω. The largest component in this resistance change is likely to be the increase in tortuosity due to the additional membrane.[20]

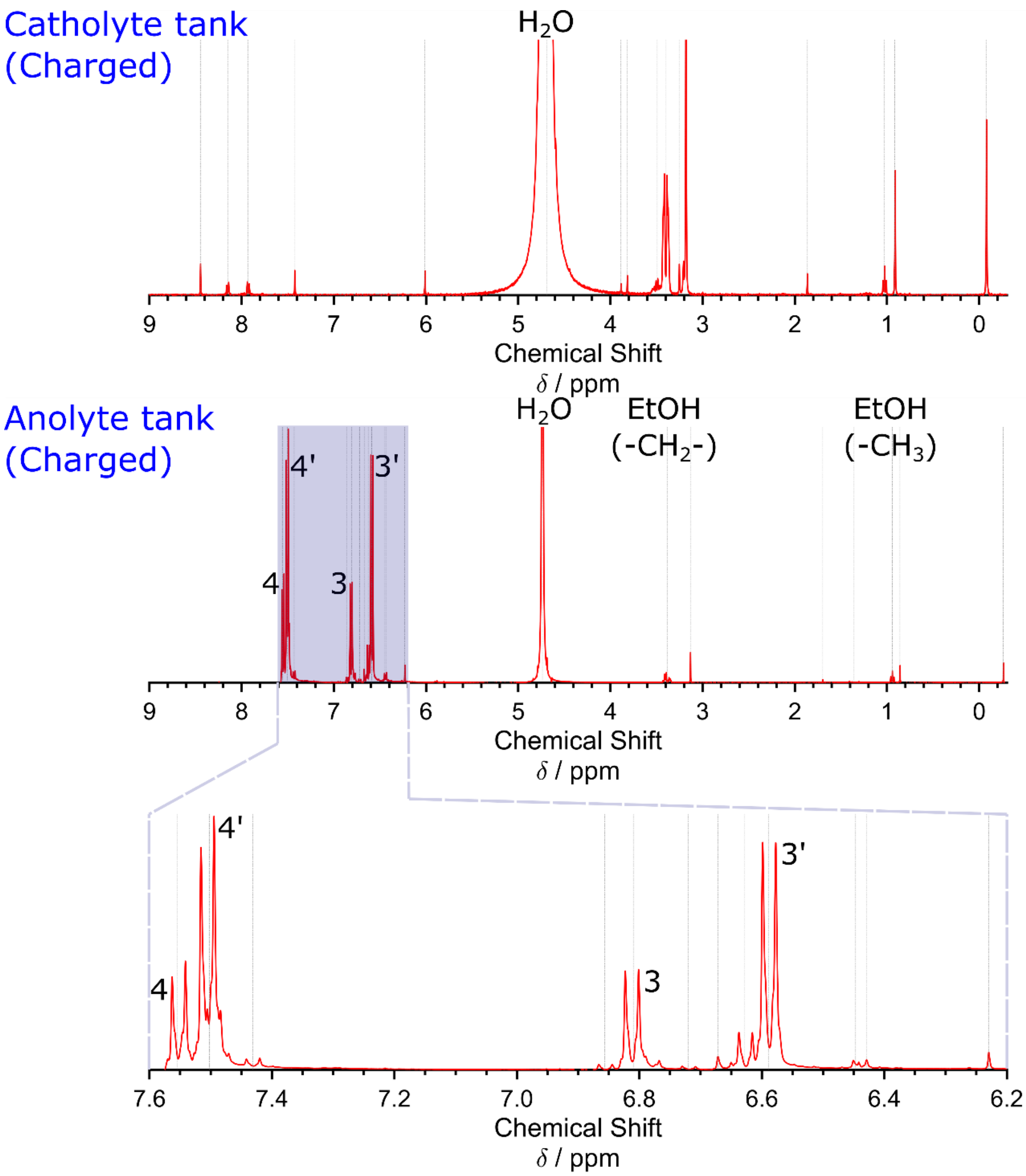

Figure S 56: Ex-situ ^{1}H NMR (400.13 MHz) taken of the charged anolyte and catholyte tanks.

2.17.1 Variable Current

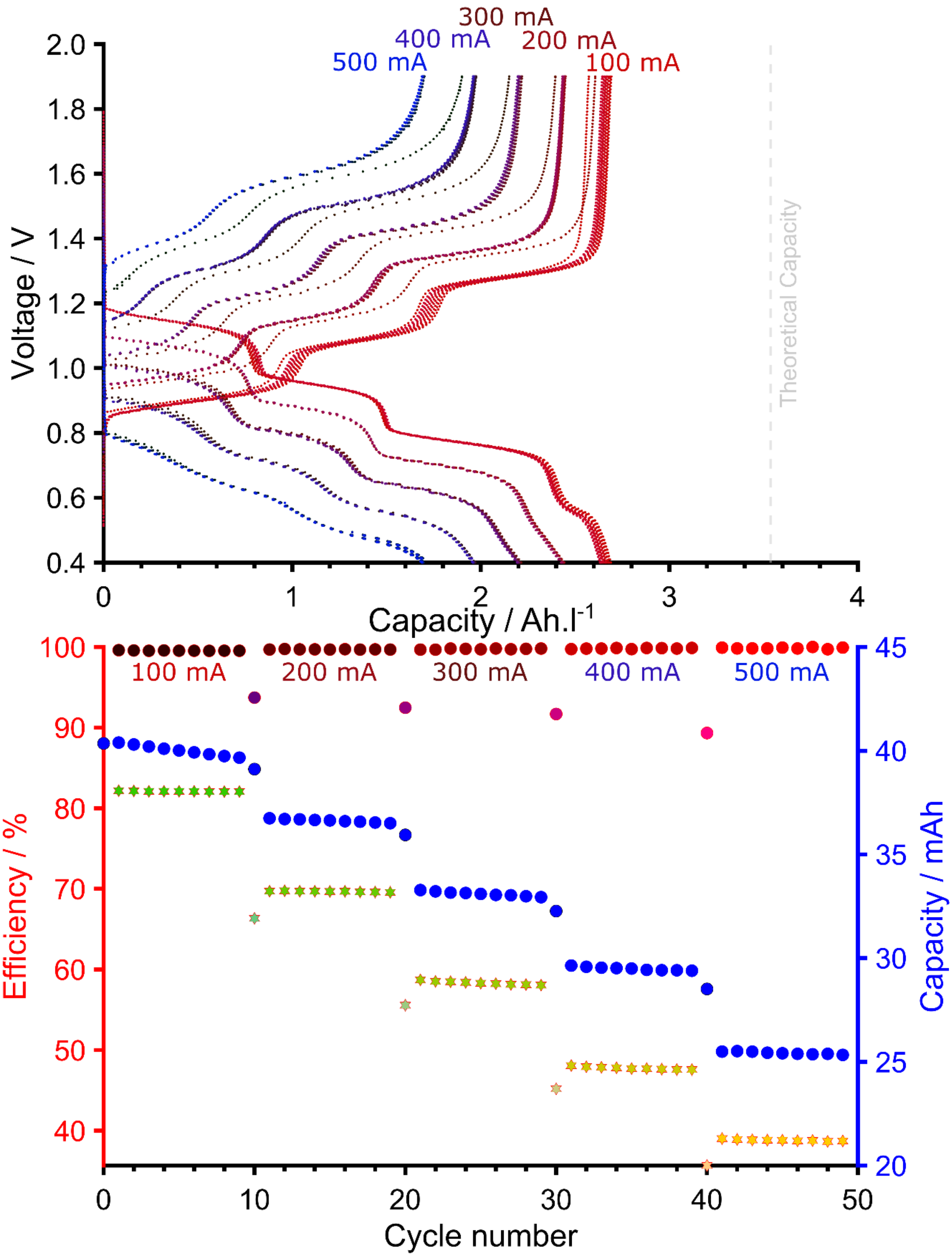

Figure S 57: Variable current data GC corresponding to a scan rates from 100-500 mA in 100 mA steps. The system was the same as in the second baked carbon paper experiment.

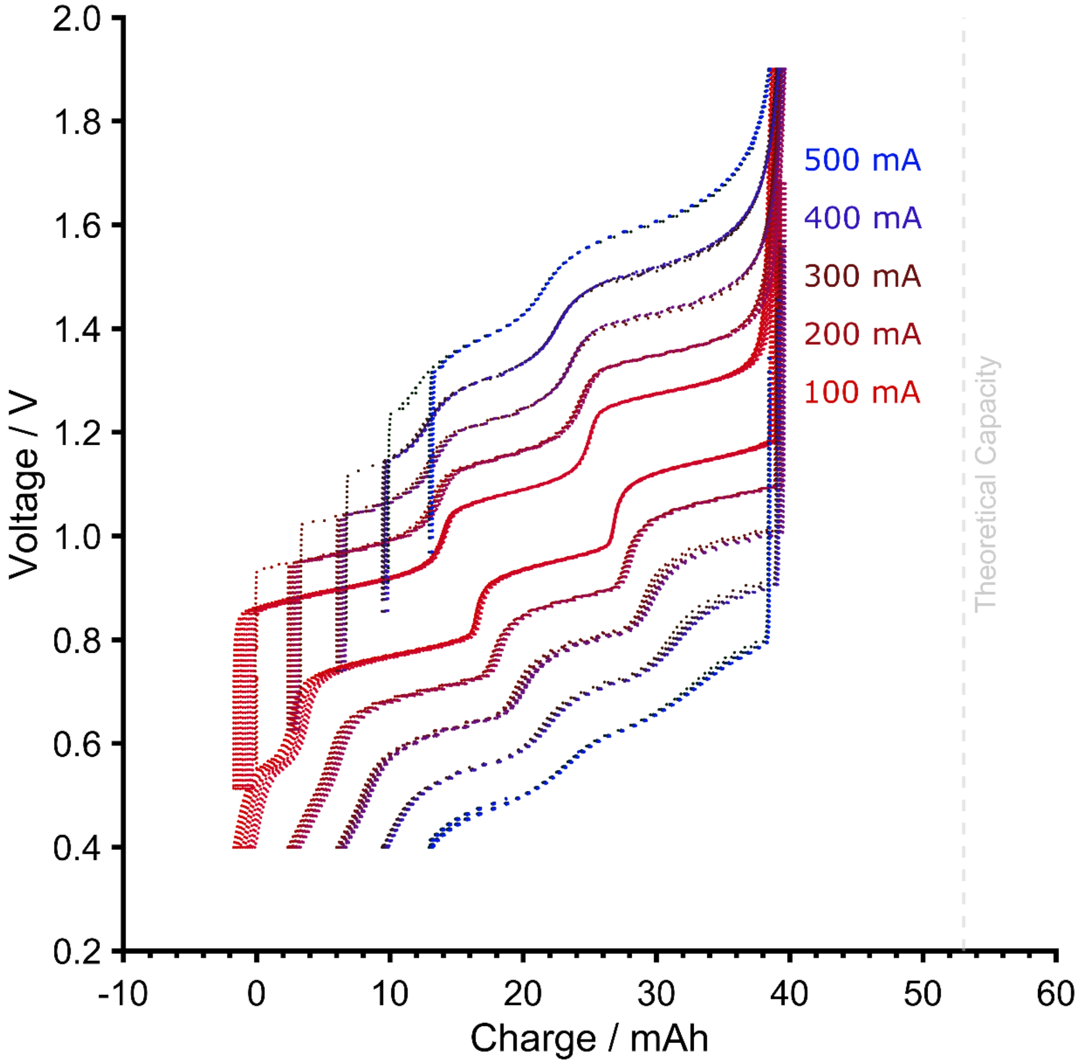

Figure S 58: Capacity-slip representation of the variable current, second baked carbon paper experiment.

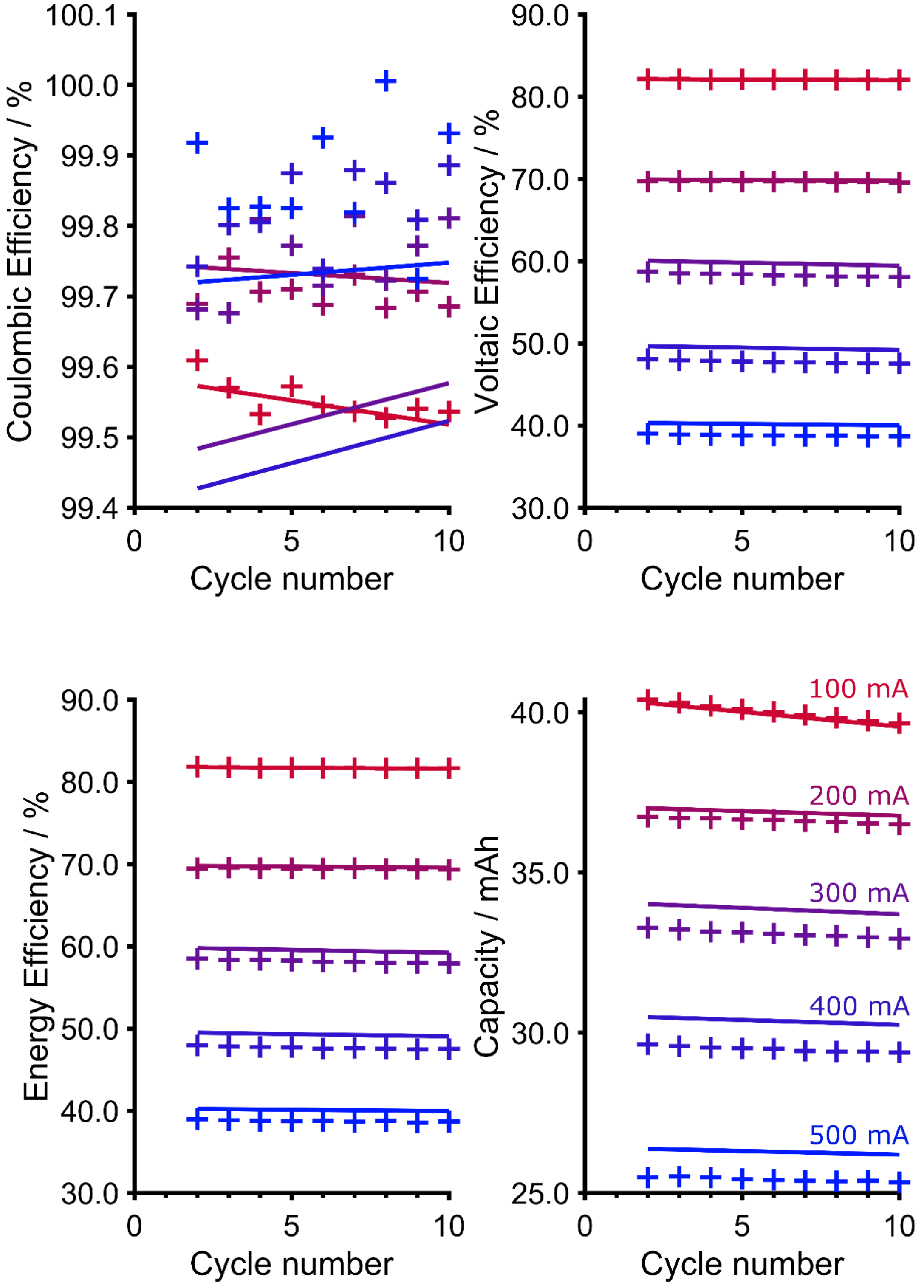

Figure S 59: Linear fits applied to the variable current, second baked carbon paper experiment.

2.18 Symmetric Cell Experiment

The figures shown in this section correspond to the electrochemical data shown in Figure 12 of the main matter. CABQ (0.5128 g) was dissolved in 1 M KOH/D_2O (20.54 ml) to make a 0.066 M anolyte solution. Ferrocyanide (2.6137 g) was dissolved in 1 M KOH/D_2O (41.25 ml) to make a catholyte solution. The anolyte solution was cycled against the ferrocyanide catholyte solution at a flow rate of 75 ml.min^{-1} (80 rpm) under a constant-current-constant-voltage charge profile to a cut off voltage of 1.9 V with a potential hold for 30 mins. The ferrocyanide solution was then replaced with anolyte solution (0.7515 g CABQ dissolved in 30.10 ml KOH/D_2O) and the cell was cycled for 600 cycles with impedance spectroscopy recorded every 100 cycles to track any change in the resistances of the system.

2.18.1 Charge cycle

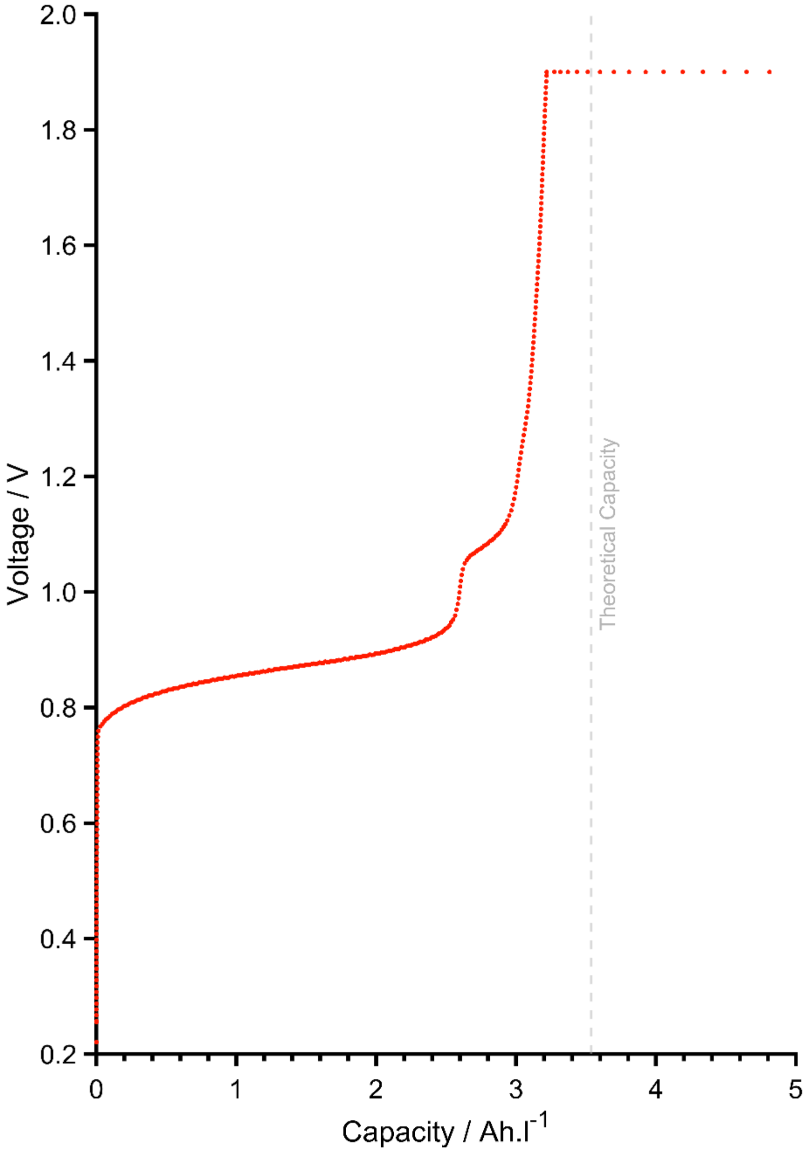

Figure S 60: Galvanostatic charge profile of symmetric cell. CABQ was cycled against $K_4Fe(CN)_6$ in 1 M KOH/D_2O.

2.18.2 Capacity Slippage Graph

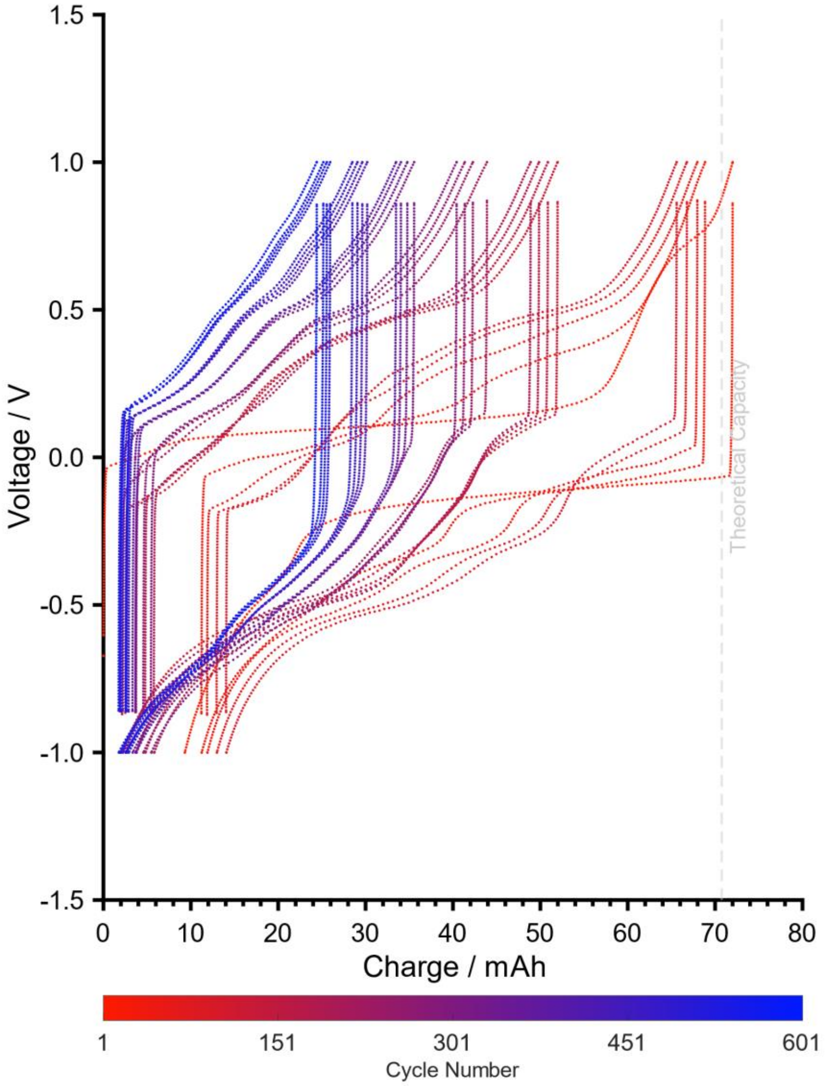

Figure S 61: Galvanostatic cycling data represented in a capacity slippage form of 0.066 M 2,5-CABQ (20 ml) in 1 M KOH/D_2O cycled at 50 ml.min^{-1} at ambient temperature against 0.066 M 2,5-CABQ (30 ml) in 1 M KOH/D_2O.

2.18.3 dQ/dV

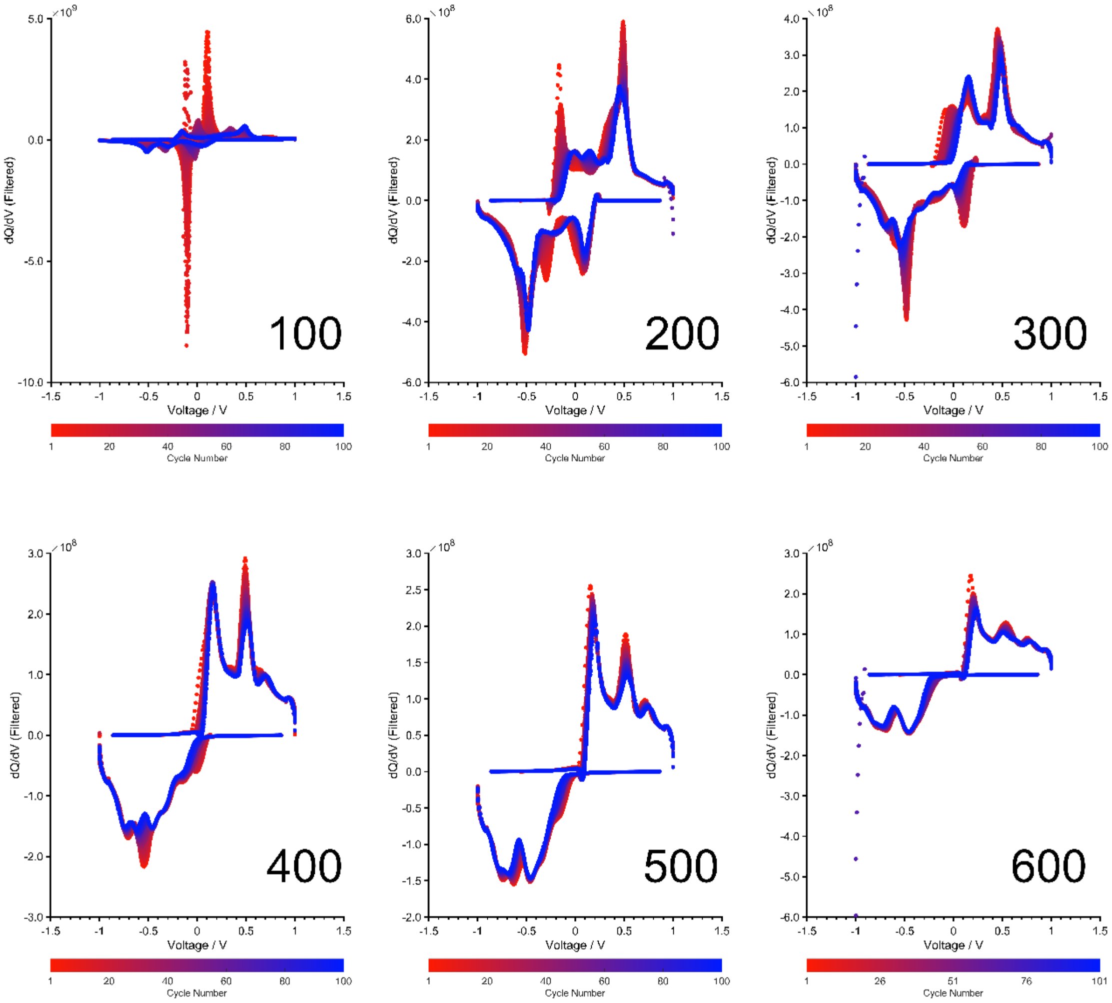

Figure S 62: dQ/dV plots of the electrochemical processes taking place in 100 cycle blocks of the symmetric cell cycling data.

2.18.4 Ex-situ NMR

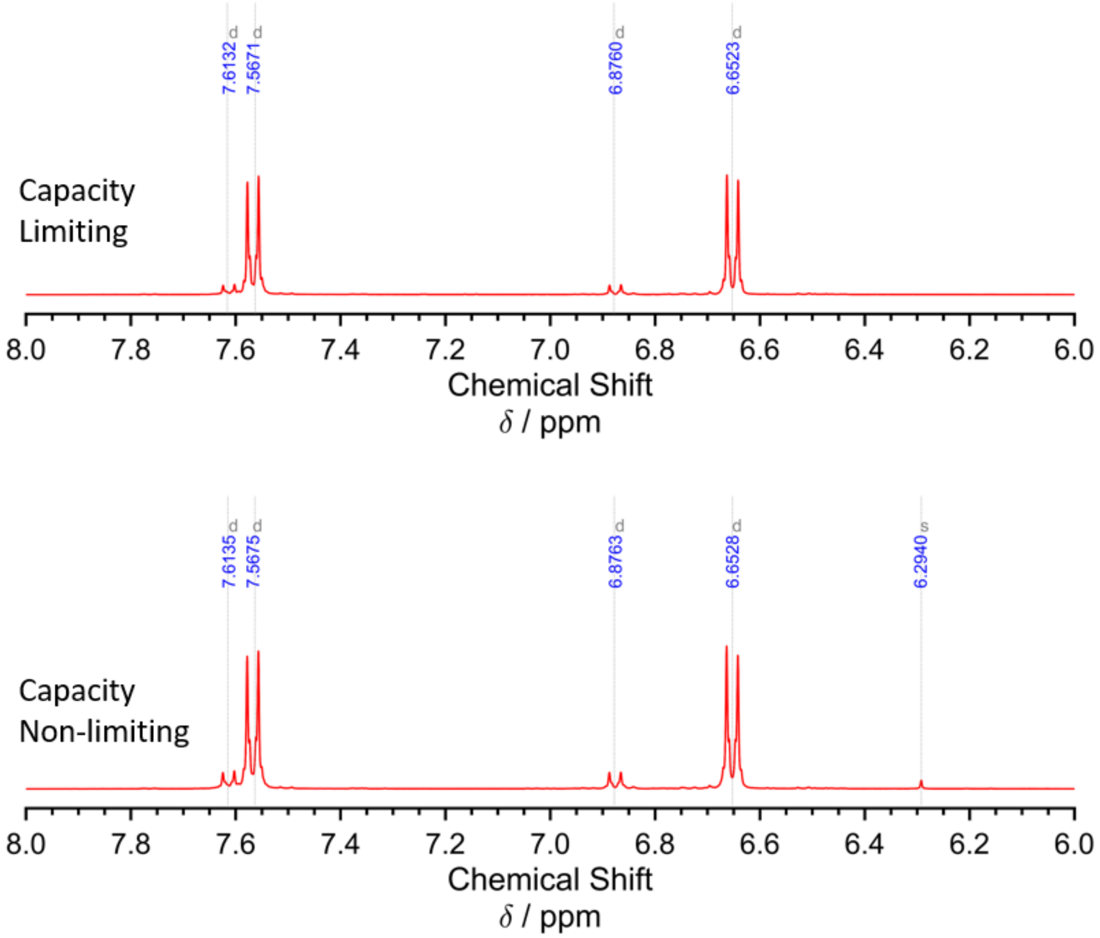

Figure S 63: Ex-situ ^{1}H NMR (400.13 MHz) of the capacity limiting and non-limiting reservoirs of the symmetric cell after cycling was complete.

2.19 DFT Calculation Results

DFT analysis was carried out at the B3LYP/def2QZVP level of theory based on the proposed reaction pathway (Scheme 3) using both water and KOH as nucleophiles. The structures were relaxed under aqueous solvated (aq) and un-solvated (gas-phase, g) environments and implicit solvation (PCM model, i.e. a polarisable continuum model) was used to both provide reasonable description of the solvent and to be computationally efficient while acquiring ground state structures. It must, however, be noted that unlike in the explicit solvent method, PCM fails to account for important interactions such as hydrogen-bonding which will significantly affect the energy of the system in an actual experimental system.

2.19.1 Calculated reactions

Gas phase

Water as nucleophile

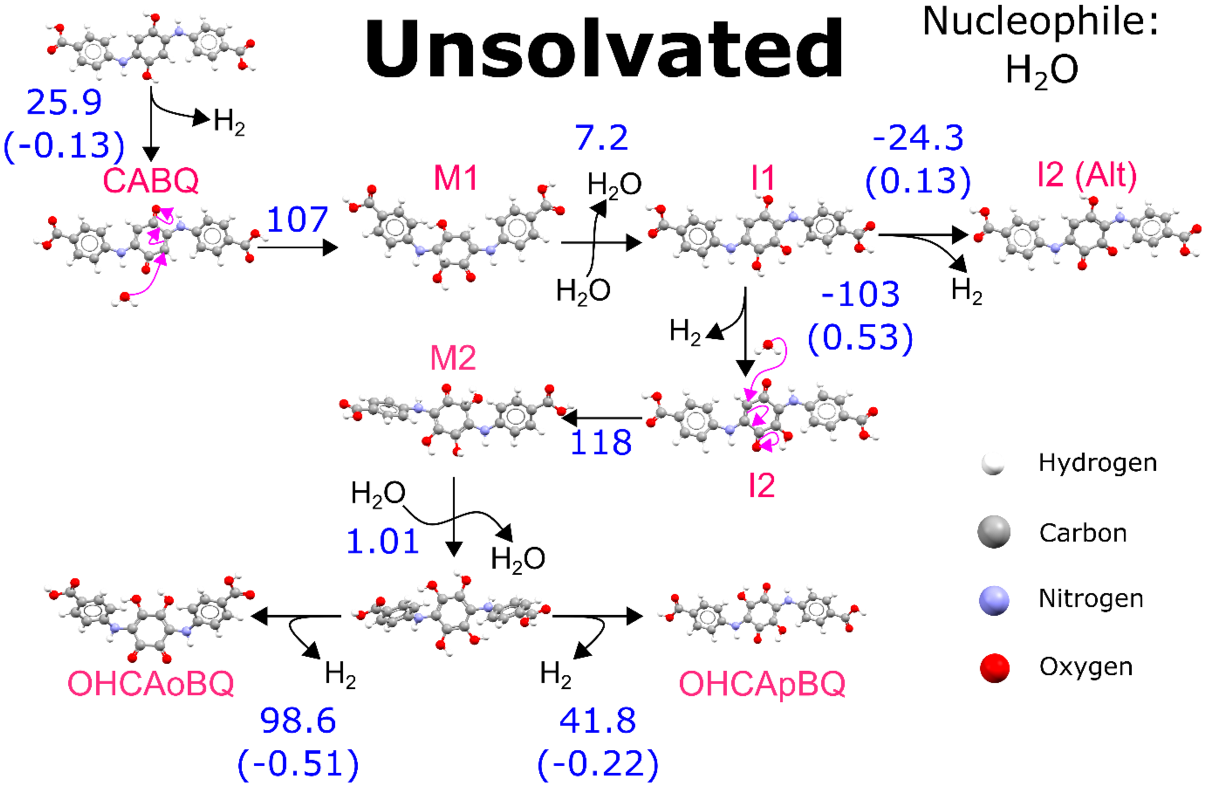

Figure S 64: DFT optimised structures and Gibbs free energies for the reactions (kJ·mol^{-1}) with water acting as the nucleophiles and all structures having been converged in the gas-phase. The numbers in brackets correspond to the potentials for those reactions in Volts.

Hydroxide as nucleophile

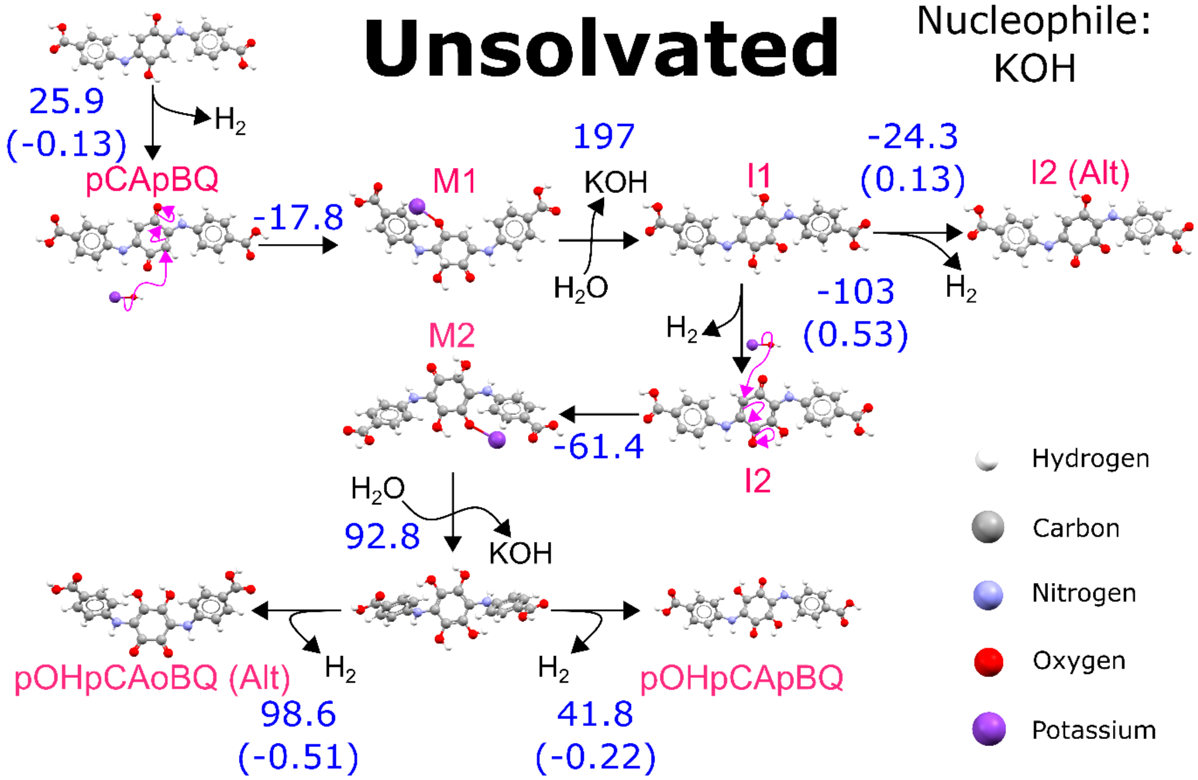

Figure S 65: DFT optimised structures and Gibbs free energies for the reactions (kJ·mol^{-1}) with potassium hydroxide acting as the nucleophiles and all structures having been converged in the gas-phase. The numbers in brackets correspond to the potentials for those reactions in Volts.

Aqueous Solvation (Implicit)

Water as nucleophile

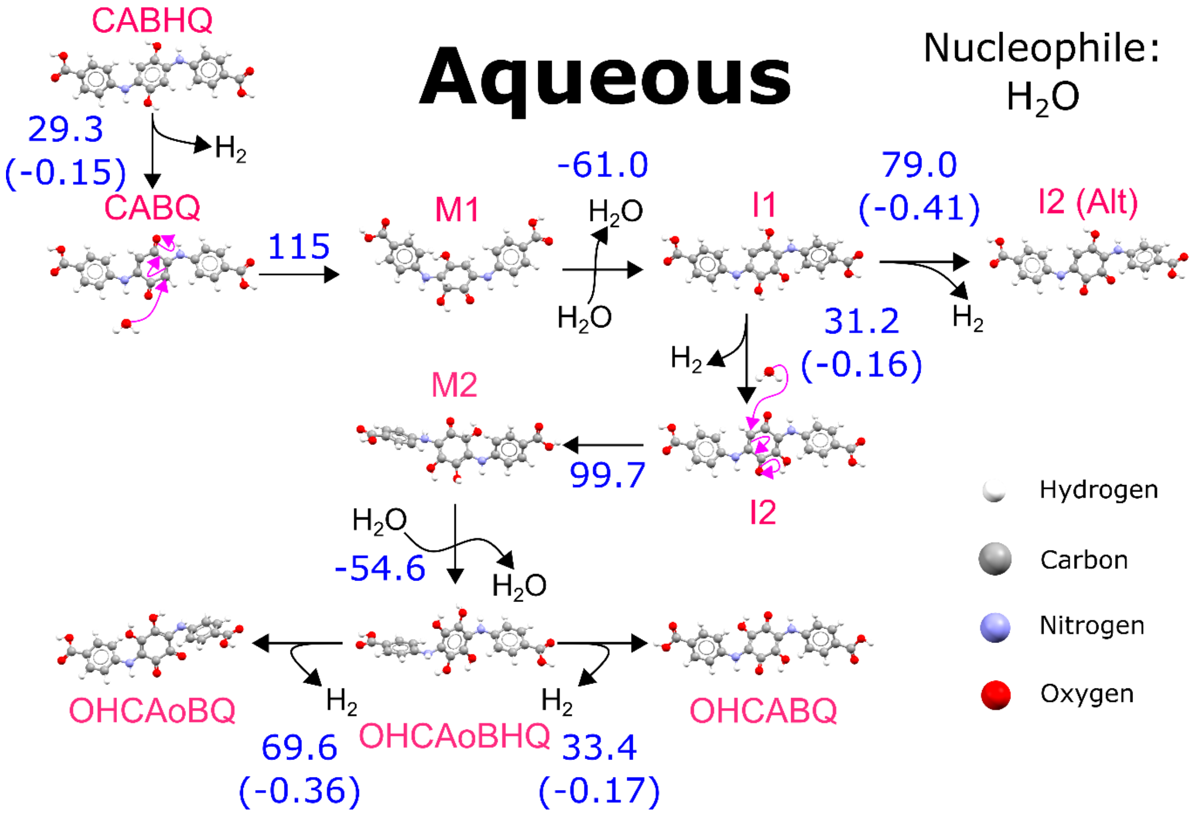

Figure S 66: DFT optimised structures with implict water and Gibbs free energies for the reactions (kJ·mol^{-1}) with water acting as the nucleophiles. The numbers in brackets correspond to the potentials for those reactions in Volts.

Hydroxide as nucleophile

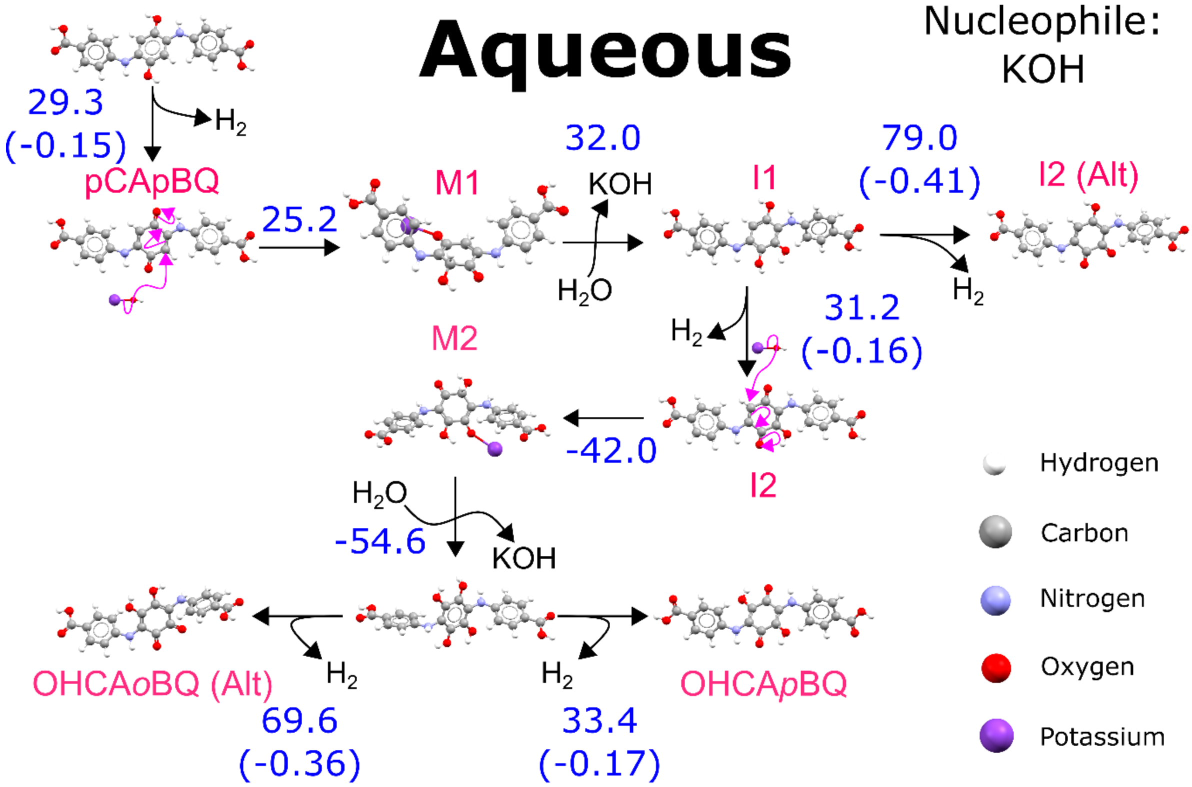

Figure S 67: DFT optimised structures with implict water and Gibbs free energies for the reactions (kJ·mol^{-1}) with water acting as the nucleophiles. The numbers in brackets correspond to the potentials for those reactions in Volts.

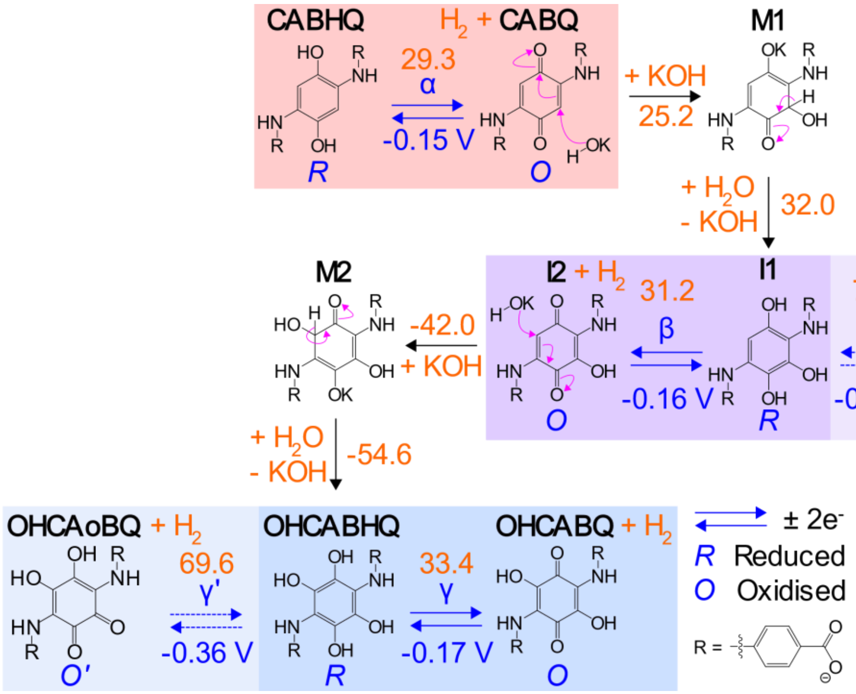

Figure S 68: DFT calculated Gibbs free energies for the reactions (in orange, kJ.mol^{-1}) with hydroxide acting as the nucleophile. The numbers in blue font correspond to the potentials for those reactions in Volts. The calculations were carried out under implicit water solvation.

2.19.2 Structures and energies

Structure	*Designation (Environment)*	*Energy /Hartree*	*Free Energy /GJ ·mol^{-1}*
	CABHQ (Gas)	-1333.318	-3.49990
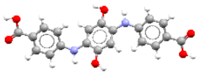	CABHQ (Water)	-1333.343	-3.49997
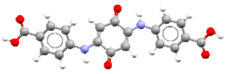	CABQ (Gas)	-1332.105	-3.49677
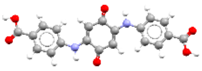	CABQ (Water)	-1332.127	-3.49683
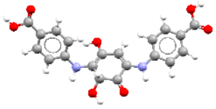	M1_H (Gas)	-1408.556	-3.69743
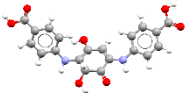	M1_H (Water)	-1408.579	-3.69749
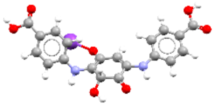	M1_K (Gas)	-2007.972	-5.27123
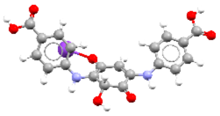	M1_K (Water)	-2008.021	-5.27136
	I1 (Gas)	-1408.575	-3.69736
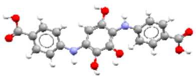	I1 (Water)	-1408.604	-3.69755
	I2 (Gas)	-1407.366	-3.69435
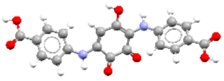	I2 (Alt) (Gas)	-1407.333	-3.69428

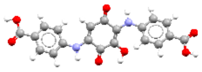	I2 (Water)	-1407.388	-3.69442
	I2 (Alt) (Water)	-1407.368	-3.69437
	M2_H (Gas)	-1483.813	-3.89500
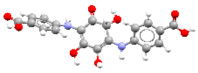	M2_H (Water)	-1483.845	-3.89509
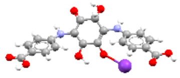	M2_K (Gas)	-2083.251	-5.46886
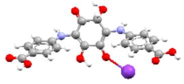	M2_K (Water)	-2083.306	-5.46902
	OHCABHQ (Gas)	-1483.846	-3.89509
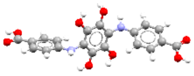	OHCABHQ (Water)	-1483.865	-3.89515
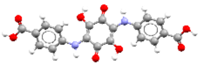	OHCABQ (Gas)	-1482.627	-3.89195
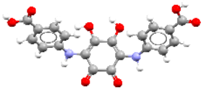	OHCAoBQ (Gas)	-1482.603	-3.89189
	OHCABQ (Water)	-1482.650	-3.89201
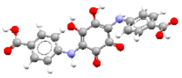	OHCAoBQ (Water)	-1482.634	-3.89197
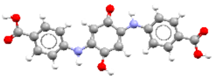	CABSQ (Gas)	-1332.669	-3.49822
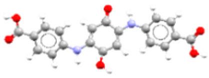	CABSQ (Water)	-1332.697	-3.49830

	OHCABSQ (Gas)	-1483.194	-3.89341
	OHCABSQ (Water)	-1483.220	-3.89348
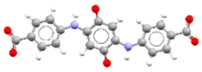	CABSQ^{3-} (Gas)	-1330.877	-3.49421
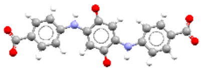	CABSQ^{3-} (Water)	-1331.301	-3.49533
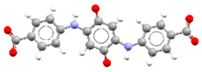	OHCABSQ^{5-} (Gas)	-1479.737	-3.88504
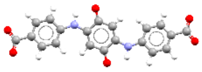	OHCABSQ^{5-} (Water)	-1480.829	-3.88791

2.19.3 Frontier Molecular Orbitals of CABQ (water)

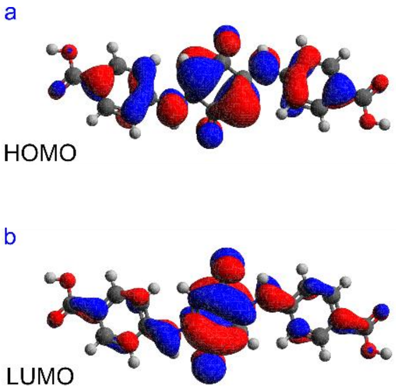

Figure S 69: **(a)** Highest occupied molecular (HOMO) orbital of CABQ. **(b)** Lowest unoccupied molecular orbital (LUMO) of CABQ.

2.19.4 Frontier Molecular Orbitals of CABHQ (water)

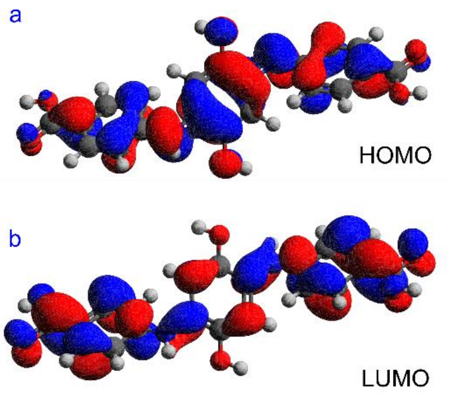

Figure S 70: **(a)** Highest occupied molecular (HOMO) orbital of CABHQ. **(b)** Lowest unoccupied molecular orbital (LUMO) of CABHQ.

2.19.5 Frontier Molecular Orbitals of OHCABQ (water)

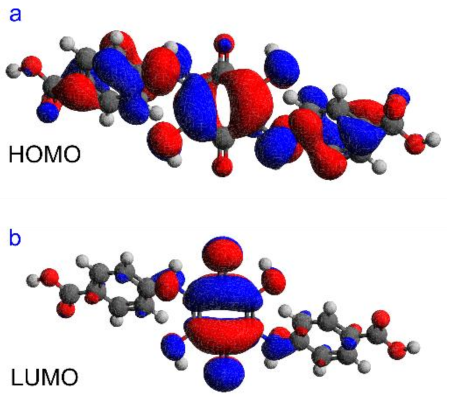

Figure S 71: **(a)** Highest occupied molecular (HOMO) orbital of OHCABQ. **(b)** Lowest unoccupied molecular orbital (LUMO) of OHCABQ.

2.19.6 Frontier Molecular Orbitals of OHCABHQ (Water)

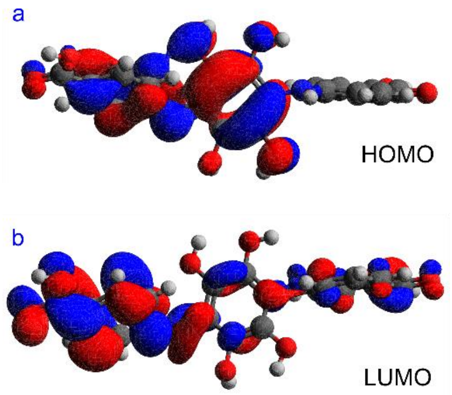

Figure S 72: **(a)** Highest occupied molecular (HOMO) orbital of OHCABHQ. **(b)** Lowest unoccupied molecular orbital (LUMO) of OHCABHQ.

2.19.7 Fermi-contact coupling constants for CABSQ

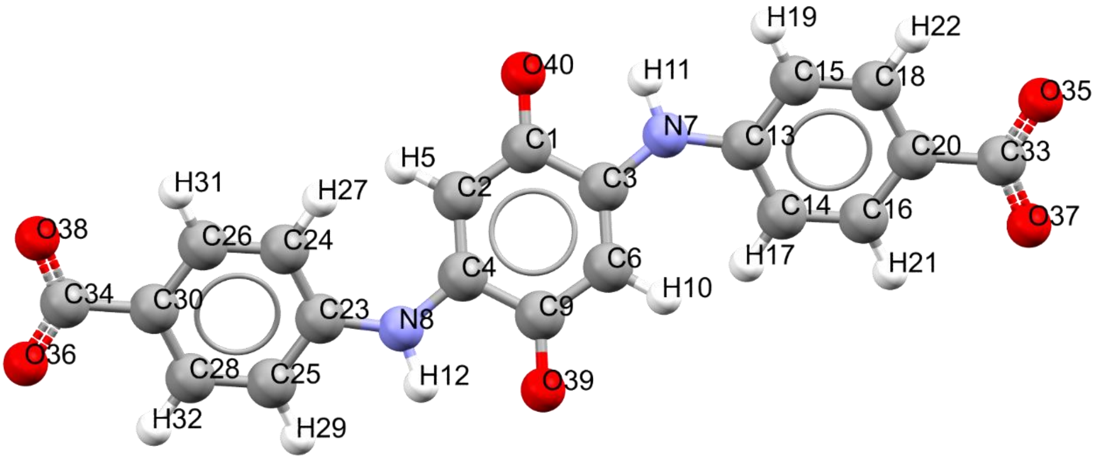

Figure S 73: CABSQ^{3-} atomic labels

Atom	*Element*	*Fermi contact coupling constant (gas phase) / MHz*	*Fermi contact coupling constant (water) / MHz*
1	C	0.29808	1.62426
2	C	-11.27530	-12.04639
3	C	6.15106	6.06079
4	C	6.15106	6.06078
5	H	0.08887	0.59135
6	C	-11.27529	-12.04634
7	N	0.53271	0.9798
8	N	0.53271	0.9798
9	C	0.29810	1.62423
10	H	0.08887	0.59133
11	H	-2.93767	-3.52843
12	H	-2.93767	-3.52843
13	C	-3.07325	-3.51597
14	C	2.18006	2.34573
15	C	1.98615	2.10458
16	C	-2.02357	-2.14092
17	H	-1.58941	-1.70366
18	C	-1.90994	-1.99621
19	H	-1.32715	-1.46369
20	C	2.55038	2.62086
21	H	0.68545	0.74358
22	H	0.60281	0.63143
23	C	-3.07324	-3.51596
24	C	2.18006	2.34573
25	C	1.98615	2.10458
26	C	-2.02357	-2.14092
27	H	-1.58941	-1.70365

28	C	-1.90994	-1.99622
29	H	-1.32715	-1.46369
30	C	2.55038	2.62086
31	H	0.68545	0.74358
32	H	0.60280	0.63143
33	C	-0.98740	-1.04719
34	C	-0.98740	-1.04719
35	O	-0.08634	-0.0993
36	O	-0.08634	-0.0993
37	O	-0.11446	-0.1279
38	O	-0.11446	-0.1279
39	O	-16.82113	-15.96901
40	O	-16.82112	-15.96901

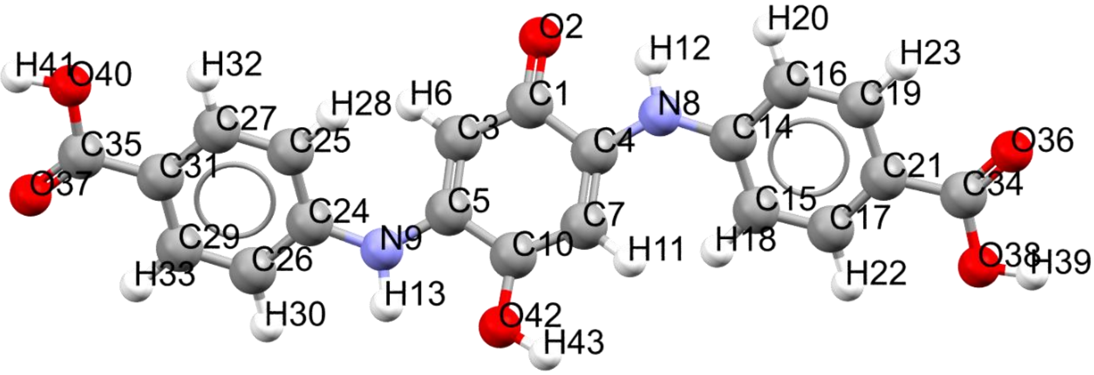

Figure S 74: CABSQ atomic labels

Atom	*Element*	*Fermi contact coupling constant (gas phase) / MHz*	*Fermi contact coupling constant (water) / MHz*
1	C	-13.43496	-8.42134
2	O	-16.78257	-15.85059
3	C	-0.57007	-4.61796
4	C	15.08576	13.35908
5	C	-8.37655	-4.57383
6	H	-4.97571	-2.57659
7	C	-21.70339	-20.14422
8	N	3.56634	3.82436
9	N	1.24636	1.59522
10	C	24.30074	20.40449
11	H	5.37036	5.02542
12	H	-8.11496	-8.02553
13	H	-2.20057	-2.41473
14	C	-6.64371	-6.83025
15	C	3.69779	3.78734
16	C	4.82394	4.67242
17	C	-3.43204	-3.50558
18	H	-2.81525	-2.88855
19	C	-2.93395	-3.07333

20	H	-2.43645	-2.52637
21	C	3.77568	3.83341
22	H	1.50698	1.50061
23	H	1.01415	1.0393
24	C	-2.17933	-2.83285
25	C	1.92210	2.11043
26	C	1.37098	1.80825
27	C	-0.86083	-1.29135
28	H	-0.81485	-1.15117
29	C	-0.93315	-1.28778
30	H	-0.74418	-1.03941
31	C	1.09583	1.51622
32	H	0.35662	0.5212
33	H	0.34161	0.44363
34	C	-1.99630	-1.9741
35	C	-0.61929	-0.82164
36	O	-0.62359	-0.65926
37	O	-0.18194	-0.26868
38	O	0.07711	0.01714
39	H	-0.18846	-0.22684
40	O	0.03274	0.01337
41	H	-0.05383	-0.09043
42	O	-7.39785	-7.66807
43	H	-4.5842	-4.80899

2.19.8 Fermi-contact coupling constants for OHCABSQ

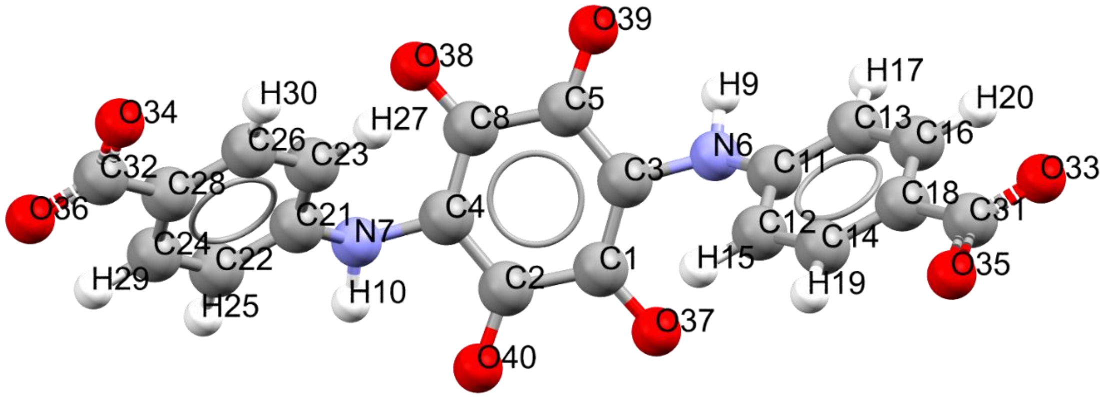

Figure S 75: OHCABSQ^{5-} atomic labels

Atom	*Element*	*Fermi contact coupling constant (gas phase) / MHz*	*Fermi contact coupling constant (water) / MHz*
1	C	0.01418	5.51329
2	C	-0.01604	7.81048
3	C	0.01729	-20.08035
4	C	0.01729	-20.09613

5	C	-0.01604	7.78589
6	N	0.04347	0.18321
7	N	0.04347	0.18105
8	C	0.01418	5.53009
9	H	0.01892	-1.36790
10	H	0.01892	-1.36617
11	C	-0.10543	-2.50514
12	C	0.32779	-0.49475
13	C	2.57623	0.01169
14	C	0.35824	0.27166
15	H	0.06307	0.26255
16	C	2.26473	0.17990
17	H	0.37591	0.09276
18	C	0.0019	-0.38465
19	H	0.04301	-0.11907
20	H	0.31929	-0.04846
21	C	-0.10543	-2.48309
22	C	2.57622	0.01131
23	C	0.32779	-0.49379
24	C	2.26474	0.18008
25	H	0.3759	0.09211
26	C	0.35824	0.27389
27	H	0.06307	0.25869
28	C	0.0019	-0.35327
29	H	0.31929	-0.04629
30	H	0.04301	-0.11679
31	C	0.35523	0.12656
32	C	0.35523	0.13384
33	O	-1.84904	0.01803
34	O	-0.26159	0.03037
35	O	-0.26158	0.02933
36	O	-1.84905	0.01910
37	O	-0.02698	-11.31836
38	O	-0.02697	-11.31876
39	O	-0.23867	-11.19949
40	O	-0.23867	-11.19941

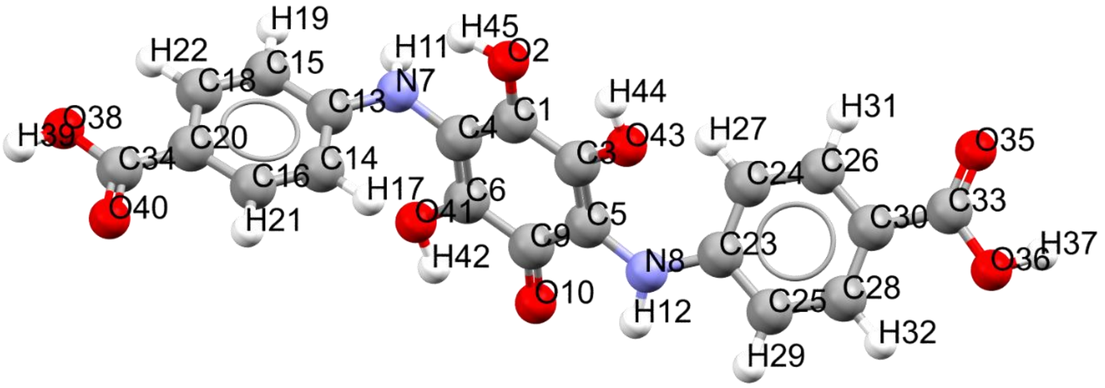

Figure S 76: OHCABSQ atomic labels

Atom	*Element*	*Fermi contact coupling constant (gas phase) / MHz*	*Fermi contact coupling constant (water) / MHz*
1	C	22.47326	21.94919
2	O	-8.56340	-9.61892
3	C	-15.17589	-12.41738
4	C	-19.61979	-21.18758
5	C	2.16441	-0.45788
6	C	10.90219	12.49022
7	N	0.27145	0.51722
8	N	3.05211	1.65976
9	C	-11.78679	-9.97106
10	O	-22.28270	-21.72763
11	H	-3.88788	-5.97524
12	H	-5.40603	-2.72973
13	C	-3.29000	-2.8439
14	C	-0.00010	-0.32547
15	C	0.04178	0.02815
16	C	0.02892	0.03263
17	H	-0.03680	0.03981
18	C	-0.04404	0.00359
19	H	0.01589	0.03958
20	C	-0.02206	-0.12433
21	H	-0.00401	-0.05752
22	H	-0.04346	-0.05182
23	C	-1.37191	0.11952
24	C	2.00569	1.11757
25	C	2.20836	1.13773
26	C	-1.70862	-1.11341
27	H	-1.38382	-0.8712
28	C	-1.76848	-1.16939
29	H	-1.36503	-0.88445
30	C	2.00046	1.2766
31	H	0.93435	0.54482
32	H	0.59033	0.38628

33	C	-1.05457	-0.66732
34	C	-0.00031	0.00885
35	O	-0.31042	-0.21269
36	O	0.06359	0.01929
37	H	-0.09040	-0.07084
38	O	0.00359	0.01079
39	H	-0.00150	-0.00157
40	O	0.00049	0.00737
41	O	-6.29507	-6.90689
42	H	-4.19892	-4.59104
43	O	0.89786	-0.20278
44	H	-0.25732	-0.89473
45	H	-4.68662	-5.71553

3. Bibliography

1 A. Nain-Perez, L. C. A. Barbosa, M. C. Picanço, S. Giberti and G. Forlani, *Chem. Biodivers.*, 2016, **13**, 1008–1017.

2 K. A. Macgregor, M. K. Abdel-Hamid, L. R. Odell, N. Chau, A. Whiting, P. J. Robinson and A. McCluskey, *Eur. J. Med. Chem.*, 2014, **85**, 191–206.

3 V. K. Tandon, S. Kumar, N. N. Mishra and P. K. Shukla, *Eur. J. Med. Chem.*, 2012, **56**, 375–386.

4 J. B. Gerken, A. Stamoulis, S.-E. Suh, N. D. Fischer, J. Kim, I. A. Guzei, S. S. Stahl, R. Li, / Chemcomm and C. Communication, *Chem. Commun*, 2020, **56**, 1199.

5 G. R. Fulmer, A. J. M. Miller, N. H. Sherden, H. E. Gottlieb, A. Nudelman, B. M. Stoltz, J. E. Bercaw and K. I. Goldberg, *Organometallics*, 2010, **29**, 2176–2179.

6 E. W. Zhao, T. Liu, E. Jónsson, J. Lee, I. Temprano, R. B. Jethwa, A. Wang, H. Smith, J. Carretero-González, Q. Song and C. P. Grey, *Nature*, 2020, **579**, 224–228.

7 E. W. Zhao, J. Jónsson, R. B. Jethwa, D. Hey, D. Lyu, A. Brookfield, P. A. A. Klusener, D. Collison and C. P. Grey, *J. Am. Chem. Soc*, 2021, **143**, 1885–1895.

8 M. J. Frisch, G. W. Trucks, H. B. Schlegel, G. E. Scuseria, M. A. Robb, J. R. Cheeseman, G. Scalmani, V. Barone, G. A. Petersson, H. Nakatsuji, X. Li, M. Caricato, A. V. Marenich, J. Bloino, B. G. Janesko, R. Gomperts, B. Mennucci, H. P. Hratchian, J. V. Ortiz, A. F. Izmaylov, J. L. Sonnenberg, D. Williams-Young, F. Ding, F. Lipparini, F. Egidi, J. Goings, B. Peng, A. Petrone, T. Henderson, D. Ranasinghe, V. G. Zakrzewski, J. Gao, N. Rega, G. Zheng, W. Liang, M. Hada, M. Ehara, K. Toyota, R. Fukuda, J. Hasegawa, M. Ishida, T. Nakajima, Y. Honda, O. Kitao, H. Nakai, T. Vreven, K. Throssell, J. Montgomery, J. A., J. E. Peralta, F. Ogliaro, M. J. Bearpark, J. J. Heyd, E. N. Brothers, K. N. Kudin, V. N. Staroverov, T. A. Keith, R. Kobayashi, J. Normand, K. Raghavachari, A. P. Rendell, J. C. Burant, S. S. Iyengar, J. Tomasi, M. Cossi, J. M. Millam, M. Klene, C. Adamo, R. Cammi, J. W. Ochterski, R. L. Martin, K. Morokuma, O. Farkas, J. B. Foresman and D. J.

Fox, 2016.
9 A. D. Becke, *J. Chem. Phys.*, 1993, **98**, 5648–5652.
10 P. J. Stephens, F. J. Devlin, C. F. Chabalowski and M. J. Frisch, *J. Phys. Chem.*, 1994, **98**, 11623–11627.
11 S. H. Vosko, S. A. And, L. W. Ilk and M. Nusair, *Can. J. Phys.*, 1980, **58**, 1200.
12 W. L. F. Armarego and C. L. L. Chai, *Purification of laboratory chemicals*, Butterworth-Heinemann, 2003.
13 C. Lee, W. Yang and R. G. Parr, *Development of the Colle-Salvetti correlation-energy formula into a functional of the electron density*, 1988, vol. 37.
14 F. Weigend, *Phys. Chem. Chem. Phys.*, 2006, **8**, 1057–1065.
15 F. Weigend and R. Ahlrichs, *Phys. Chem. Chem. Phys.*, 2005, **7**, 3297–3305.
16 V. Barone, in *Recent Advances in Density Functional Methods, Part I*, ed. D. P. Chong, World Scientific Publ. Co., Singapore, 1995, pp. 287–335.
17 G. Scalmani and M. J. Frisch, *J. Chem. Phys.*, 2010, **132**, 114110.
18 P. (University of O. Atkins and J. (Haverford C. de Paula, *Atkins' Physical Chemistry*, Oxford University Press, New York, Seventh., 2002.
19 A. J. Bard and L. R. Faulkner, in *Electrochemical Methods: Fundamentals and Applications*, Wiley, 2nd edn., 2001, pp. 239–244.
20 Y. A. Gandomi, D. S. Aaron, J. R. Houser, M. C. Daugherty, J. T. Clement, A. M. Pezeshki, T. Y. Ertugrul, D. P. Moseley and M. M. Mench, *J. Electrochem. Soc.*, , DOI:10.1149/2.0601805jes.